CHAPTER 5

LASER SPECTROSCOPIC TECHNIQUES

5.1 ADVANTAGES OF LASER SPECTROSCOPY

In standard absorption spectroscopy, radiation sources have a spectrally wide continuous emission. The sources typically used were lamps.

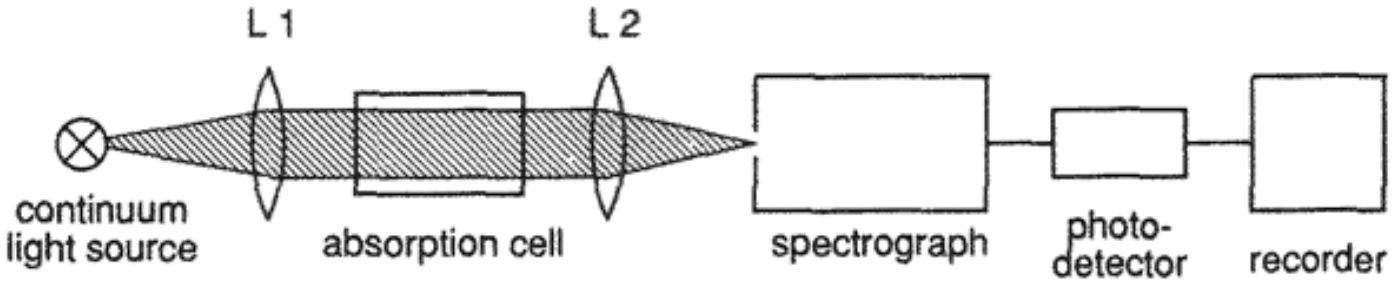

The radiation emitted by the source is collimated by a lens lente L_1 to pass through a cell containing the absorbent gas.

The light exiting from the absorption cell is focused by a lens lente L_2 on a dispersing instrument (spectrometer or interferometer) to select the different spectral components. In this way, the intensity $I_T(\lambda)$ of the transmitted light is measured as a function of the wavelength λ.

5.1 ADVANTAGES OF LASER SPECTROSCOPY

By comparing $I_T(\lambda)$ with the reference beam $I_R(\lambda)$ (it can be acquired, for example, by removing the absorption cell), the absorption spectrum can be derived:

$$I_A(\lambda) = a[I_0(\lambda) - I_T(\lambda)\,] = a[bI_R(\lambda) - I_T(\lambda)\,]$$

where the constants a and b are introduced to consider the non-wavelength-dependent losses of $I_R(\lambda)$ and $I_T(\lambda)$.

The **spectral resolution** is limited by the resolving power of the spectrometer. Only by using expensive and bulky tools (e.g. Fourier spectrometers), the Doppler limit can be reached.

The **detection limit** is determined by the minimum absorbed power that the detector can reveal. In many cases, this is limited by the noise level of the optical detector and the fluctuations in intensity of the light source. Typically, the absorption limit that can be reached is $\frac{\Delta I}{I} \geq 10^{-4} - 10^{-5}$.

5.1 ADVANTAGES OF LASER SPECTROSCOPY

We will see that these limits can be overcome by employing advanced spectroscopy techniques.

In contrast to radiation sources with large spectral emission, laser sources can be tuned in wavelength and can cover a wide spectral region, from UV to infrared, with extremely narrow line widths. In addition, their spectral power density can exceed those of broadband, incoherent sources by several orders of magnitude.

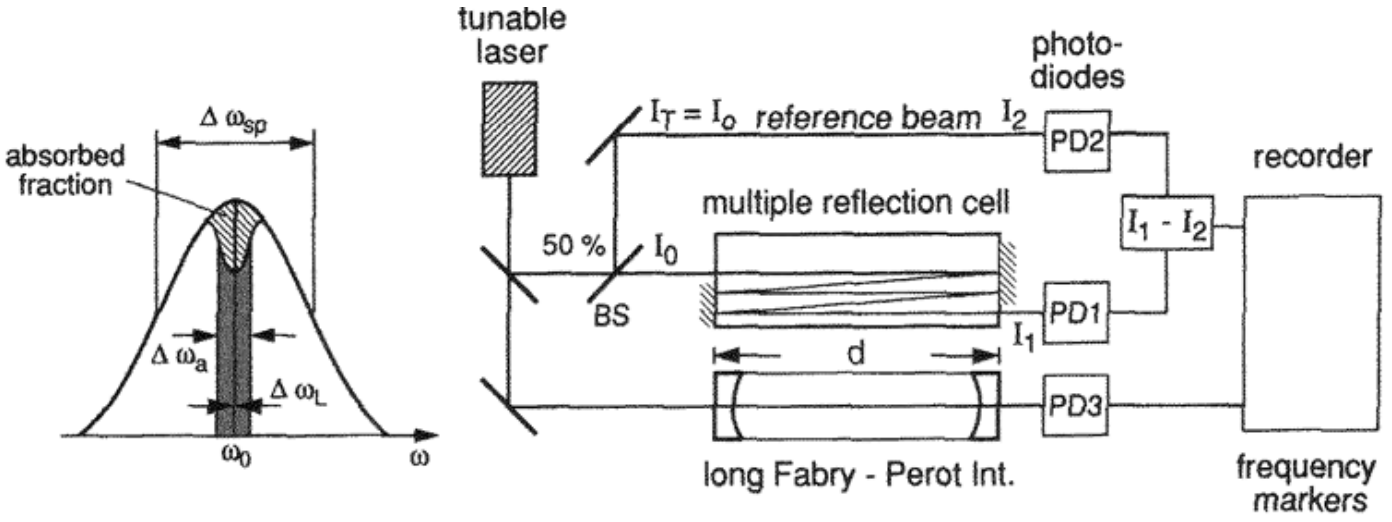

5.1 ADVANTAGES OF LASER SPECTROSCOPY

The main advantages of laser spectroscopy are:

- Monochromators are not needed, since the spectral dispersion of the absorption coefficient $\alpha(\omega)$ can be directly measured by the difference $\Delta I(\omega) = a[I_R(\omega) - I_T(\omega)]$ between the intensities of the reference beam $I_R = I_2$ and the transmitted beam $I_T = I_1$.

  - Because the spectral power density of a laser is high, detector noise is typically negligible. Fluctuations in intensity of a laser source, which limit the sensitivity of detection, can be greatly reduced by using techniques for the stabilization in intensity.

  - Thanks to excellent collimation of the beam reachable with laser sources, long optical paths can be achieved, even through multiple reflections on small spaces (multi-pass absorption cells). Increasing the optical path allows the measurement of optical transitions even with small absorption coefficients.

5.1 ADVANTAGES OF LASER SPECTROSCOPY

- If a small portion of the laser beam is sent to a Fabry-Perot interferometer with a separation d between the mirrors, the PD3 photodiode measures peak value in intensity whenever the laser frequency υ_L coincides with the maximum transmission $\upsilon = mc/2d$. These peaks can be used as a sort of wavelength markers, which can be used to calibrate the separation between adjacent spectral lines. With $d = 1\,m$, the spectral separation between successive peaks will be: $\Delta\nu_P = \frac{c}{2d} = 150\ MHz$.
-
    - In conditions of non-saturation, the Doppler broadening of a molecular transition is the dominant spectral mechanism and, at room temperature and at atmospheric pressure, it can reach values of a few tens of GHz. The linewidth of a laser emission is typically a few tens of MHz. This means that by varying the wavelength of emission of the laser, it is possible to reconstruct the profile of the absorption line of an optical transition with an extremely fine spectral sampling.

5.2 DIRECT ABSORPTION

The simplest method for measuring the absorption spectrum of a gas species is to determine the absorption coefficient $\alpha(\omega)$ using the Lambert-Beer law:

$$I_T(\omega) = I_0 e^{-\alpha(\omega)x}$$

which allows to calculate the radiation transmitted I_T after passing through an optical path of length x.

In the approximation of small absorptions $\alpha(\omega)x \ll 1$, using the approximation $e^{-\alpha(\omega)x} \ll 1 - \alpha(\omega)x$, lambert-Beer's law can be reduced to:

$$I_T(\omega) \simeq I_0[1 - \alpha(\omega)x]$$

By measuring the intensity I_0, the absorption coefficient can be retrieved as:

$$\alpha(\omega) = \frac{I_0 - I_T(\omega)}{xI_0} = \frac{\Delta I}{xI_0}$$

where $\Delta I = I_0 - I_T(\omega)$.

5.2 DIRECT ABSORPTION

The absorption coefficient $\alpha_{ik}(\omega)$ of the transition $|i\rangle \rightarrow |k\rangle$ with absorption cross section $\sigma_{ik}(\omega)$ is determined by the density of the absorbing molecules N_i :

$$\alpha_{ik}(\omega) = \left[N_i - \left(\frac{g_i}{g_k}\right) N_k\right] \sigma_{ik}(\omega) = \Delta N \sigma_{ik}(\omega)$$

If N_k is much smaller than N_i, it is possible to calculate the minimum detectable density of absorbers N_i over an optical absorption path $x = L$:

$$N_i \geq \frac{\Delta I}{I_0 L \sigma_{ik}(\omega)}$$

$$\alpha(\omega) = \frac{\Delta I}{x I_0}$$

The minimum detectable density of absorbers directly depends on:

a. the absorption cross section σ_{ik}

b. the length of the optical path L

c. the minimum detectable change in intensity $\frac{\Delta I}{I_0}$ caused by absorption.

5.2 DIRECT ABSORPTION

To achieve high detection sensitivities, $L\sigma_{ik}$ must be as large as possible and the minimum detectable value $\frac{\Delta I}{I_0}$ as small as possible.

$$N_i \geq \frac{\Delta I}{I_0 L \sigma_{ik}(\omega)}$$

In the case of small absorptions, measuring $\frac{\Delta I}{I_0}$ involves estimating small differences $I_0 - I_T$ of two large quantities I_0 and I_T .

The two main contributions that negatevely affect the accuracy of the measurement of $\frac{\Delta I}{I_0}$ ar:

- Fluctuations in I_0 that can be reduced using methods that increase the stabilization of the intensity of a laser.
- The noise level of the photodetector.

5.3 MODULATION TECHNIQUES

5.3.1 Amplitude modulation

Since the noise level of a photodetector affects the ultimate detection sensitivity, we analyze the typical noise spectrum of a photodetector, i.e., the noise level as a function of the working frequency. The typical spectrum of a detector is represented in Figure.

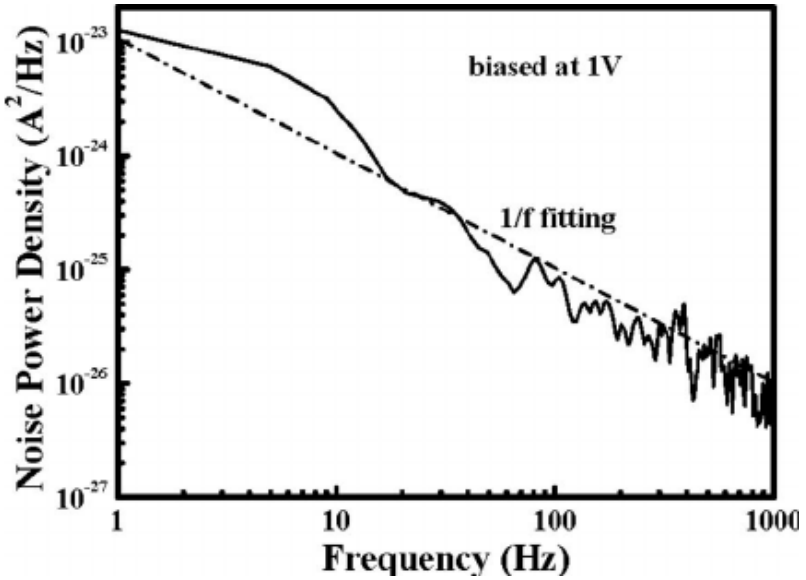

We observe that the noise level significantly decreases when the photodetector operates at higher frequencies. For example, it is reduced by several orders of magnitude when moving from frequencies of the order of Hz up to frequencies of the order of kHz, following indicatively the Flicker noise trend $1/f$.

5.3 MODULATION TECHNIQUES

5.3.1 Amplitude modulation

This suggests that rather than working with a continuous-wave (CW) laser beam, it is more convenient to modulate the light intensity at a certain frequency, and then to filter the signal from the photodetector to extract only the spectral component at the working frequency. This approach is called **Amplitude Modulation Spectroscopy**.

A typical apparatus for amplitude modulation spectroscopy is shown in Figure:

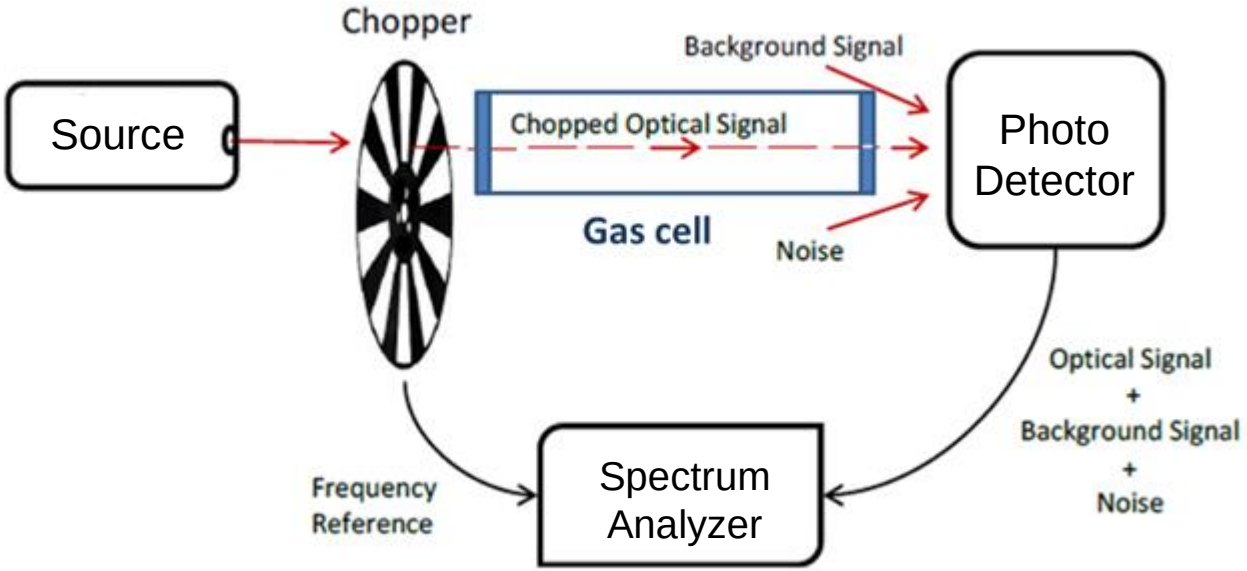

5.3 MODULATION TECHNIQUES

5.3.1 Amplitude modulation

The laser beam with continuous emission is modulated in intensity using a mechanical modulator (chopper) with a duty-cycle, typically, of 50 %. The light transmitted by the cell containing the absorbent gas sample is sent to a photodetector, which generates an electrical signal proportional to the concentration of the absorbent gas.

The signal is then sent to a spectrum analyzer that extracts the spectral component at the frequency of modulation of the beam by a Fourier analysis of the input signal. An alternative to the spectrum analyzer is a lock-in amplifier.

Being Ω the modulation frequency, the light intensity incident on the gas sample can be represented as a square wave at the Ω frequency.

This means that in the Lamber-Beer equation for small absorptions, $I_T(\omega) = I_0[1 - \alpha(\omega)x]$, I_0 has itself a square wave shape.

If the wavelength of the laser is fixed on the peak of the absorption line, I_T will also be a square wave in the time domain as well as the signal S_T acquired by the detector.

5.3 MODULATION TECHNIQUES

5.3.1 Amplitude modulation

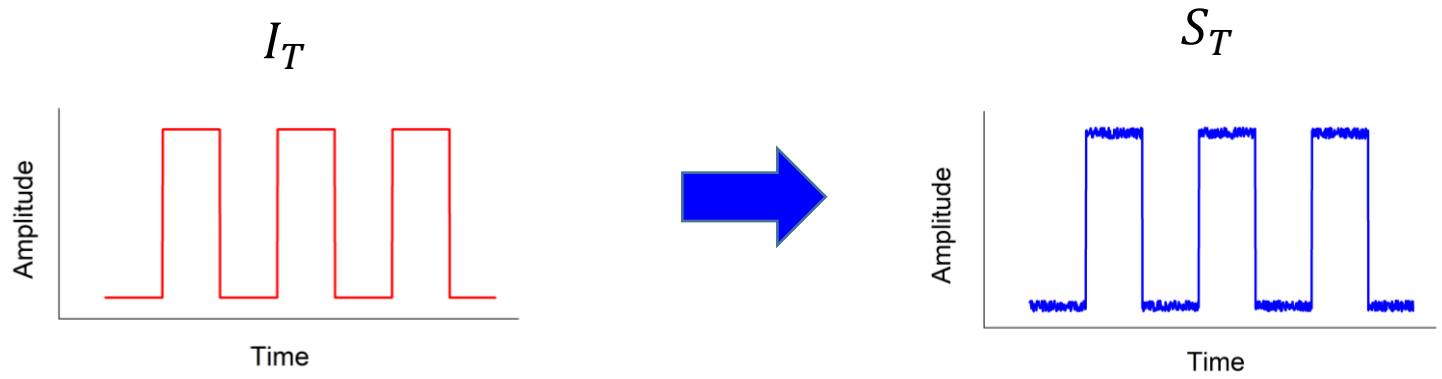

The detector signal S_T is sent to a spectrum analyzer to extract only the component at the Ω frequency, i.e., at the modulation frequency of the laser intensity.

In the frequency domain, square waves with a duty cycle of 50% can be expressed as a Fourier series:

$$\psi_{square} = \frac{4}{\pi}\sum_{k=1}^{\infty}\frac{sen[(2k-1)\Omega t]}{(2k-1)}$$

$$= \frac{4}{\pi}\left[sen(\Omega t) + \frac{1}{3}sen(3\Omega t) + \frac{1}{5}sen(5\Omega t) + \cdots\right]$$

5.3 MODULATION TECHNIQUES

5.3.1 Amplitude modulation

Only the odd harmonics are present: the third one with amplitude equal to one third of the fundamental, the fifth harmonic with amplitude equal to one fifth of the fundamental, and so on.

So, in the acquired spectrum there will be unwanted contributions even to the higher harmonics.

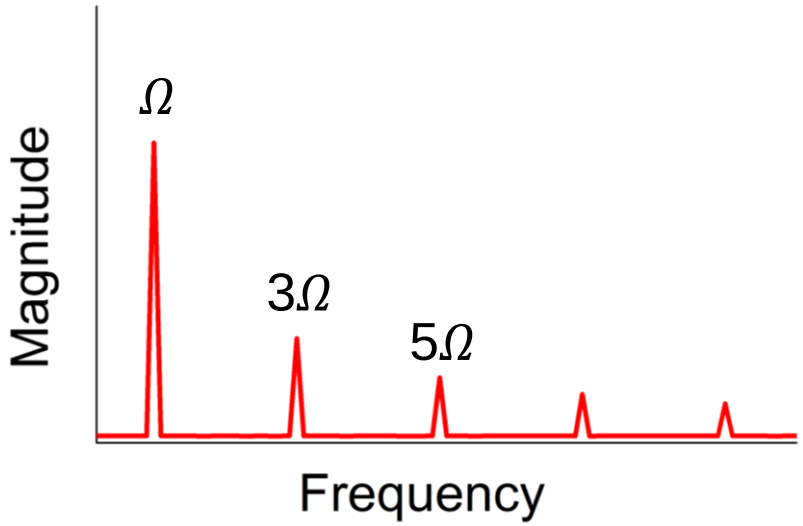

If only the spectral component of I_T at the Ω frequency is extracted, I_T/I_0 as a function of the frequency of the light will follow the trend of the absorption coefficient $\alpha(\omega)$, as in the case of direct absorption with the advantage of a significantly lower photodetector noise level.

5.3 MODULATION TECHNIQUES

5.3.2 Frequency modulation

Amplitude modulation involves the use of a mechanical modulator that hardly allows to reach modulation frequencies > 5 KHz. At such frequencies, mechanical choppers tend to suffer from frequency instabilities. In addition, they are bulky and noisy.

A simpler alternative is to modulate the laser current. If the injection current is modulated with an amplitude such as to alternate at a frequency Ω the condition of laser on with that of laser off (laser below threshold), the result will be identical to that of a mechanical modulator. However, this condition is not advisable as abrupt variations in the current injected at such high frequencies can lead to instability of the source generated by the alternation of heat accumulation and subsequent dissipation.

To overcome this issue, it is preferred to polarize the laser with a direct current above the threshold and apply a modulation with an amplitude such that the laser is always above the threshold. This condition is known in the literature as **dithering**.

5.3 MODULATION TECHNIQUES

5.3.2 Frequency modulation

When a dither is applied, the square wave is not the best solution as we have seen that there will be unwanted contributions to the higher harmonics as well.

For this reason, it is preferred to apply a sinusoidal dither at a frequency Ω, to have only one contribution in frequency, without distortions due to higher harmonics.

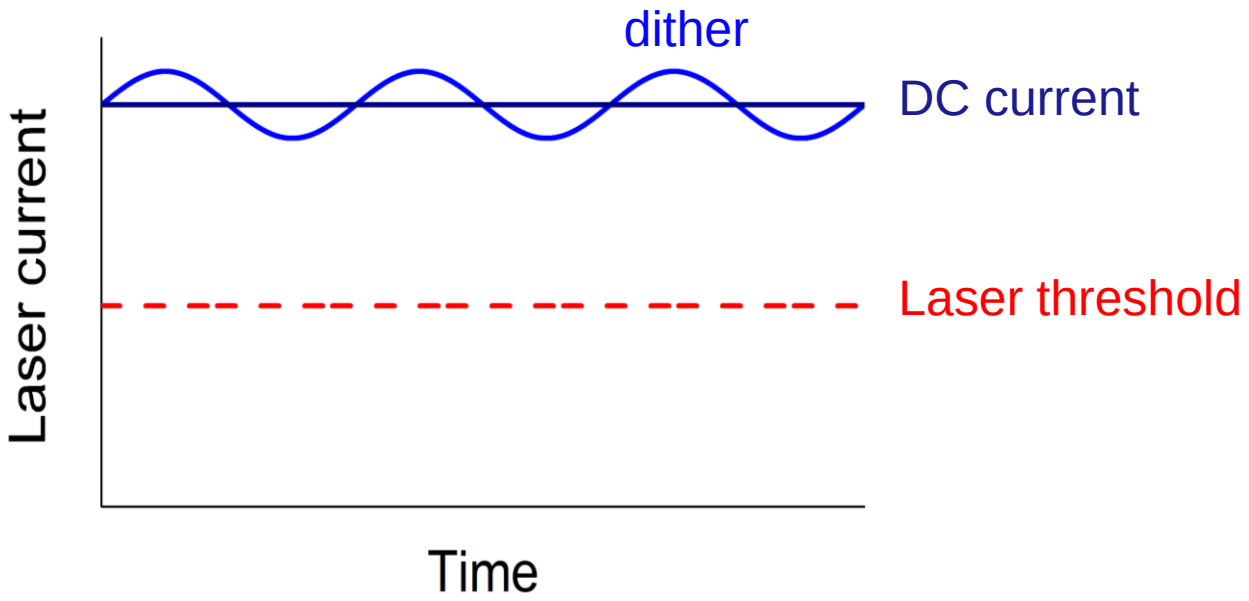

5.3 MODULATION TECHNIQUES

5.3.2 Frequency modulation

If the intensity of the laser varies linearly with the electric current, a sinusoidal dither applied to the current will correspond to a modulation of the current at the same frequency, without distortion. This is the case with laser diodes, in which above the lasing threshold, the light intensity varies linearly with the injected current.

Unfortunately, for diode lasers, the emission wavelength also varies linearly with the electric current, as a result of the dependence of the refractive index on the temperature of the active medium.

So, if we apply a dither of amplitude Δi at the frequency Ω to the DC current i_{DC}, with $\Delta i \ll i_{DC}$, the instantaneous current will be (we neglect any type of phase shift):

$$i(t) = i_{\mathrm{DC}} + \Delta \mathrm{i} \cos(\Omega t)$$

and the laser intensity will vary with the same trend:

$$I_0(t) = I_{\mathrm{DC}} + \Delta \mathrm{I} \cos(\Omega t)$$

and simultaneously the emission frequency will be modulated at the same frequency Ω :

$$\omega(t) = \omega_0 + \Delta\omega \cos(\Omega t)$$

5.3 MODULATION TECHNIQUES

5.3.2 Frequency modulation

This technique is known as **Frequency Modulation**. In the literature, it is usually referred a Frequency Modulation if Ω is in the range of MHz, while it is known as **Wavelength Modulation** if Ω < 100 kHz.

In the case of small absorptions:

$$I_T(\omega) = I_0[1 - \alpha(\omega)x]$$

Since the absorption coefficient is a function of frequency:

$$\alpha(\omega) \propto \frac{\left(\frac{\gamma}{2}\right)^2}{(\omega - \omega_0)^2 + \left(\frac{\gamma}{2}\right)^2}$$

If $\frac{\Delta\omega}{\omega_0} \ll 1$, a Taylor expansion around the central frequency ω_0 can be performed, with the addiction of a contribution α_0 that does not depend, or weakly depends, on the frequency of the laser (for example, absorption by optical surfaces) such that it can be considered constant:

5.3 MODULATION TECHNIQUES

5.3.2 Frequency modulation

$$\alpha[\omega(t)] = \alpha_0 + \left.\frac{\partial\alpha}{\partial\omega}\right|_{\omega=\omega_0} \Delta\omega\cos(\Omega t) + \frac{1}{2}\left.\frac{\partial^2\alpha}{\partial\omega^2}\right|_{\omega=\omega_0} (\Delta\omega)^2\cos^2(\Omega t)+\dots$$

Inserting $I_0(t)$ and the Taylor series expansion of $\alpha[\omega(t)]$ into the Lambert-Beer law for small absorptions, we get:

$$I_T(\omega) = I_0[1-\alpha(\omega)x]$$

$$I_0(t) = I_{\mathrm{DC}} + \Delta\mathrm{I}\cos(\Omega t)$$

$$I_t(t) = [I_{\mathrm{DC}} + \Delta\mathrm{I}\cos(\Omega t)]\left[1 - L\left(\alpha_0 + \left.\frac{\partial\alpha}{\partial\omega}\right|_{\omega=\omega_0} \Delta\omega\cos(\Omega t) + \frac{1}{2}\left.\frac{\partial^2\alpha}{\partial\omega^2}\right|_{\omega=\omega_0} (\Delta\omega)^2\cos^2(\Omega t)+\dots\right)\right]$$

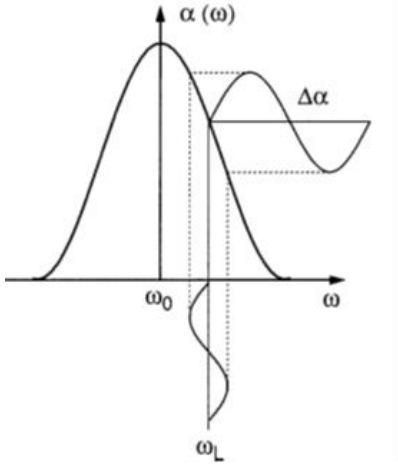

5.3 MODULATION TECHNIQUES

5.3.2 Frequency modulation

By developing the product, you get:

$$
\begin{aligned}
& I_t(t) \\
& = I_{\mathrm{DC}} - L I_{\mathrm{DC}} \alpha_0 - L I_{\mathrm{DC}} \left.\frac{\partial \alpha}{\partial \omega}\right|_{\omega=\omega_0} \Delta\omega \cos(\Omega t) \\
& - L I_{\mathrm{DC}} \left.\frac{1}{2}\frac{\partial^2 \alpha}{\partial \omega^2}\right|_{\omega=\omega_0} (\Delta\omega)^2 \cos^2(\Omega t) + \Delta \mathrm{I} \cos(\Omega t) - \mathrm{L}\alpha_0 \Delta \mathrm{I} \cos(\Omega t) \\
& - L \Delta \mathrm{I} \Delta\omega \left.\frac{\partial \alpha}{\partial \omega}\right|_{\omega=\omega_0} \cos^2(\Omega t) + O[\cos^3(\Omega t)]
\end{aligned}
$$

We observe that the intensity transmitted has three types of contribution:

- one not dependent on the frequency Ω
- one proportional to $\cos(\Omega t)$
- one proportional to $\cos^2(\Omega t)$

5.3 MODULATION TECHNIQUES

5.3.2 Frequency modulation

If we acquire the only spectral component at the frequency Ω of the signal $I_t(t)$ and suppose we filter all the others, we will have that:

$$I_t(t)\Big|_{cos\Omega t} = \Delta I(1-L)\alpha_0 - LI_{DC}\Delta\omega\frac{\partial\alpha}{\partial\omega}\Big|_{\omega=\omega_0}$$

By linearly varying i_{DC} to spectrally scan the absorption line, we will have that $I_t(t)|_{cos\Omega t}$ will consists of two contributions:

- a constant contribution, $\Delta I(1-L)\alpha_0$, not dependent on the shape of the absorption line,
- a constant contribution proportional to the derivative before the absorption line.

This technique is known as **wavelength modulation and 1f detection**, as you acquire the signal at the same frequency at which you modulate it.

Assuming a Lorentzian lineshape, $I_t(t)|_{cos\Omega t}$ will be:

5.3 MODULATION TECHNIQUES

5.3.2 Frequency modulation

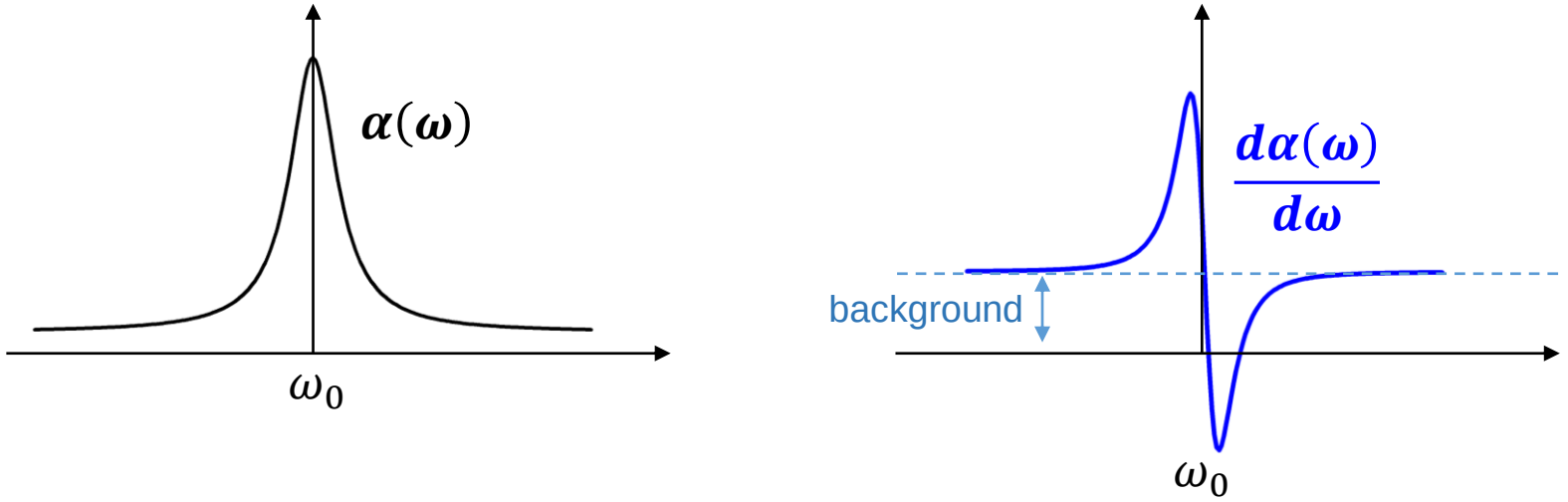

Working in these conditions, there are three major disadvantages:

1. The acquired line shape is heavily distorted
2. It is not background-free, which means that post-processing techniques must be adopted to remove the contribution due to the background
3. Once the background contribution is removed, $I_t(t)|_{cos\Omega t} = 0$ at the maximum absorption. This is not particularly useful for extracting information about the concentration of the absorbent gas.

5.3 MODULATION TECHNIQUES

5.3.2 Frequency modulation

$I_t(t)$ have components proportional to $\cos^2(\Omega t)$.

From the trigonometry, we know that $cos^2(\Omega t) = \frac{1+\cos(2\Omega t)}{2}$, so $cos^2(\Omega t)$-component are proportional to the first harmonic (2Ω).

In other words, if we modulate the current of a laser diode at Ω, $I_t(t)$ will have components at the fundamental and components at the first harmonic.

If we acquire only the components at the first harmonic, going to filter the fundamental ones, the signal be in the form of:

$$I_t(t)\Big|_{cos2\Omega t} = -L\Delta \mathrm{I}\Delta\omega \frac{\partial\alpha}{\partial\omega}\Big|_{\omega=\omega_0} - LI_{\mathrm{DC}}(\Delta\omega)^2 \frac{1}{2}\frac{\partial^2\alpha}{\partial\omega^2}\Big|_{\omega=\omega_0}$$

By scanning the absorption line of the absorbing gas, $I_t(t)|_{cos2\Omega t}$ will have two contributions: one proportional to the first derivative of the lineshape and the other one proportional to the second derivative.

5.3 MODULATION TECHNIQUES

5.3.2 Frequency modulation

This technique is known as **wavelength modulation and 2f detection**: the laser is modulated at a frequency Ω and the signal acquired at the first harmonic 2Ω.

Assuming that the absorption lineshape is Lorentzian one, the second derivative will have the form:

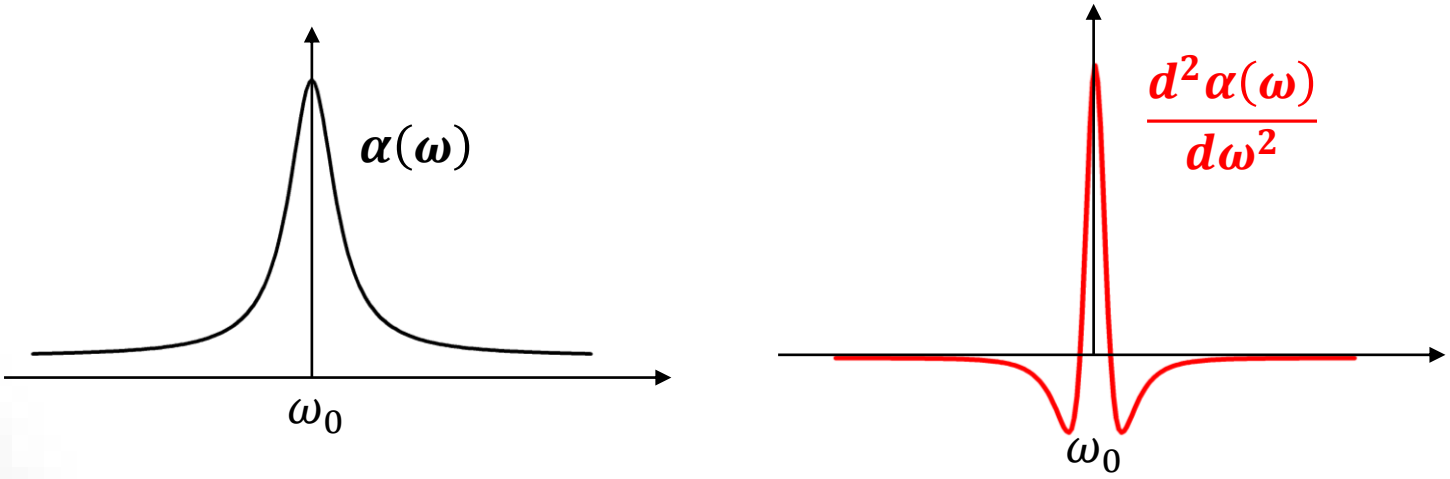

The central peak is at the maximum of the absorption; there are two symmetrical lobes of opposite sign on two sides with respect to the central peak.

5.3 MODULATION TECHNIQUES

5.3.2 Frequency modulation

Adding the contribution due to the first derivative, it is easy to verify that the resulting effect will be to make the two lateral lobes asymmetrical, without altering the intensity of the central peak, since the first derivative before a Lorentzian function is zero at the maximum absorption, and changes sign depending on the side.

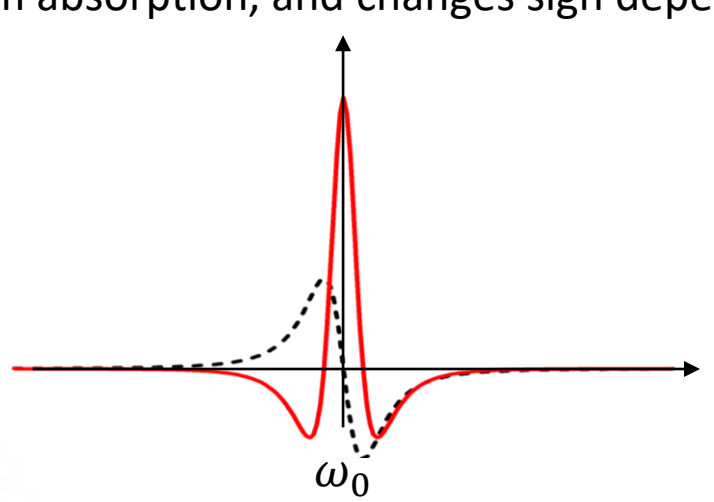

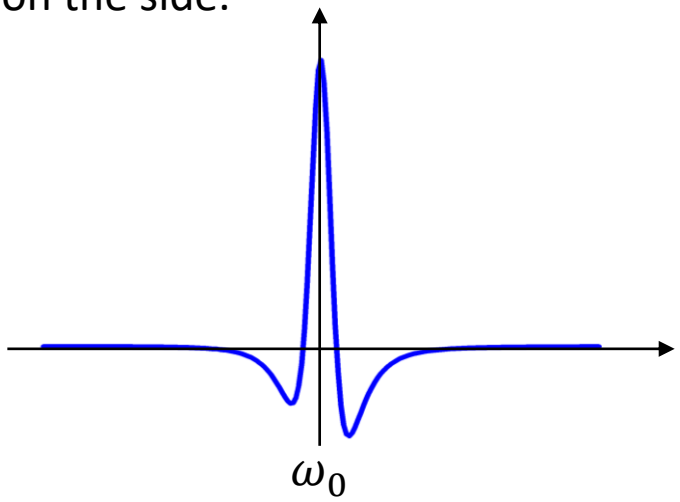

For this reason, the contribution due to the first derivative is known as *Residual Amplitude Modulation (*RAM). In conclusion, working in wavelength modulation and 2f detection alters the shape of the absorption line, but the maximum signal is still at the maximum absorption. The great advantage lies in the fact that the technique is background-free, eliminating all the inconvenient introduced in post-processing to remove the background contribution from the signal.

5.3 MODULATION TECHNIQUES

5.3.3 Lock-in Detection

Working in amplitude or frequency modulation requires that the signal acquired by the photodetector is sent to a spectrum analyzer to extract the desired component (the fundamental or the first harmonic).

Spectrum analyzers are expensive and require complex computational processing, based on the Fourier transform. The same functions of filtering a single component from an analog signal can be performed using a **lock-in amplifier**.

A lock-in amplifier is an instrument used for the analysis of AC signals of low intensity, up to nV or characterized by high background noise, which can sometimes be even higher than the intensity of the signal itself.

The principle of operation is based on the extraction from the input signal, typically noisy, only the component with the desired frequency and phase, going to filter the remaining components, whose contribution of noise is then canceled. The technique is therefore called Phase-Sensitive Detection (PSD) and allows to measure the amplitude of the only desired component.

5.3 MODULATION TECHNIQUES

5.3.3 Lock-in Detection

Figure shows the block diagram of a typical lock-in amplifier.

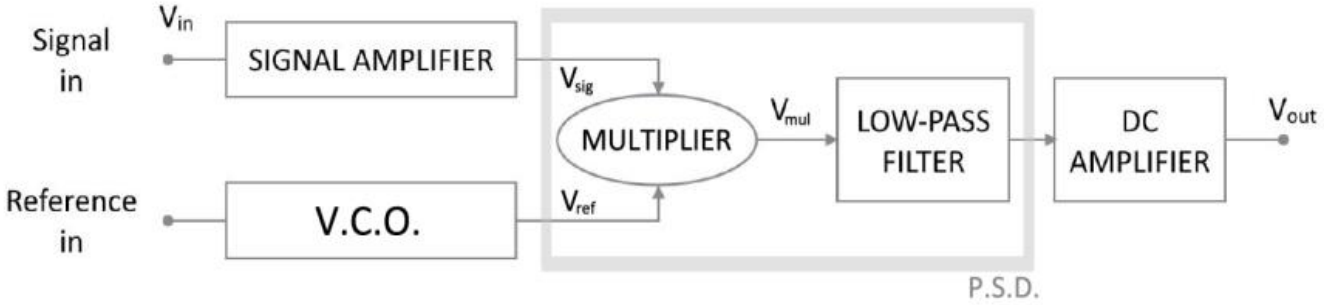

The structure consists of:

- **Voltage Controlled Oscillator (V.C.O.):** Typically, an oscillator, or waveform generator, adjustable in frequency and phase and used to generate the reference signal (in commercial amplifiers it is usually integrated).
- **Phase-Sensitive Detector (P.S.D.):** composed of the multiplier of electrical signals (Multiplier) and the low-pass filter with adjustable threshold;
- **DC amplifier:** DC signal amplifier used to amplify the output signal from the PSD in a controlled way.

5.3 MODULATION TECHNIQUES

5.3.3 Lock-in Detection

To evaluate the principle of operation of the PSD, the heart of the lock-in technique, let us consider the reference signal V_{ref} as a periodic signal that can be represented as a sine wave of frequency Ω_{ref},

$$V_{ref} = A_{ref} cos\left(\Omega_{ref} t + \varphi_{ref}\right)$$

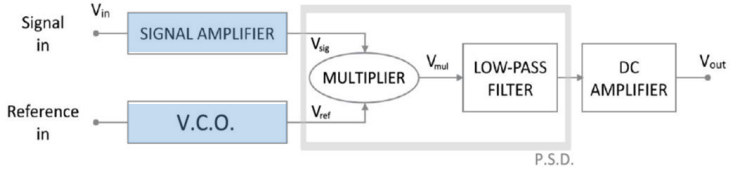

and the signal to be measured V_{sign} as

$$V_{sig} = A_{sig} cos\left(\Omega_{sig} t + \varphi_{sig}\right) + \sum_{\Omega_{noise}} A_{sign} cos(\Omega_{noise} t + \varphi_{noise})$$

which can be expanded in the Fourier series as the superposition of a sinusoidal signal at the frequency Ω_{sig}, to be extracted, with all the other spectral components that are the background noise to be subtracted.

5.3 MODULATION TECHNIQUES

5.3.3 Lock-in Detection

The signals V_{ref} and V_{sig} are then multiplied each other. Then, the signal at the exit of the multiplier we be:

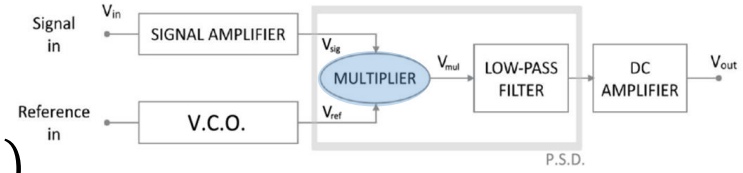

$$V_{ref} \times V_{sig}$$
$$= A_{ref}A_{sig}cos(\Omega_{ref}t + \varphi_{ref})cos(\Omega_{sig}t + \varphi_{sig})$$
$$+ A_{ref}cos(\Omega_{ref}t + \varphi_{ref}) \sum_{\omega_{noise}} A_{noise}cos(\Omega_{noise}t + \varphi_{noise})$$

Using the trigonometric relation $cos\alpha cos\beta = \frac{1}{2}[\cos(\alpha + \beta) + \cos(\alpha - \beta)]$:

$$V_{ref} \times V_{sig}$$
$$= \frac{1}{2}A_{ref}A_{sig}\{\cos[(\Omega_{sig} + \Omega_{ref})t + (\varphi_{sig} + \varphi_{ref})]$$
$$+ \cos[(\Omega_{sig} - \Omega_{ref})t + (\varphi_{sig} - \varphi_{ref})]\}$$
$$+ \frac{1}{2}A_{ref}\left\{\sum_{\omega_{noise}} A_{noise}\left[\cos[(\Omega_{ref} + \Omega_{noise})t + (\varphi_{ref} + \varphi_{noise})]\right.\right.$$
$$\left.\left. + cos[(\Omega_{ref} - \Omega_{noise})t + (\varphi_{ref} - \varphi_{noise})]\right]\right\}$$

5.3 MODULATION TECHNIQUES

5.3.3 Lock-in Detection

The output signal from the multiplier is sent to the low-pass filter, which is set to a cutting frequency that only the continuous component of the signal pass through:

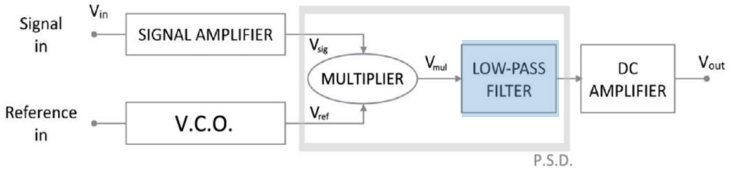

As a result, all the terms are canceled, except for those that the frequencies of the two signals coincide, namely $\Omega_{sig} = \Omega_{ref}$; similarly for the noise contribution, $\Omega_{ref} = \Omega_{noise}$.

$$
\begin{aligned}
&V_{ref} \times V_{sig} \\
&= \frac{1}{2} A_{ref} A_{sig} \{\cos[(\Omega_{sig} + \Omega_{ref})t + (\varphi_{sig} + \varphi_{ref})] \\
&+ \boldsymbol{\cos[(\Omega_{sig} - \Omega_{ref})t + (\varphi_{sig} - \varphi_{ref})]}\} \\
&+ \frac{1}{2} A_{ref} \left\{ \sum_{\omega_{noise}} A_{noise} \left[\cos[(\Omega_{ref} + \Omega_{noise})t + (\varphi_{ref} + \varphi_{noise})]\right.\right. \\
&\left.\left. + \boldsymbol{\cos[(\Omega_{ref} - \Omega_{noise})t + (\varphi_{ref} - \varphi_{noise})]}\right]\right\}
\end{aligned}
$$

5.3 MODULATION TECHNIQUES

5.3.3 Lock-in Detection

The final result at the output of the low-pass filter will be:

$$V_{PSD} = \frac{1}{2} A_{ref} A_{sig} \cos(\varphi_{sig} - \varphi_{ref}) + \frac{1}{2} A_{ref} A_{noise} \cos(\varphi_{ref} - \varphi_{noise})$$

As a result, the system is sensitive to the phase difference between the signal to be measured and the reference signal. In addition, the generated signal V_{PSD} is affected only by the noise component at the reference frequency.

By knowing the amplitude of the reference signal (A_{ref}) it is possible to retrieve the A_{sig} measurement; in addition, it is possible to determine the phase of the signal with respect to the reference.

Thus, the output of the lock-in amplifier will be:

$$V_{out} \propto A_{sig} \cos\varphi$$

where $\varphi = \varphi_{sig} - \varphi_{ref}$

5.3 MODULATION TECHNIQUES

5.3.3 Lock-in Detection

This dependence on the phase difference between the two signals can be eliminated by using a dual-phase lock-in amplifier.

The figure shows the block diagram of a dual-phase lock-in amplifier.

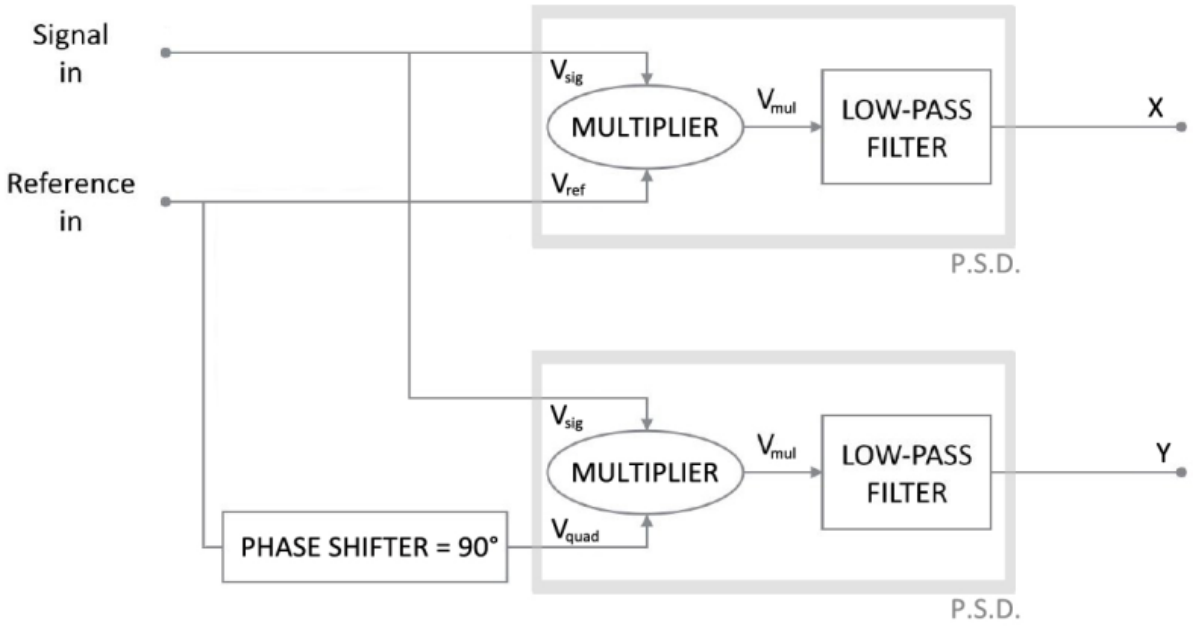

A dual-phase lock-in has an additional PSD that measures the quadrature component of the signal , i.e. the signal component at 90° compared to that measured by the first channel.

5.3 MODULATION TECHNIQUES

5.3.3 Lock-in Detection

In this way, simultaneous measurement of the amplitude and phase of the signal is possible.

Assuming then that the quadrature component has the form:

$$V_{quad} = A_{quad} cos\left(\Omega_{ref} t + \varphi_{ref} + \frac{\pi}{2}\right)$$

Repeating the same steps made previously, the output signal from the second PSD will be:

$$V_{quad} \times V_{sig}$$
$$= \frac{1}{2} A_{sig} A_{quad} \left\{\cos\left[\left(\varphi_{sig} - \varphi_{ref} + \frac{\pi}{2}\right)\right]\right\}$$
$$+ \frac{1}{2} A_{quad} A_{noise} \left\{\cos\left(\varphi_{ref} - \varphi_{noise} + \frac{\pi}{2}\right)\right\}$$
$$= \frac{1}{2} A_{sig} A_{quad} \{\text{sen}(\varphi_{sig} - \varphi_{ref})\} + \frac{1}{2} A_{quad} A_{noise} \{\text{sen}(\varphi_{ref} - \varphi_{noise})\}$$

5.3 MODULATION TECHNIQUES

5.3.3 Lock-in Detection

At the output of the low-pass filter the overall signal will be:

$$V_{PSD2} = \frac{1}{2} A_{quad} A_{sig} \operatorname{sen}(\varphi_{sig} - \varphi_{ref}) + \frac{1}{2} A_{quad} A_{noise} \operatorname{sen}(\varphi_{ref} - \varphi_{noise})$$

Finally, at the output of the dual-phase lock-in amplifier, neglecting the contribution of noise, two signals are obtained:

$$X \propto A_{sig} \cos\varphi$$

$$Y \propto A_{sig} \operatorname{sen}\varphi$$

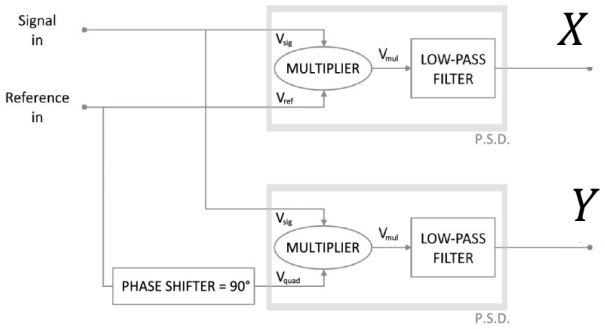

the first is called a in-pahse signal, since it is maximized when the phase difference φ is zero, while the second represents the quadrature component.

The, the amplitude R of the signal and the phase φ can be easily calculated by using the relations:

$$R = \sqrt{X^2 + Y^2} \propto A_{sig} \qquad \varphi = arctg\left(\frac{Y}{X}\right)$$

R is proportional to the amplitude of the component Ω_{sig} of the acquired signal.

5.4 SPECTROSCOPY WITH MULTIPASS CELLS

The amplitude or frequency modulation techniques involve the modulation of the laser source and the demodulation of the photodetector signal. These approaches allow an increase of the detection sensitivity as a consequence of the reduction of the noise of the photodetector itself.

Modulation techniques are therefore not related to the gas-radiation interaction.

That is why modulation techniques can be coupled with other spectroscopy techniques that are focused on the increase the optical pathway.

$$N_i \geq \frac{\Delta I}{I_0 L \sigma_{ik}(\omega)}$$

The Lambert-Beer law clearly expresses the dependence of the intensity transmitted by the optical path.
Allowing radiation to travel longer distances allows the possibility to detect small concentrations of absorbing molecules and thus to increase the ultimate sensitivity of detection.
Obviously, it is unthinkable to build gas cells with lengths of several meters.

The correct approach is **to increase the total optical path by forcing the radiation to remain confined within small and constant volume**.

5.4 SPECTROSCOPY WITH MULTIPASS CELLS

This can be accomplished in two ways:

- Through multiple reflections between two large convex mirrors positioned opposite each other, so that with each reflection on a mirror the beam travels a different optical path to reach the other mirror. Cells of this type are called **multipass cells**.

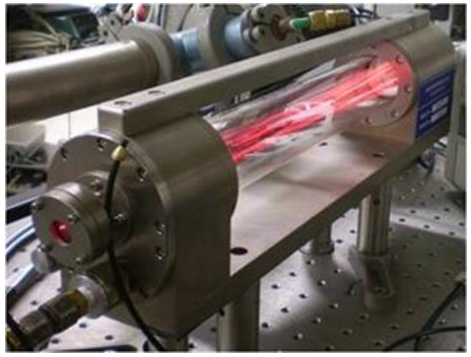

- By means of **optical cavities**. The laser beam introduced into the cavity always travels the same optical path through multiple reflections on highly reflective mirrors, until a standing wave is formed inside it.

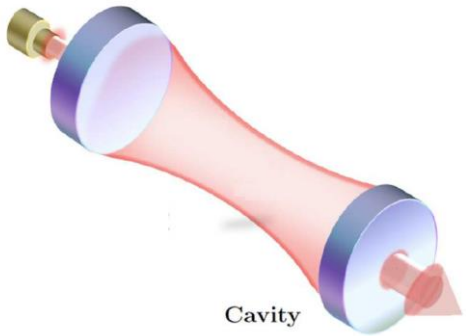

The most used multistep cells are of two types.

- **White Multipass Cell**
- **Herriott Multipass Cell**

5.4 SPECTROSCOPY WITH MULTIPASS CELLS

5.4.1 White Multipass Cell

White Multipass Cell consists of three spherical, concave mirrors with the same radius of curvature.

The principle of operation of such a multi-pass system for a beam of light is easily obtained through the use of geometric optics.

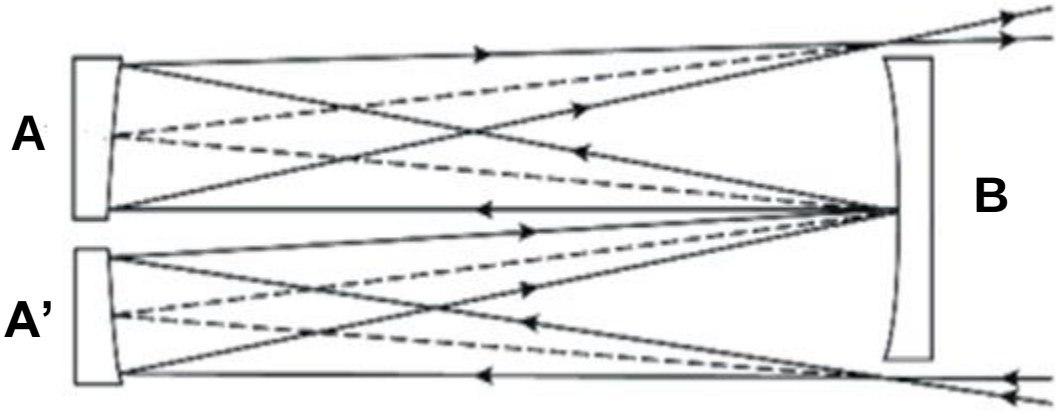

Two mirrors A and A' are next to each other and form one end of the absorption cell; mirror B is placed at the other end of the cell. The centers of curvature of A and A' lie on the surface of B, and the center of curvature of B is between mirror A and A'.

5.4 SPECTROSCOPY WITH MULTIPASS CELLS

5.4.1 White Multipass Cell

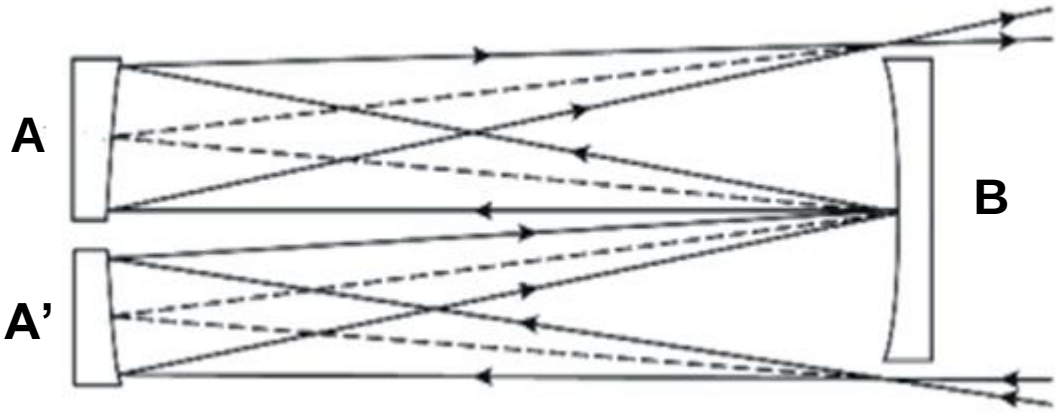

This arrangement creates a system of conjugated points on the reflective surfaces of the mirrors, according to which all the light that leaves at any point A is focused from B to the corresponding point on A', and all the light that leaves A' from this point is focused backwards on the original point of A.

With these rules, let's see how you can use a multipass cell to achieve long optical paths.

5.4 SPECTROSCOPY WITH MULTIPASS CELLS

5.4.1 White Multipass Cell

The positions of subsequent images can all be identified by the rule that the points of the object and the image near the center of curvature of a spherical mirror are always on a straight line whose midpoint falls on the center of curvature.

Thus, mirror A forms an image 1 of the input slit on the surface of B distant from the center of curvature of A, as far as the input slit is distant from the center of curvature of A.

Then, since the center of curvature of B is between A and A', B forms an image of A in A'.

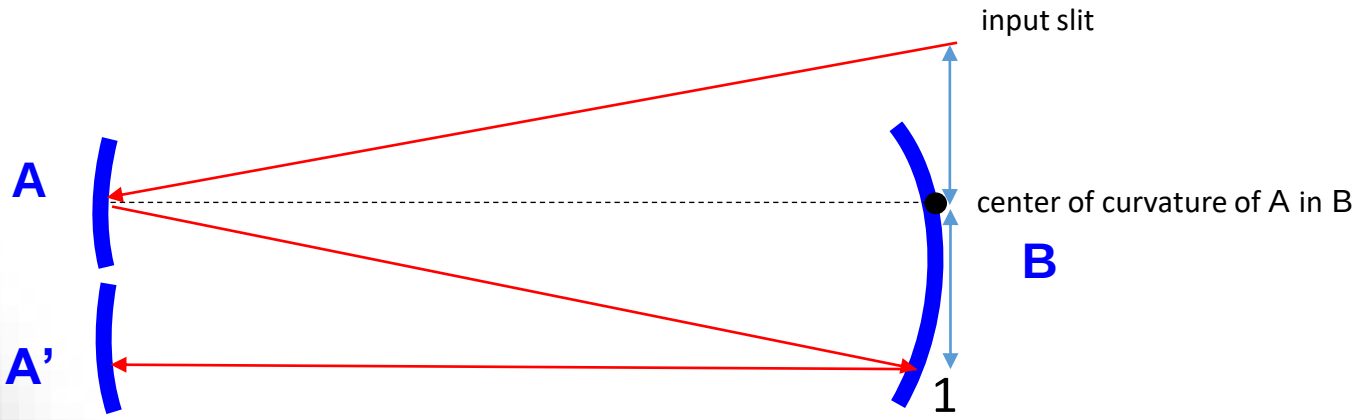

5.4 SPECTROSCOPY WITH MULTIPASS CELLS

5.4.1 White Multipass Cell

Then, the mirror A' forms in B a second image 2 of the input slit, whose position is determined by the distance between 1 and the radius of curvature of A' .

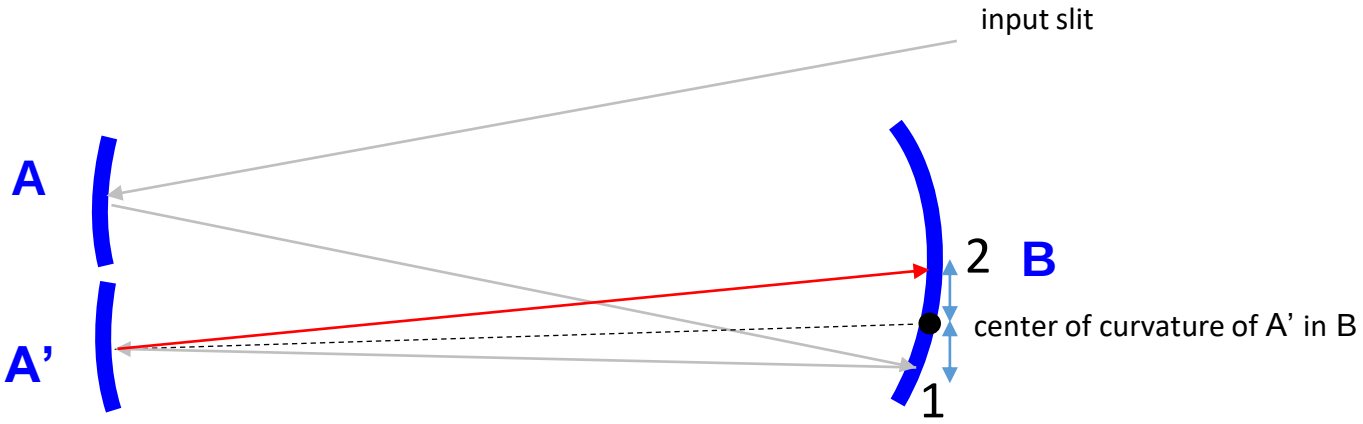

Mirror B will form an image of A' in A and then a will form an image 3 of the slit in B

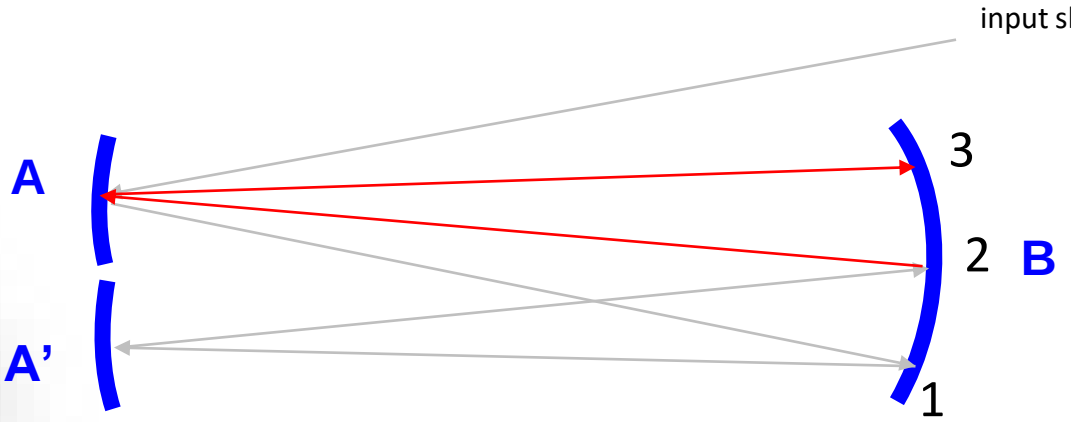

5.4 SPECTROSCOPY WITH MULTIPASS CELLS

5.4.1 White Multipass Cell

Image 3 will be sent back to A' to get out the pair of mirrors.

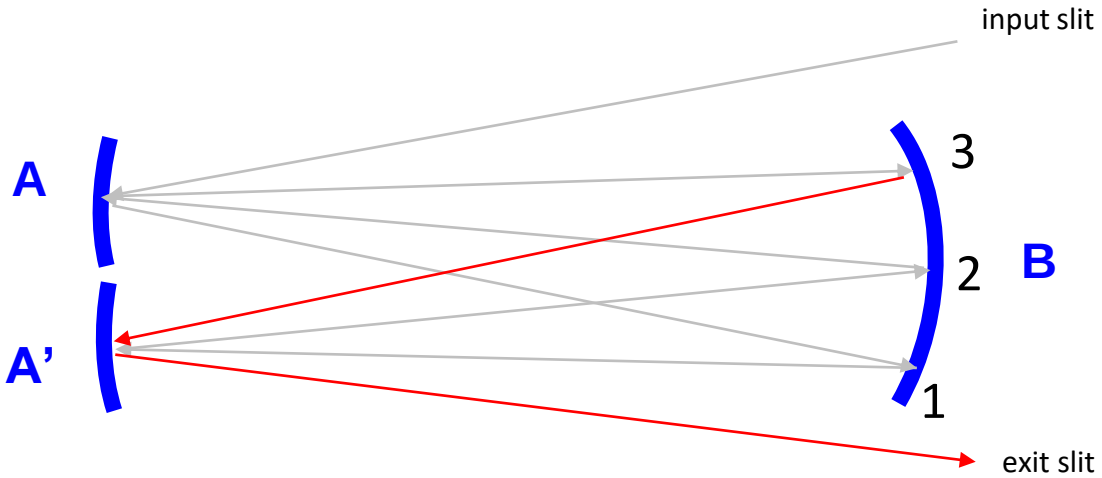

The resulting optical path is the one determined in Figure.

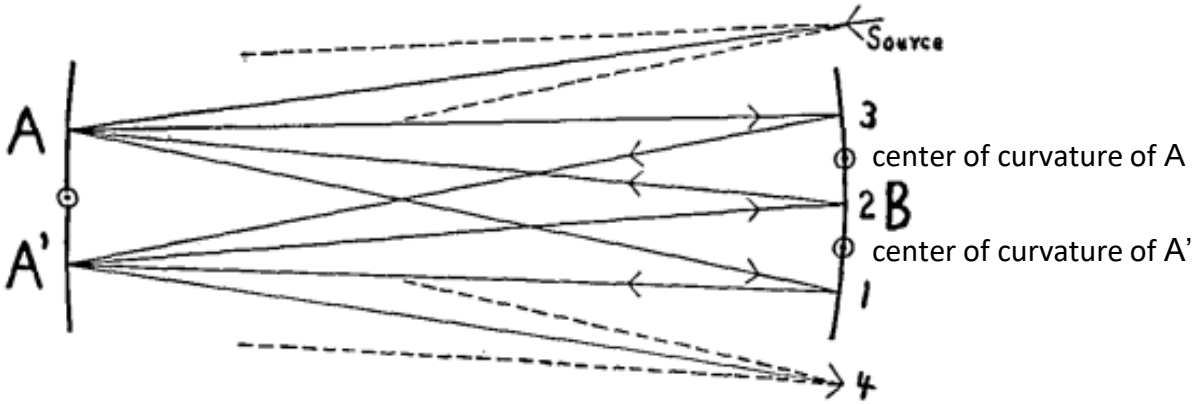

5.4 SPECTROSCOPY WITH MULTIPASS CELLS

5.4.1 White Multipass Cell

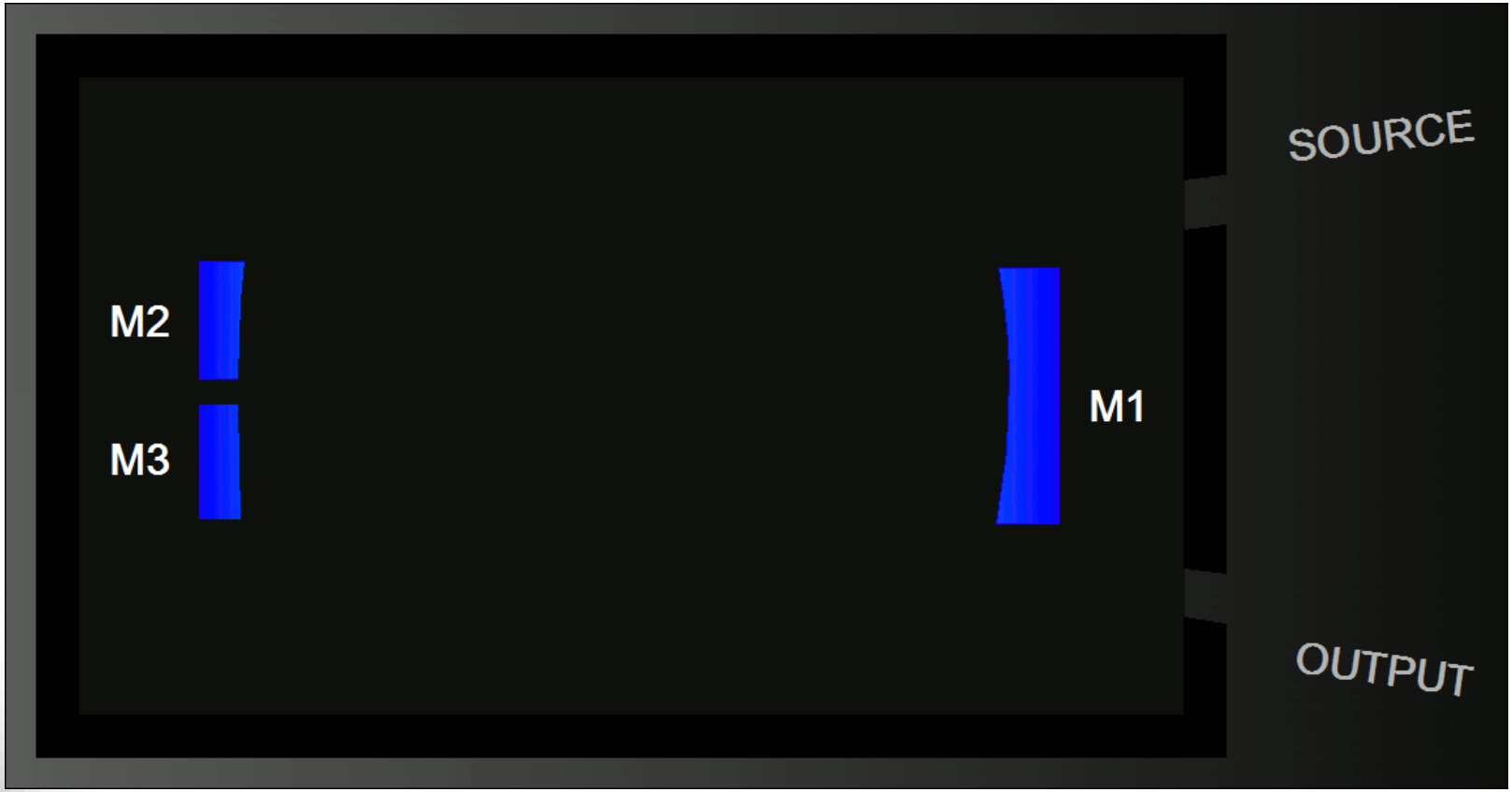

5.4 SPECTROSCOPY WITH MULTIPASS CELLS

5.4.1 White Multipass Cell

- Light is injected into the multi-pass cell out of the optical axis of the system (off-axis).
- It is easy to verify that a White multi-pass cell allows the use of beams with large numerical aperture, if you do not impact the edges of the mirror.
- The optical alignment of the system is not critical: it can be done manually, without using micrometric movements.
- The most critical point is the separation of the centers of curvature of mirrors A and A' on B: if A and A' are adjusted symmetrically with respect to B and its center of curvature, each image on B is separated from adjacent ones exactly by the distance between the centers of curvature of A and A'.

The ratio of the length of B to this separation determines honw many times light passes through the cell. These can be 4 if you form a single image on B, 8 in the case of three images, 12 in the case of 5 images, 14 for 7 images and so on. Intermediate numbers are not possible.

5.4 SPECTROSCOPY WITH MULTIPASS CELLS

5.4.2 Herriott Multipass Cell

A Herriott cell consists of a spherical mirrors (M1 and M2) positioned on opposite sides, on the same optical axis.

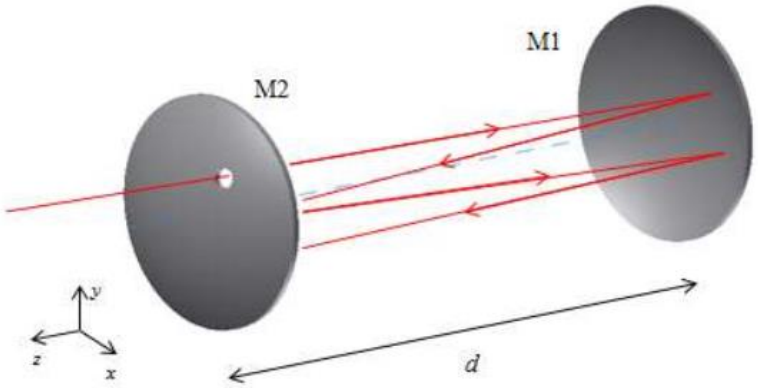

The laser beam enters the cell through an opening created on one of the two mirrors and comes out either from the same opening, or from another opening created on the mirror M1.

When the laser beam is introduced inside the cell in a direction not parallel to the optical axis, the reflection spots on the mirrors form a pattern that are arranged in such a way as to form an ellipse.

5.4 SPECTROSCOPY WITH MULTIPASS CELLS

5.4.2 Herriott Multipass Cell

The conditions for a good alignment of a multi-pass cell must are mainly two:

1) Beams must not overlap each other, to avoid interference effects;

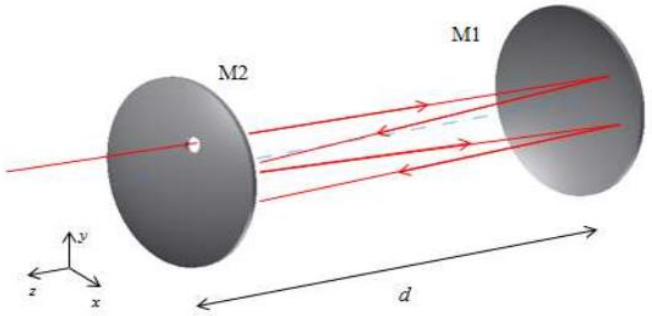

2) After a series of n reflections the system must return to its initial conditions. In addition, the system must be closed and not diverge, to avoid the escape of the radiation from the system.

A multipass cell can be modelled by using geometric optics, in paraxial approximation.

For the mathematical description of the system, it is possible to use the ABCD matrices formalism.

5.4 SPECTROSCOPY WITH MULTIPASS CELLS

5.4.2 Herriott Multipass Cell

The ABCD matrix formalism of Gaussian optics involves the introduction of the complex radius of curvature $q(z)$, where z is the direction of propagation of the wave, which contains information about both the real radius of curvature $R(z)$ and the beam diameter $w(z)$,by the relation:

$$\frac{1}{q(z)} = \frac{1}{R(z)} - i\frac{\lambda}{\pi w^2(z)}$$

where λ is the wavelength.

The formalism of ABCD matrices allows to calculate how the radius of complex curvature evolves as the wave propagates.

Each interaction of the beam with an optical element (mirror, lens...) or a propagation can be associated with a transformation matrix $\begin{pmatrix} A & B \\ C & D \end{pmatrix}$ that allows to estimate the evolution of $q(z)$ in space.

Knowing q_1 at a certain point in space, q_2 will be expressed as:

$$q_2 = \frac{Aq_1 + B}{Cq_1 + D}$$

5.4 SPECTROSCOPY WITH MULTIPASS CELLS

5.4.2 Herriott Multipass Cell

If the wave propagates for a path d, the transformation matrix for the complex radius of curvature will be:

$$\begin{pmatrix} A & B \\ C & D \end{pmatrix} = \begin{pmatrix} 1 & d \\ 0 & 1 \end{pmatrix}$$

If the wave experiences a reflection to a convex mirror with a radius of curvature R:

$$\begin{pmatrix} A & B \\ C & D \end{pmatrix} = \begin{pmatrix} 1 & 0 \\ -\frac{2}{R} & 1 \end{pmatrix}$$

If the wave passes through a converging lens of focal length f:

$$\begin{pmatrix} A & B \\ C & D \end{pmatrix} = \begin{pmatrix} 1 & 0 \\ -\frac{1}{f} & 1 \end{pmatrix}$$

If the wave passes through several situations in succession, the total transformation matrix will be the row-by-column multiplication of the individual transformation matrices.

5.4 SPECTROSCOPY WITH MULTIPASS CELLS

5.4.2 Herriott Multipass Cell

The situation inside the cell can be split into two distinct steps: a free propagation in the space that separates the two mirrors and a reflection on the spherical mirror.

Considering a cavity in which the two mirrors are at a distance L and have a radius of curvature R, the ABCD matrix of the system, in paraxial approximation, will be:

$$\begin{pmatrix} A & B \\ C & D \end{pmatrix} = \begin{pmatrix} 1 & 0 \\ -\frac{2}{R} & 1 \end{pmatrix} \cdot \begin{pmatrix} 1 & L \\ 0 & 1 \end{pmatrix}$$

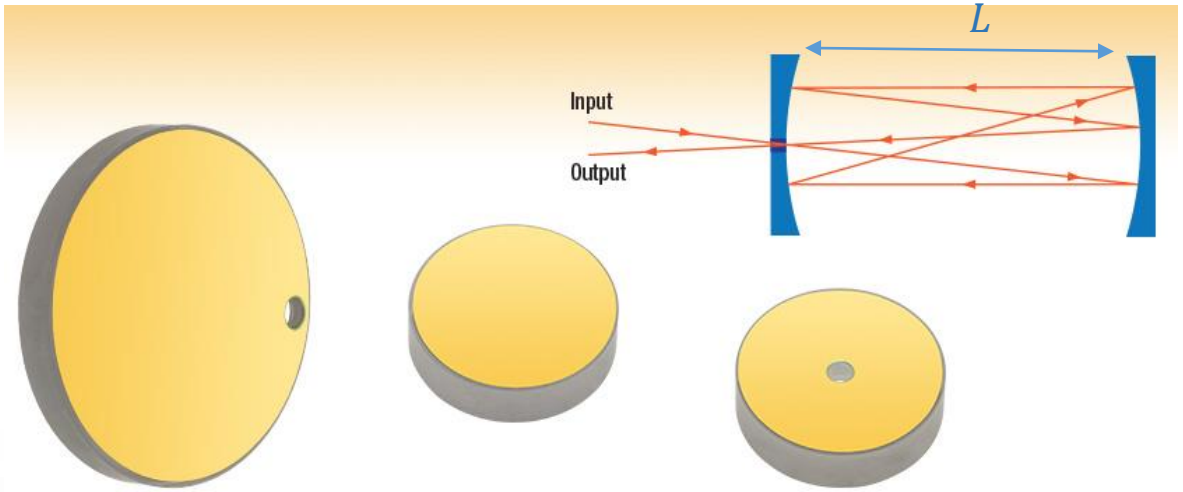

5.4 SPECTROSCOPY WITH MULTIPASS CELLS

5.4.2 Herriott Multipass Cell

Once the XY plane has been identified as the plane orthogonal to the optical axis of the cell, x_n and y_n are the positions on the XY plane of the beam spot at the point where it is reflected by the mirror, at the n-th passage.

x'_n and y'_n indicate the angles of reflection.

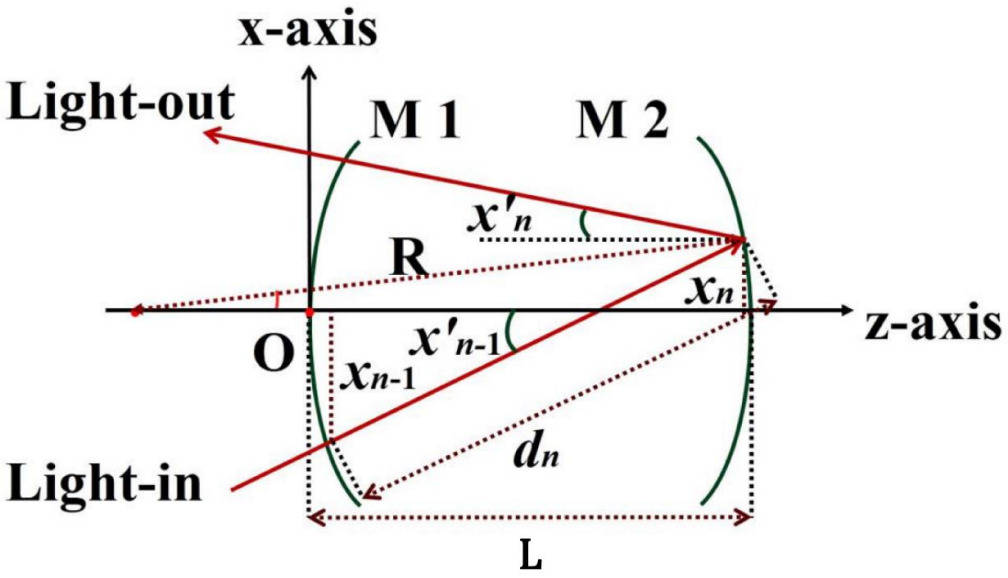

The optical pathlength in the cell, at the n-th passage will be indicated as d_n.

In paraxial approximation, $L \approx d_n$.

5.4 SPECTROSCOPY WITH MULTIPASS CELLS

5.4.2 Herriott Multipass Cell

To calculate the positions in which the rays inside the cell are reflected, and therefore the relative pattern, it is necessary to solve the systems:

$$\begin{pmatrix} x_{n+1} \\ x_{n+1}' \end{pmatrix} = \begin{pmatrix} A & B \\ C & D \end{pmatrix} \begin{pmatrix} x_n \\ x_n' \end{pmatrix}$$
$$\begin{pmatrix} y_{n+1} \\ y_{n+1}' \end{pmatrix} = \begin{pmatrix} A & B \\ C & D \end{pmatrix} \begin{pmatrix} y_n \\ y_n' \end{pmatrix}$$

$$\begin{pmatrix} A & B \\ C & D \end{pmatrix} = \begin{pmatrix} 1 & 0 \\ -\frac{2}{R} & 1 \end{pmatrix} \cdot \begin{pmatrix} 1 & L \\ 0 & 1 \end{pmatrix}$$

Substituting the ABCD matrix written above is:

$$\begin{cases} x_{n+1} = x_n + L\, x_n' \\ x_{n+1}' = {}^{-2}/_{R}\; x_n + ({}^{-2D}/_{R} + 1)\, x_n' \end{cases}$$

Similarly, it will be for y_{n+1} and y_{n+1}'

The approach to the problem can be either analytical (going to solve the problem considering that the ABCD matrix is multiplied m times by itself), or iterative.

5.4 SPECTROSCOPY WITH MULTIPASS CELLS

5.4.2 Herriott Multipass Cell

In the analytical approach, it is necessary to solve the matrix system:

$$\begin{pmatrix} x_{n+1} \\ x'_{n+1} \end{pmatrix} = \begin{pmatrix} A & B \\ C & D \end{pmatrix}^n \begin{pmatrix} x_n \\ x'_n \end{pmatrix}$$

After n reflections, the coordinates x_{n+1} and x'_{n+1} will be:

$$\begin{cases} x_{n+1} = Ax_n + Bx'_n \\ x'_{n+1} = Cx_n + Dx'_n \end{cases}$$

We determine the equation that governs the dynamics for x_{n+1} by removing the explicit dependence on the angle.

From the first equation we get:

$$x'_n = \frac{x_{n+1} - Ax_n}{B}$$

We replace $n \rightarrow n+1$:

$$x'_{n+1} = \frac{x_{n+2} - Ax_{n+1}}{B}$$

5.4 SPECTROSCOPY WITH MULTIPASS CELLS

5.4.2 Herriott Multipass Cell

Replace: $x'_n = \frac{x_{n+1} - Ax_n}{B}$ $x'_{n+1} = \frac{x_{n+2} - Ax_{n+1}}{B}$ in: $x'_{n+1} = Cx_n + Dx'_n$

and you get:

$$x_{n+2} = (A + D)x_{n+1} + (\mathrm{BC} - \mathrm{AD})x_n$$

Introduce: $b = \frac{A + D}{2}$

$$\boldsymbol{M} = \begin{pmatrix} A & B \\ C & D \end{pmatrix}$$

and we note that $AD - BC$ is the determinant of the ABCD matrix:

Therefore:

$$x_{n+2} = 2bx_{n+1} - F^2 x_n$$

with:

$$F^2 = \det[\boldsymbol{M}]$$

5.4 SPECTROSCOPY WITH MULTIPASS CELLS

5.4.2 Herriott Multipass Cell

$$x_{n+2} = 2bx_{n+1} - F^2 x_n$$

A periodic solution of the equation must now be determined.

We show that the geometric solution:

$$x_n = x_0 h^n$$

with constant h meets the requirement of a periodic solution.

Imposing it as a solution:

$$x_0 h^{n+2} = 2bx_0 h^{n+1} - F^2 x_0 h^n$$

we get the condition for h:

$$h^2 - 2bh + F^2 = 0$$

This can be solved in the variable h:

$$h = b \pm i\sqrt{F^2 - b^2}$$

5.4 SPECTROSCOPY WITH MULTIPASS CELLS

5.4.2 Herriott Multipass Cell

$$h = b \pm i\sqrt{F^2 - b^2}$$

This can be rewritten in a more elegant way by introducing the variable:

$$\varphi = cos^{-1}\left(\frac{b}{F}\right)$$

so that:

$$b = Fcos\varphi$$

$$\sqrt{F^2 - b^2} = \sqrt{F^2 - F^2cos^2\varphi} = Fsen\varphi$$

Substituting it in the roots:

$$h = F(cos\varphi \pm isen\varphi)$$

giving as solution:

$$x_n = x_0 F^n e^{\pm im\varphi}$$

$x_n = x_0 h^n$

5.4 SPECTROSCOPY WITH MULTIPASS CELLS

5.4.2 Herriott Multipass Cell

The condition to be imposed is:

$$\varphi = cos^{-1}\left(\frac{b}{F}\right)$$

$$\frac{b}{F} \leq 1$$

Since $F^2 = \det[\boldsymbol{M}]$:

$$\det[\boldsymbol{M}] = det\begin{bmatrix} A & B \\ C & D \end{bmatrix} = det\left[\begin{pmatrix} 1 & 0 \\ -\frac{2}{R} & 1 \end{pmatrix} \cdot \begin{pmatrix} 1 & L \\ 0 & 1 \end{pmatrix}\right] = det\begin{bmatrix} 1 & L \\ -\frac{2}{R} & -\frac{2}{R}L + 1 \end{bmatrix}$$

$$= -\frac{2}{R}L + 1 - -\frac{2}{R}L = 1$$

So the condition to be imposed is:

$$b = \frac{A + D}{2}$$

$$b \leq 1$$

leading to:

$$\frac{1}{2}|A + D| \leq 1 \rightarrow \left|1 - {}^{L}/_{R}\right| \leq 1 \quad \Rightarrow \quad L \leq 2R$$

5.4 SPECTROSCOPY WITH MULTIPASS CELLS

5.4.2 Herriott Multipass Cell

So, if the positions of the spots on the mirror are repeated after m cycles, the total number of reflections will be equal to $2m$ before the beam leaves the multipass cell. Thus, the total optical path will be equal to $2mL$.

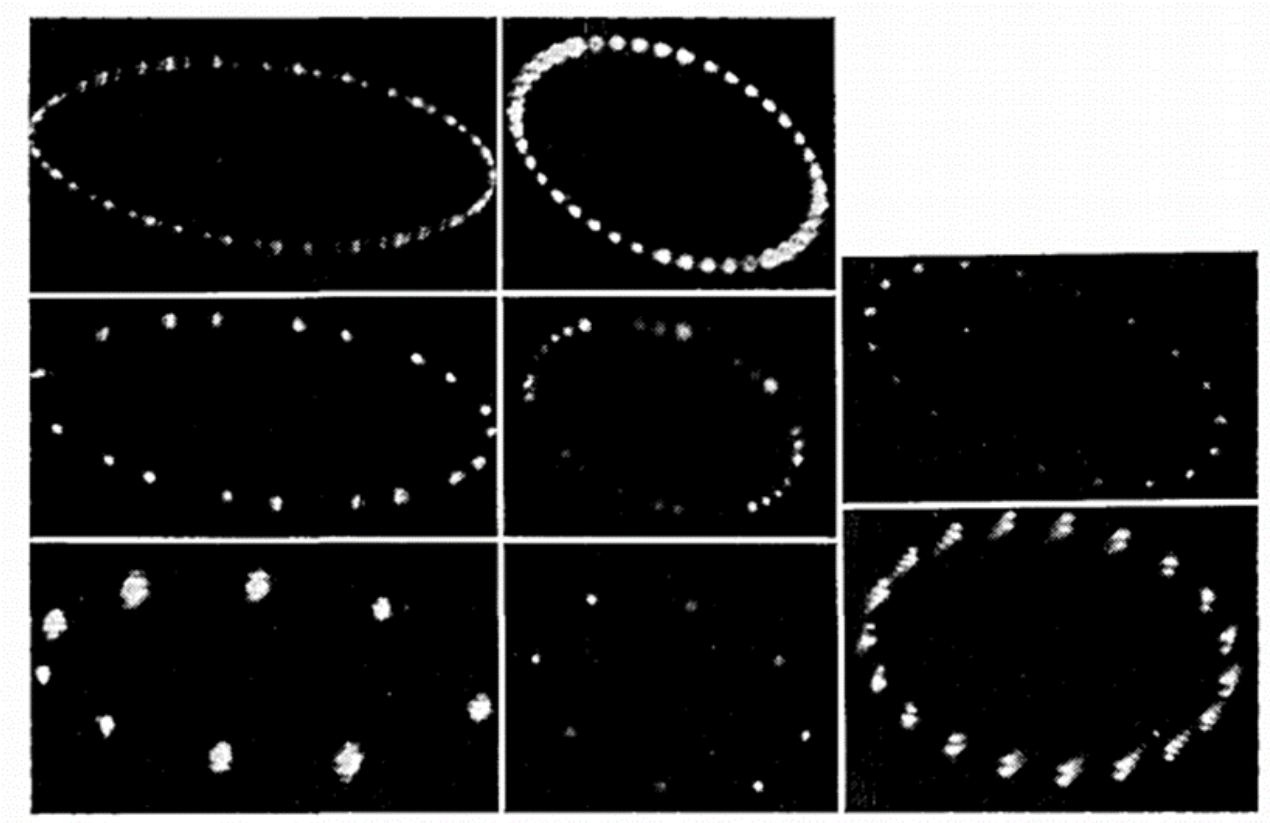

5.4 SPECTROSCOPY WITH MULTIPASS CELLS

5.4.2 Herriott Multipass Cell

Advantages of Herriott cell:

- The total optical path depends only on the distance between the two mirrors
- The cell structure is simple, consisting of two mirrors aligned on the same optical axis
- Opto-mechanical stability is very good

Disadvantages:

- It does not accept beams with large numerical apertures
- A large part of the mirror surface is not used
- Large mirrors are needed to make long optical paths.

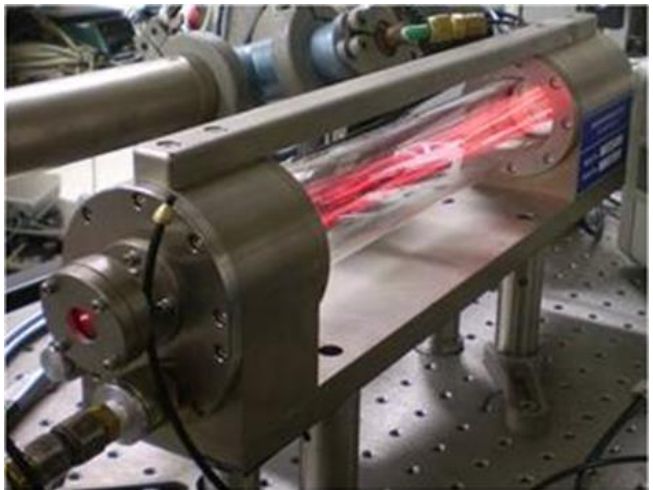

5.5 SPECTROSCOPY WITH RESONANT CAVITIES

5.5.1 Longitudinal modes of cavities

A different way to increase the optical path is to place the gas sample inside a resonant optical cavity. The light transmitted by the cavity will be related to the leaks in the cavity. Losses in cavities will be due to optical absorption that can be estimated by analyzing the transmitted light.

According to classical physics, the standing waves created inside the cavity can be seen as an overlap of waves traveling back and forth as a result of reflection to the mirrors, so the final optical path is a multiple of the physical length of the cavity. The resulting effect is an increase in optical power inside the cavity due to the constructive overlap of waves propagating back and forth.

According to quantum mechanics, a photon travels q times back and forth between mirrors before leaving the cavity. Thus, the single photon has a q times higher probability of being absorbed by the gas sample.

Consider the simple case of a linear cavity consisting of two mirrors. The amount of light reflected and transmitted by the cavity depends mainly on the frequency of the incident beam and the reflectivity and transmittivity of the two mirrors.

5.5 SPECTROSCOPY WITH RESONANT CAVITIES

5.5.1 Longitudinal modes of cavities

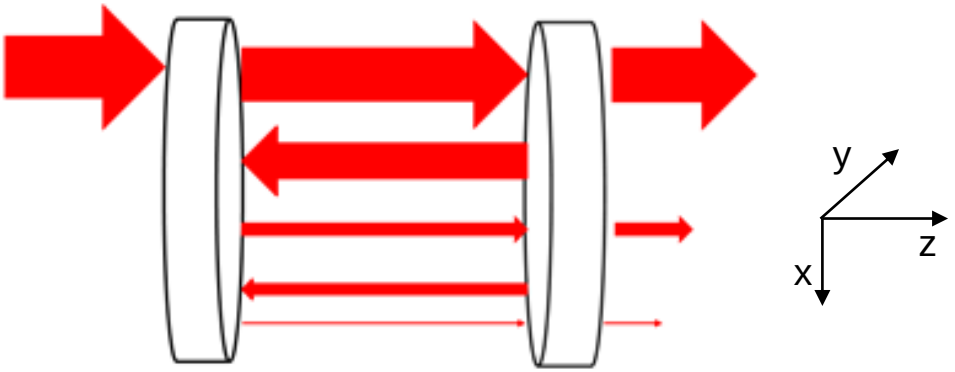

A cavity is an optical resonator in which the electromagnetic field inside the cavity is excited (and therefore increases in amplitude) by incident light at certain frequencies, called resonance frequencies of the cavity.

Let us consider only the cavity resonances associated with the TEM_{nm} cavity modes, so-called longitudinal modes because the wave vector of propagation of the wave remains parallel to the optical axis of the cavity (z axis) during reflections, with electric and magnetic field aligned in the transverse plane to the direction of propagation.

5.5 SPECTROSCOPY WITH RESONANT CAVITIES

5.5.1 Longitudinal modes of cavities

For TEM_{nm} modes, the distribution of the electric field can be described as the product of two Hermite polynomials of order n and m (non-negative integers, corresponding to the x and y directions, respectively) and two Gaussian functions. It follows that the intensity distribution of these modes has n nodes in the x direction and m nodes in the y direction.

$$E_{nm}(x,y,z) \propto H_n(x)H_m(y)e^{-\frac{x^2}{w^2(z)}}e^{-\frac{y^2}{w^2(z)}}$$

where $H_n(x)$ and $H_m(y)$ are the Hermite polynomials and $w(z)$ is the waist of the beam within the cavity.

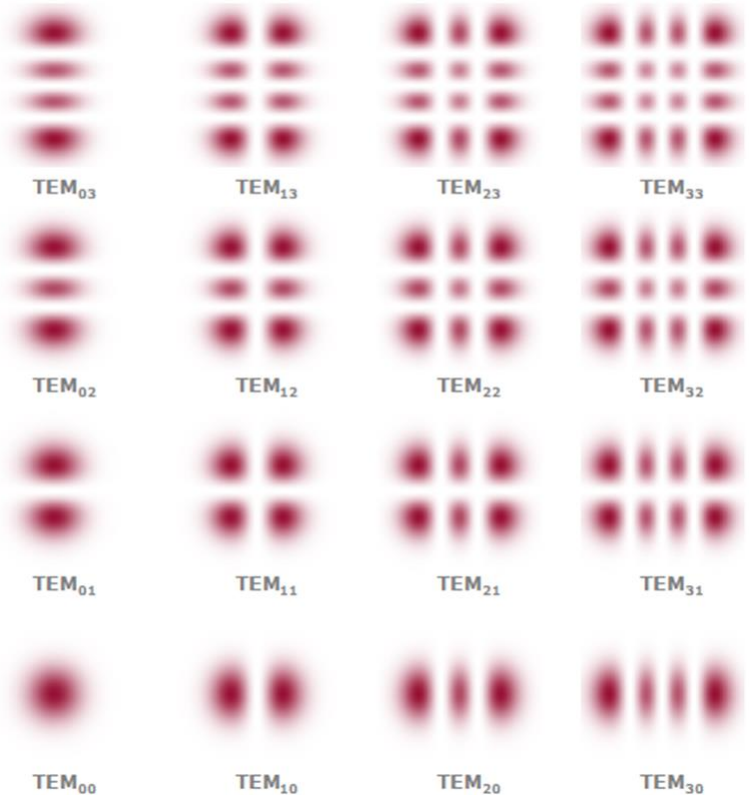

5.5 SPECTROSCOPY WITH RESONANT CAVITIES

5.5.1 Longitudinal modes of cavities

The mode $n = m = 0$ is known as the fundamental mode and the distribution of the intra-cavity intensity resembles a Gaussian distribution. The other modes are called higher-order modes. For simplicity, we will consider on only the TEM_{00} inside the cavity.

As for cavity frequency selectivity, this can be obtained by considering the cavity as a Fabry-Perot resonator: the waves that can propagate inside the cavity are those that have minimal losses at reflection on the mirrors, namely all the waves whose wavelength satisfies the condition:

$$\lambda_n = \frac{2n_r L}{n}$$

where $2L$ is the length of a round trip and n_r is the refractive index of the cavity medium.

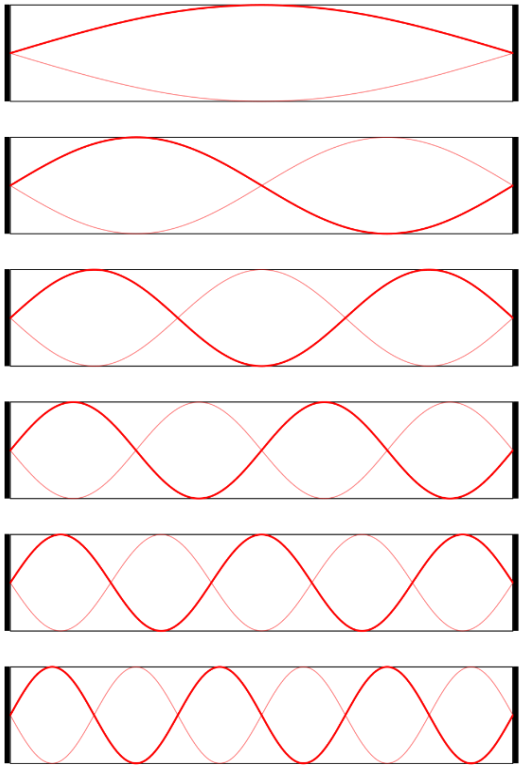

5.5 SPECTROSCOPY WITH RESONANT CAVITIES

5.5.1 Longitudinal modes of cavities

In the frequency domain:

$$\upsilon_n = \frac{nc}{2n_r L}$$

$$\lambda_n = \frac{2n_r L}{n}$$

where c is the speed of light.

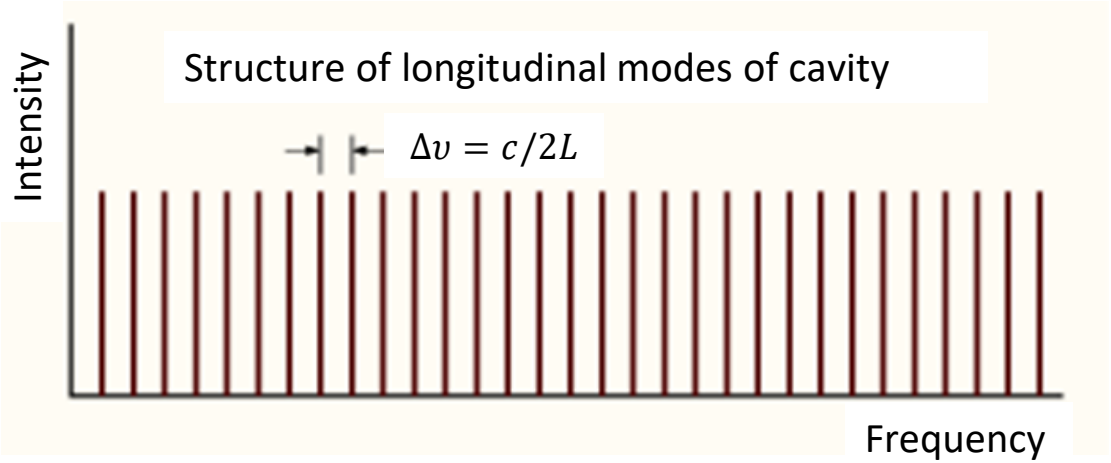

The spectral distance between two consecutive modes (n and $n+1$) is known as Free Spectral Range (FSR) of the cavity:

$$FSR = \frac{c}{2n_r L}$$

5.5 SPECTROSCOPY WITH RESONANT CAVITIES

5.5.2 Finesse and spectral bandwidth

Let's determine the spectral characteristics of the cavity. Suppose a monochromatic wave with Gaussian profile along the transverse directions x and y, incident along the optical axis z:

$$E_{in}(x,y,z,t) = E_0(x,y)e^{i(\omega t - kz)}$$

Let's suppose the two mirrors are identical, so they have the same reflectivity R and the same transmittivity T. The beam is transmitted by the first mirror and when it reaches the second mirror, the resulting wave will be:

$$E_0(x,y)Te^{i(\omega t - kz)}e^{-i\omega\frac{L}{c}}$$

5.5 SPECTROSCOPY WITH RESONANT CAVITIES

5.5.2 Finesse and spectral bandwidth

The wave is reflected by the second mirror, retraces the cavity to be reflected by the first mirror, retraces the cavity and then reaches the second mirror again. This is the first round-trip and the field will be the sum between:

$$E_0(x,y)Te^{i(\omega t-kz)}e^{-i\omega\frac{L}{c}}\left(1+R^2e^{-i\omega 2\frac{L}{c}}\right)$$

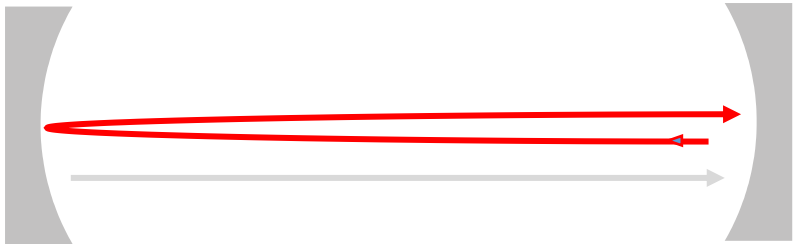

Then, after p round-trip, the field inside the cavity will be:

$$E_0(x,y)Te^{i(\omega t-kz)}e^{-i\omega\frac{L}{c}}\sum_{p}\left(R^2e^{-i\omega 2\frac{L}{c}}\right)^p$$

With a high number of round-trips, namely $p\to\infty$, the intra-cavity field becomes:

$$E_0(x,y)Te^{i(\omega t-kz)}e^{-i\omega\frac{L}{c}}\sum_{p=0}^{\infty}\left(R^2e^{-i\omega 2\frac{L}{c}}\right)^p$$

5.5 SPECTROSCOPY WITH RESONANT CAVITIES

5.5.2 Finesse and spectral bandwidth

If the field is transmitted by the second mirror after an infinite number of round trips:

$$E_{out} = E_0(x,y)T^2 e^{i(\omega t - kz)} e^{-i\omega\frac{L}{c}} \sum_{p=0}^{\infty} \left(R^2 e^{-i\omega 2\frac{L}{c}}\right)^p$$

It is worth noticing that the series is convergent because $|R| < 1$. For for $p \to \infty$:

$$\sum_{p=0}^{\infty} \left(R^2 e^{-i\omega 2\frac{L}{c}}\right)^p = \frac{1}{1 - R^2 e^{-i\omega 2\frac{L}{c}}}$$

Replacing:

$$E_{out} = E_0(x,y) e^{i(\omega t - kz)} \frac{T^2 e^{-i\omega\frac{L}{c}}}{1 - R^2 e^{-i\omega 2\frac{L}{c}}} = E_{in}(x,y,z,t) \frac{T^2 e^{-i\omega\frac{L}{c}}}{1 - R^2 e^{-i\omega 2\frac{L}{c}}}$$

5.5 SPECTROSCOPY WITH RESONANT CAVITIES

5.5.2 Finesse and spectral bandwidth

The intensity is equal to:

$$I_{out} = 2c\varepsilon_0 E_{out} {E_{out}}^*$$

Being $\tau = 2\frac{L}{c}$ we have:

$$E_{out} = E_{in}(x,y,z,t)\frac{T^2 e^{-i\omega\frac{L}{c}}}{1 - R^2 e^{-i\omega 2\frac{L}{c}}}$$

$$I_{out} = 2c\varepsilon_0 T^4 |E_{in}|^2 \frac{e^{-i\omega\frac{\tau}{2}}}{1 - R^2 e^{-i\omega\tau}} \cdot \frac{e^{i\omega\frac{\tau}{2}}}{1 - R^2 e^{i\omega\tau}}$$

$$= 2c\varepsilon_0 T^4 |E_{in}|^2 \frac{1}{1 - R^2 e^{-i\omega\tau} - R^2 e^{i\omega\tau} + R^4}$$

$$= 2c\varepsilon_0 T^4 |E_{in}|^2 \frac{1}{1 + R^4 - 2R^2 cos\omega\tau}$$

$$= 2c\varepsilon_0 T^4 |E_{in}|^2 \frac{1}{1 + R^4 - 2R^2 + 2R^2 - 2R^2 cos\omega\tau}$$

$$= 2c\varepsilon_0 T^4 |E_{in}|^2 \frac{1}{(1 - R^2)^2 + 2R^2(1 - cos\omega\tau)}$$

5.5 SPECTROSCOPY WITH RESONANT CAVITIES

5.5.2 Finesse and spectral bandwidth

Imposing $I_{in} = 2c\varepsilon_0|A_0|^2$ and using the trigonometric identity: $sen^2\left(\frac{\phi}{2}\right) = \frac{1-cos\phi}{2}$, we can rewrite the intensity of the reflected wave as:

$$I_{out} = I_{in}\frac{T^4}{(1-R^2)^2 + 4R^2 sen^2\left(\frac{\omega\tau}{2}\right)}$$

$$= I_{in}\frac{T^4}{(1-R^2)^2}\frac{1}{1+\left(\frac{2R}{1-R^2}\right)^2 sen^2\left(\frac{\omega\tau}{2}\right)}$$

$$I_{out} = 2c\varepsilon_0 T^4|E_{in}|^2\frac{1}{(1-R^2)^2 + 2R^2(1-cos\omega\tau)}$$

In the absence of mirror losses, $T^2 = 1 - R^2$ and the expression is simplified as:

$$I_{out} = I_{in}\frac{1}{1+\left(\frac{2R}{1-R^2}\right)^2 sen^2\left(\frac{\omega\tau}{2}\right)}$$

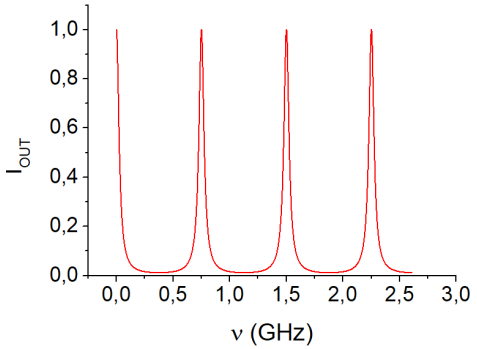

5.5 SPECTROSCOPY WITH RESONANT CAVITIES

5.5.2 Finesse and spectral bandwidth

The full-width half-maximum $\Delta\omega = \left|\frac{\omega_1\tau}{2} - \frac{\omega_2\tau}{2}\right|$ corresponding to $I_{out}\left(\frac{\omega_1\tau}{2}\right) = I_{out}\left(\frac{\omega_2\tau}{2}\right) = I_{in}/2$ of the transmission peak can be calculated as:

$$\frac{I_{in}}{2} = I_{in}\frac{1}{1+\left(\frac{2R}{1-R^2}\right)^2 sen^2\left(\frac{\omega_1\tau}{2}\right)}$$

$$sen^2\left(\frac{\omega_1\tau}{2}\right) = \left(\frac{1-R^2}{2R}\right)^2$$

$$\omega_1 = \frac{2}{\tau} arcsen\left(\frac{1-R^2}{2R}\right)$$

$$I_{out} = I_{in}\frac{1}{1+\left(\frac{2R}{1-R^2}\right)^2 sen^2\left(\frac{\omega\tau}{2}\right)}$$

Thus:

$$\Delta\omega = \frac{4}{\tau} arcsen\left(\frac{1-R^2}{2R}\right)$$

5.5 SPECTROSCOPY WITH RESONANT CAVITIES

5.5.2 Finesse and spectral bandwidth

If we assume $R \approx 1$, then $(1 - R^2) \ll R$ and so:

$$\Delta\omega \approx \frac{4}{\tau}\left(\frac{1-R^2}{2R}\right) = \frac{2}{\tau}\left(\frac{1-R^2}{R}\right)$$

$$\Delta\omega = \frac{4}{\tau} arcsen\left(\frac{1-R^2}{2R}\right)$$

In frequency unit:

$$\Delta\upsilon = \frac{\Delta\omega}{2\pi} = \frac{1}{\pi\tau}\left(\frac{1-R^2}{R}\right)$$

Then, the finesse of the cavity will be:

$$F^* = \frac{FSR}{\Delta\upsilon}$$

Since $FSR = \frac{c}{2L}$ and $\tau = 2\frac{L}{c} = \frac{1}{FSR}$, you get:

$$F^* = \pi\frac{R}{1-R^2}$$

5.5 SPECTROSCOPY WITH RESONANT CAVITIES

5.5.2 Finesse and spectral bandwidth

Since the finesse represents the number of waves that overlap constructively in cavities, the intra-cavity power will be proportional to the input optical power for the cavity finesse.

So, to increase the amplification of the intra-cavity intensity, the parameter to optimize is the reflectivity of the mirrors.

$$F^* = \tau \frac{R}{1 - R^2}$$

The question is: how much the reflectivity of the mirrors must be increased to achieve a substantial increase in the optical path? Considering a cavity length L = 20 cm

$$I_{out} = I_{in} \frac{1}{1 + \left(\frac{2R}{1-R^2}\right)^2 sen^2\left(\frac{\omega\tau}{2}\right)}$$

$$\Delta\upsilon = \frac{1}{\pi\tau}\left(\frac{1-R^2}{R}\right)$$

R = 0.8

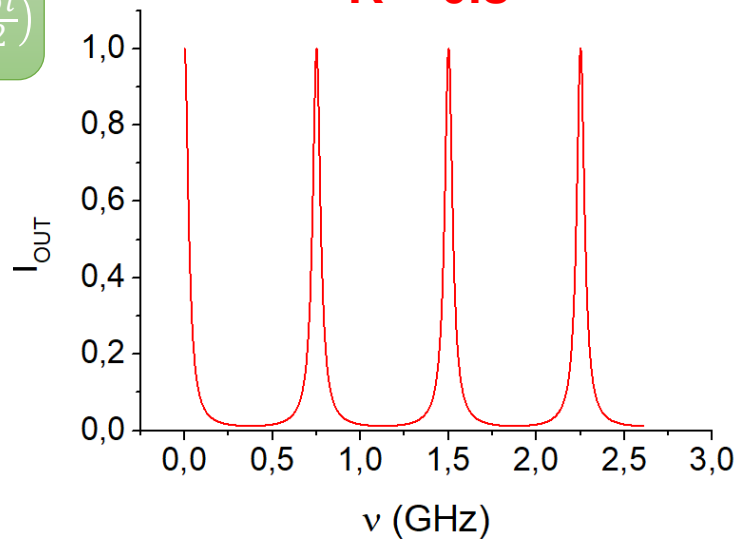

$$FSR = \frac{c}{2L} = 0.75\ GHz$$

$$\tau_r = \frac{1}{FSR} = 1.3\ ns$$

$$\Delta\upsilon = 53.41\ MHz$$

$$F^* = \frac{FSR}{\Delta\upsilon} = \frac{750\ MHz}{53.41\ MHz} = 14$$

5.5 SPECTROSCOPY WITH RESONANT CAVITIES

5.5.2 Finesse and spectral bandwidth

R = 0.9

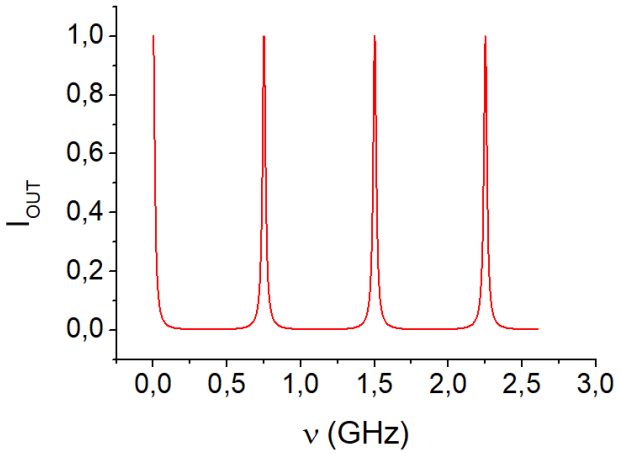

$$FSR = \frac{c}{2L} = 0.75\ GHz$$

$$\tau_r = \frac{1}{FSR} = 1.3\ ns$$

$$\Delta\upsilon = 25.17\ MHz$$

$$F^* = 29.8$$

R = 0.95

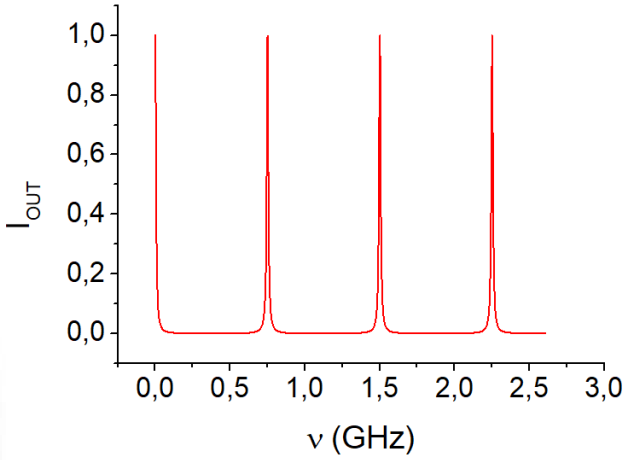

$$FSR = \frac{c}{2L} = 0.75\ GHz$$

$$\tau_r = \frac{1}{FSR} = 1.3\ ns$$

$$\Delta\upsilon = 12.25\ MHz$$

$$F^* = 61$$

5.5 SPECTROSCOPY WITH RESONANT CAVITIES

5.5.2 Finesse and spectral bandwidth

R = 0.99

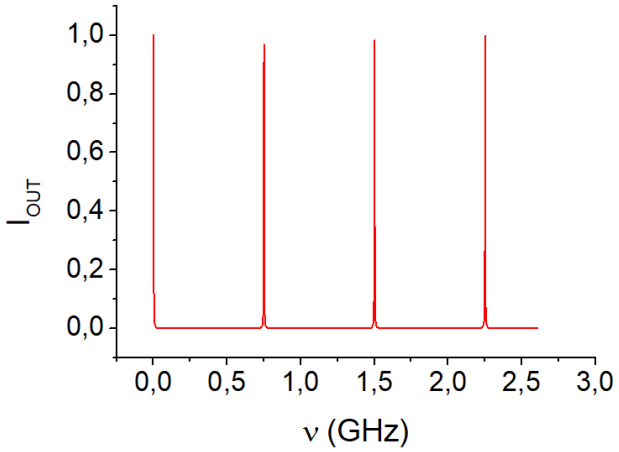

$$FSR = \frac{c}{2L} = 0.75\ GHz$$

$$\tau_r = \frac{1}{FSR} = 1.3\ ns$$

$$\Delta\upsilon = 2.4\ MHz$$

$$F^* = 312$$

R = 0.995

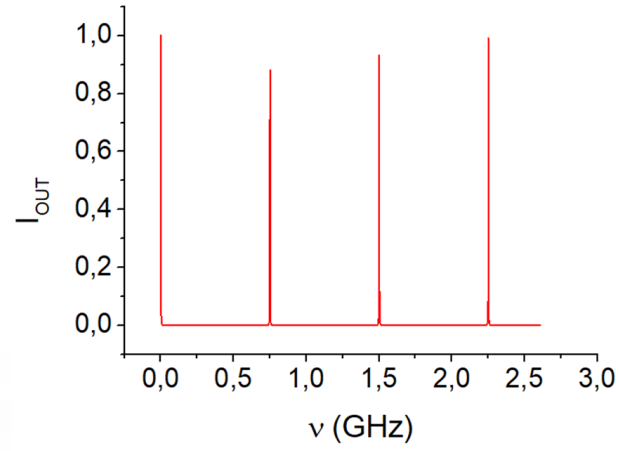

$$FSR = \frac{c}{2L} = 0.75\ GHz$$

$$\tau_r = \frac{1}{FSR} = 1.3\ ns$$

$$\Delta\upsilon = 1.19\ MHz$$

$$F^* = 630$$

5.5 SPECTROSCOPY WITH RESONANT CAVITIES

5.5.2 Finesse and spectral bandwidth

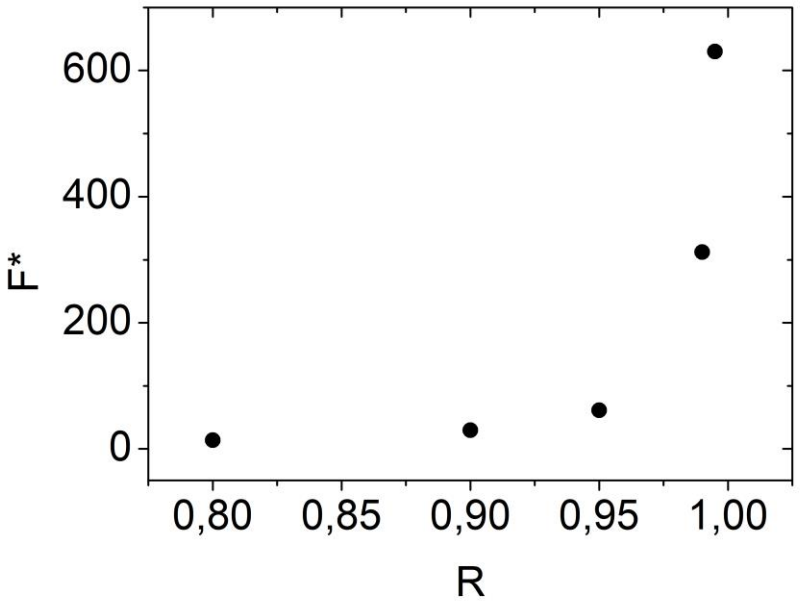

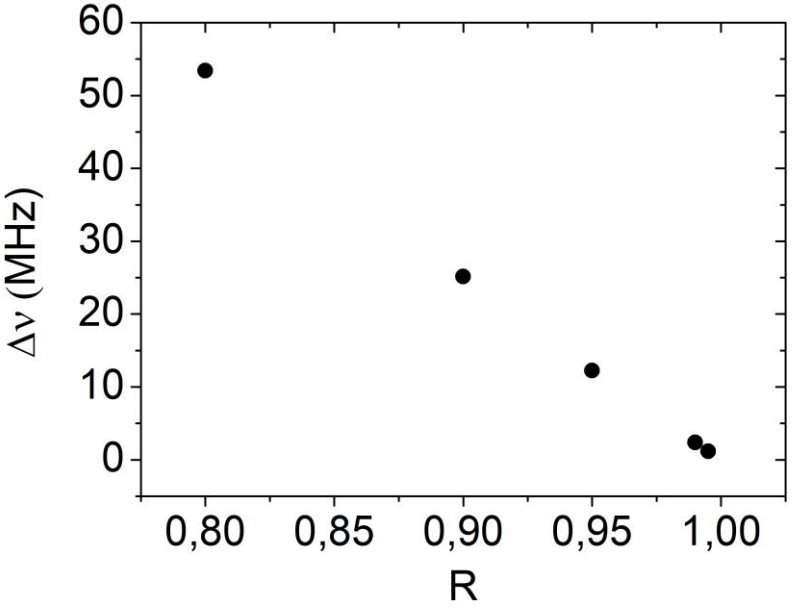

$$F^* = \tau \frac{R}{1 - R^2}$$

$$\Delta \upsilon = \frac{1}{\pi \tau} \left(\frac{1 - R^2}{R} \right)$$

For $R > 0.99$, as the finesse (and therefore the amplification of the intra-power) the width of the cavity mode becomes narrower and narrower. Which is the conseguence?

5.5 SPECTROSCOPY WITH RESONANT CAVITIES

5.5.2 Finesse and spectral bandwidth

The linewidth of a laser emission is not strictly monochromatic. In diode lasers, the spectral broadening of the laser radiation is mainly determined by current fluctuations of the current driver, which in turn generate fluctuations in wavelength. Typically, using standard current drivers, the spectral linewidth of a laser emission line is around 50 MHz. When coupled with cavity modes having linewidth < 50 MHz, all laser power spectrally distributed out of the cavity mode is not coupled into cavities, to be back reflected by the input mirror.

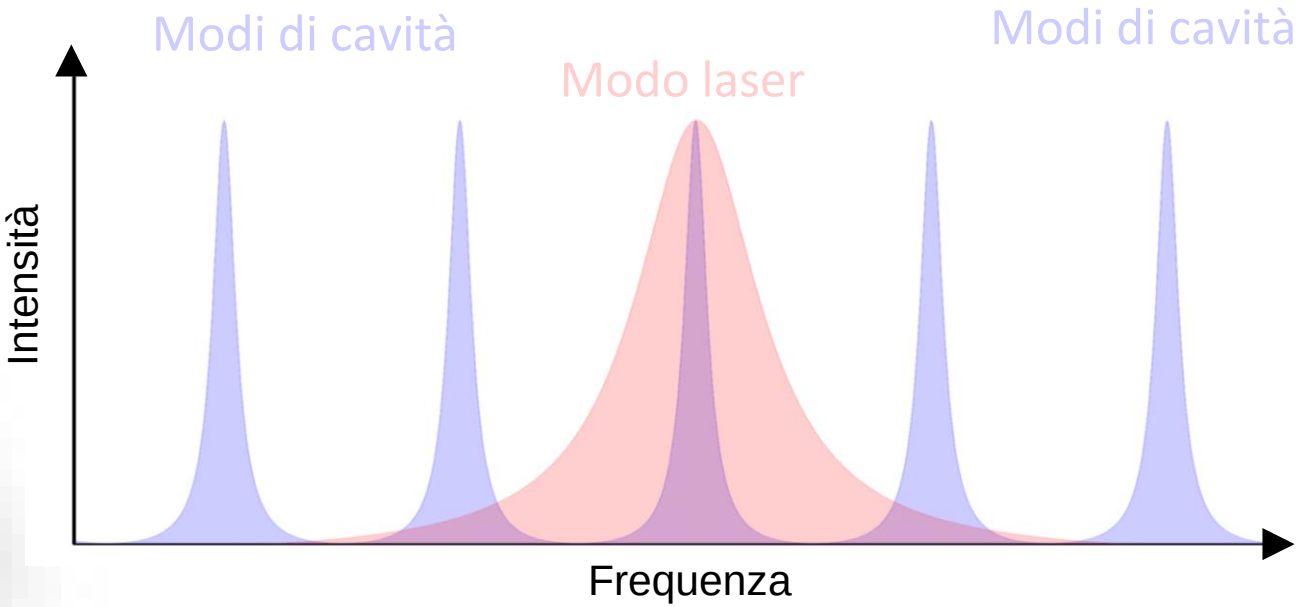

5.5 SPECTROSCOPY WITH RESONANT CAVITIES

5.5.2 Finesse and spectral bandwidth

For high finesses $F^{*}{\sim}300$, $\Delta\upsilon \sim 2\ MHz$ (corresponding to $R{\sim}0.99$). Hence, to ensure an optimal coupling, it is necessary that the linewidth of the laser emission mode is less than MHz. For semiconductor lasers, this can be achieved by using ultra-low noise current drivers, which can reduce the linewidth even below MHz.

Let us suppose that the linewidth of the laser was reduced in order to be comparable with the linewidth of the cavity mode. The next step is to spectrally overlap the laser mode with one of the cavity modes.

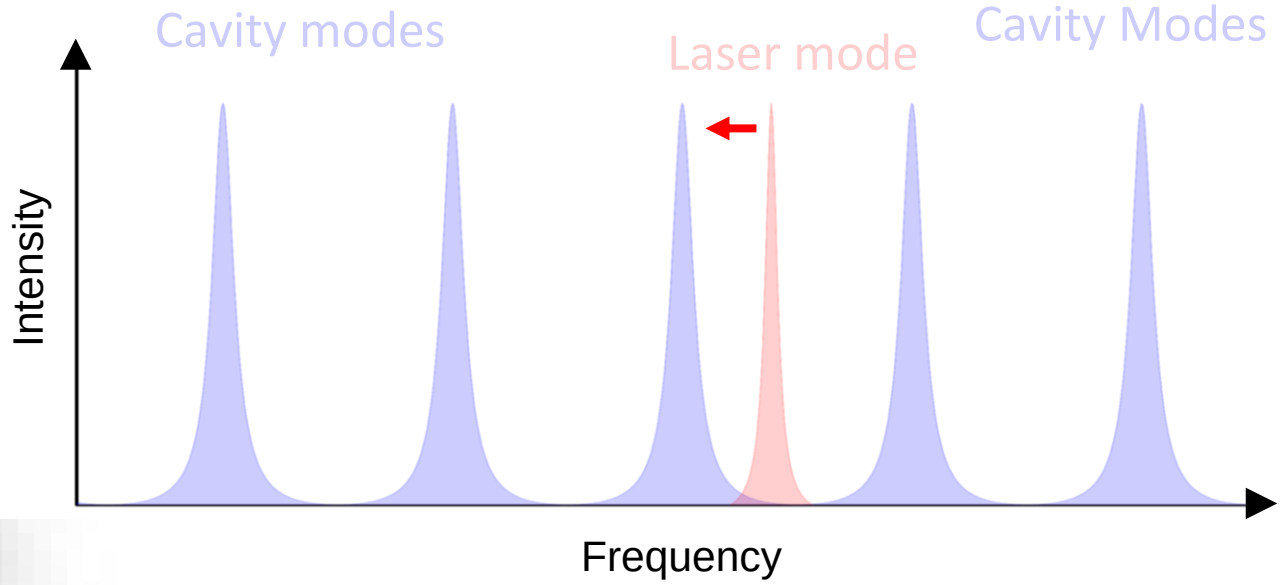

5.5 SPECTROSCOPY WITH RESONANT CAVITIES

5.5.2 Finesse and spectral bandwidth

By keeping the laser wavelength fixed, the overlap can be achieved by varying the length of the cavity which produces a variation of the $FSR = \frac{c}{2L}$.

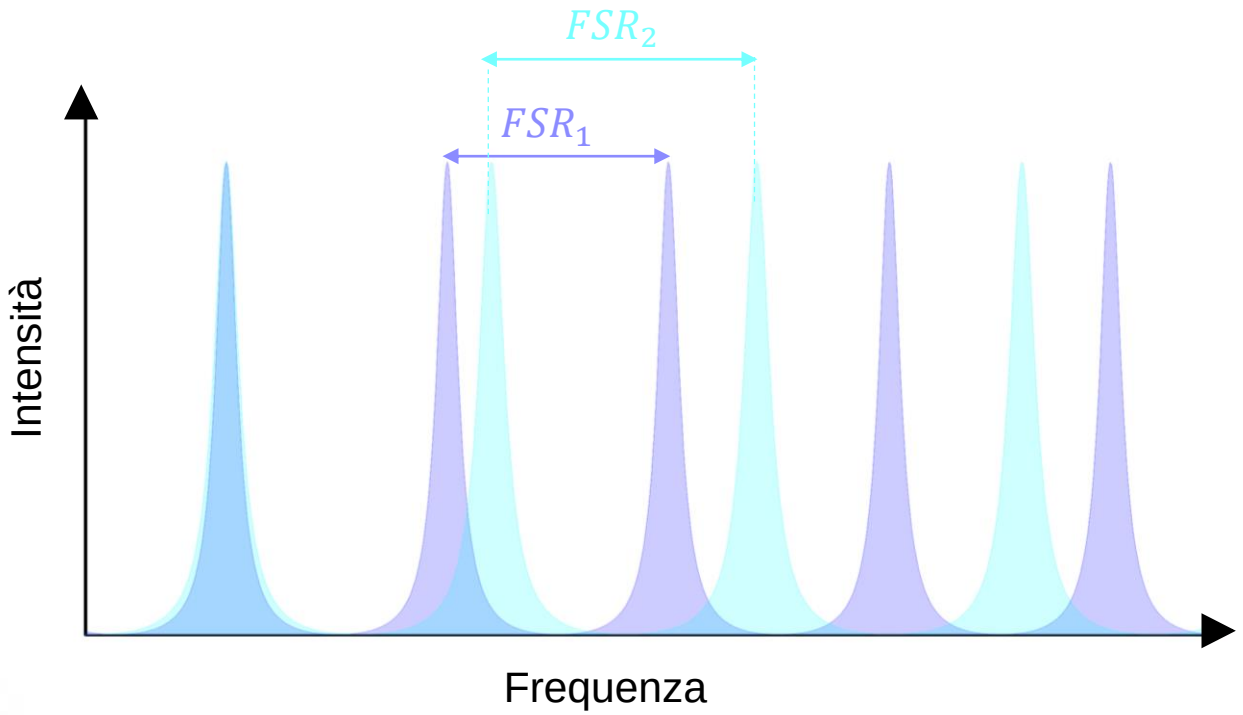

Varying the FSR is equivalent to changing the position of the cavity peaks, without altering the width of the mode and the finesse that depend on the reflectivity of the mirrors.

5.5 SPECTROSCOPY WITH RESONANT CAVITIES

5.5.2 Finesse and spectral bandwidth

Let us assume that both the cavity modes and the laser mode have a linewidth of 1 MHz. An accurate control of the spectral overlap requires a change of the FSR with an accuracy below 1 MHz, to have the possibility that the peak of the laser mode coincides as much as possible with one of the cavity peaks.

If we ask an accuracy of $\partial FSR = 0.1\ MHz$ for the FSR, which is the correspondent variation of the length L of the cavity required to reach such an accuracy?

Being $FSR = \frac{c}{2L}$, deriving with respect to L:

$$\partial FSR = \left|\frac{c}{2L^2}\right| \partial L$$

corresponding to:

$$\partial L = \partial FSR \left|\frac{2L^2}{c}\right|$$

For $L = 15\ cm$, being $c = 30\ cm \cdot GHz$, we obtain that it is necessary to change the length of the cavity with an accuracy of $\partial L = 15\ \mu m$. Such precision can be achieved if one of the two mirrors is mounted on a piezoelectric motor (piezo-actuators).

5.5 SPECTROSCOPY WITH RESONANT CAVITIES

5.5.3 Optical coupling of a laser beam in a cavity

Let us suppose we have realized a linear cavity with two identical plane-convex mirrors placed at a distance equal to twice the focal length of the two mirrors.
How can we couple the light into the cavity in order to have amplification? The most used method is to directly use one of the two mirrors as an entrance mirror.

In order to optimize the amount of light coupled into the cavity, an anti-reflection coating (AR) is deposited on the flat surface of the mirror (to minimize the reflective losses of the incoming beam), while a highly reflective coating (HR) is deposited on the convex side of the mirror.

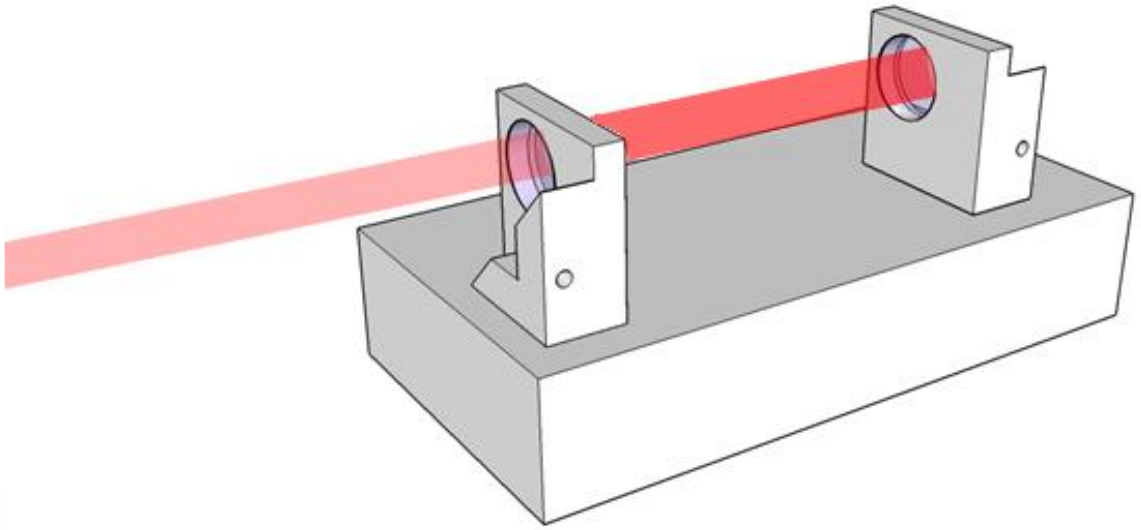

5.5 SPECTROSCOPY WITH RESONANT CAVITIES

5.5.3 Optical coupling of a laser beam in a cavity

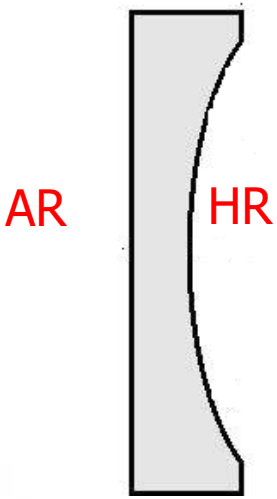

Spectral characteristics of a highly reflective coating

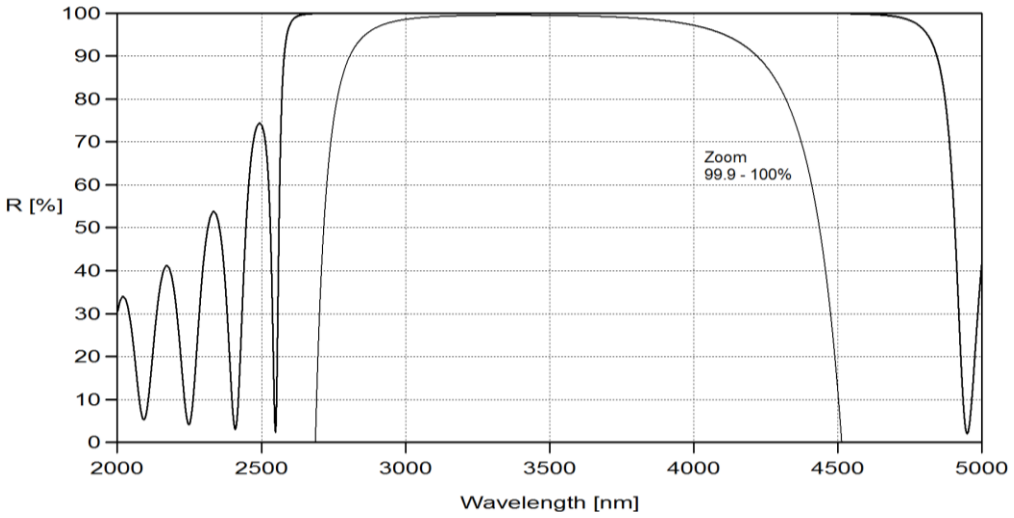

Spectral characteristics of an anti-reflective coating

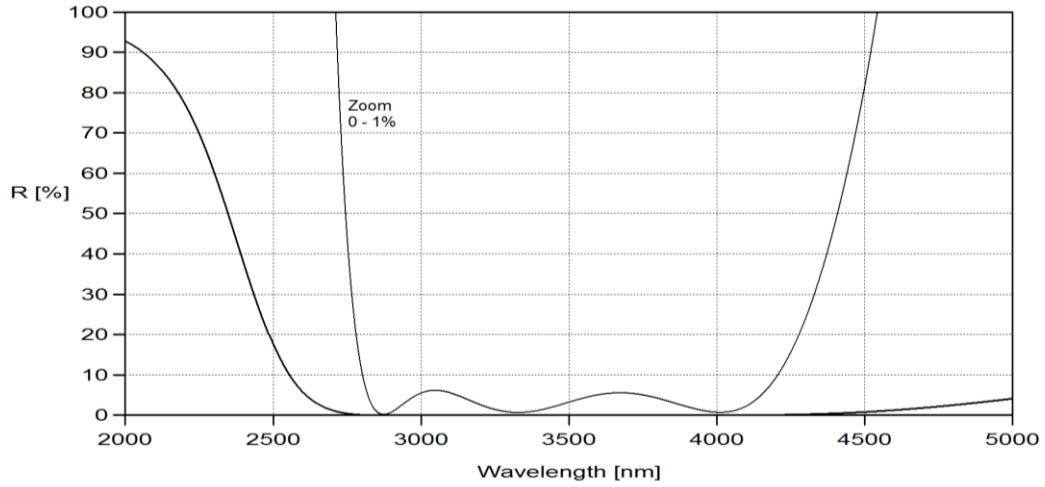

5.5 SPECTROSCOPY WITH RESONANT CAVITIES

5.5.3 Optical coupling of a laser beam in a cavity

Which are the characteristics must the incoming laser beam have to be spatially coupled with the cavity?

Let us consider only the fundamental longitudinal mode with Gaussian intensity distribution. The intro-cavity field reaches its smallest dimensions (beam waist) at the center of the cavity.

The optical coupling of a laser beam in a cavity is called as **mode-matching**. A perfect mode-matching is reached when the radius of curvature and the wavefront of the input beam overlap perfectly with those of the longitudinal mode TEM_{00} of the cavity. If the input laser beam is collimated, this condition can be achieved using a focusing lens.

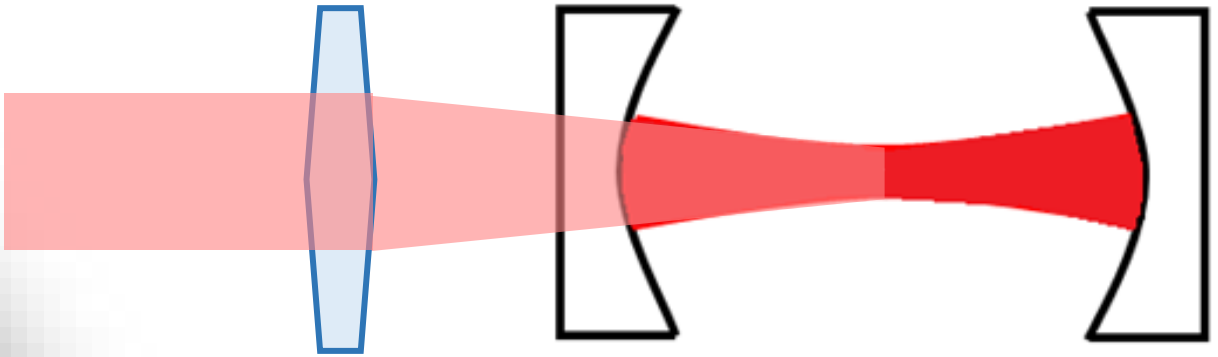

5.5 SPECTROSCOPY WITH RESONANT CAVITIES

5.5.3 Optical coupling of a laser beam in a cavity

To decide which lens to use you need to calculate the beam waist of the cavity.

We use ABCD matrix formalism to estimate the size of the beam at the center of the cavity formed by two identical mirrors of radius of curvature R placed at a distance L. Starting from the center of the cavity, being $q(z_1)$ the complex radius of curvature, the transformation matrix after a round-trip into cavities will be:

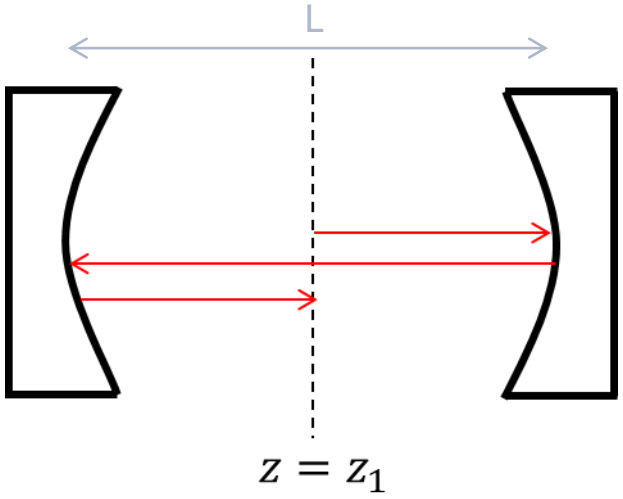

$$\begin{pmatrix} \boldsymbol{A} & \boldsymbol{B} \\ \boldsymbol{C} & \boldsymbol{D} \end{pmatrix} = \begin{pmatrix} 1 & \frac{L}{2} \\ 0 & 1 \end{pmatrix} \begin{pmatrix} 1 & 0 \\ -\frac{2}{R} & 1 \end{pmatrix} \begin{pmatrix} 1 & L \\ 0 & 1 \end{pmatrix} \begin{pmatrix} 1 & 0 \\ -\frac{2}{R} & 1 \end{pmatrix} \begin{pmatrix} 1 & \frac{L}{2} \\ 0 & 1 \end{pmatrix}$$

5.5 SPECTROSCOPY WITH RESONANT CAVITIES

5.5.3 Optical coupling of a laser beam in a cavity

Exploiting the row-by-column multiplication:

$$\begin{pmatrix} \boldsymbol{A} & \boldsymbol{B} \\ \boldsymbol{C} & \boldsymbol{D} \end{pmatrix} = \begin{pmatrix} \dfrac{2L^2 - 4LR + R^2}{R^2} & \dfrac{L(L^2 - 3LR + 2R^2)}{R^2} \\ \dfrac{4(L-R)}{R^2} & \dfrac{2L^2 - 4LR + R^2}{R^2} \end{pmatrix}$$

After a round-trip, the beam in the center of the cavity must have the same parameters as the starting one, namely:

$$q(z_1 + round\ trip) = q(z_1)$$

leading to:

$$q(z_1) = \frac{Aq(z_1) + B}{Cq(z_1) + D}$$

5.5 SPECTROSCOPY WITH RESONANT CAVITIES

5.5.3 Optical coupling of a laser beam in a cavity

Since at the waist beam point the real radius of curvature is infinite $R(z_1) = \infty$,

$$\frac{1}{q(z_1)} = -i\frac{\lambda}{\pi w^2(z_1)}$$

Imposing to be real:

$$w(z_1) = \sqrt{\frac{q(z_1)\lambda}{\pi}}$$

Once $q(z_1)$ is calculated, the beam waist can be easily determined.

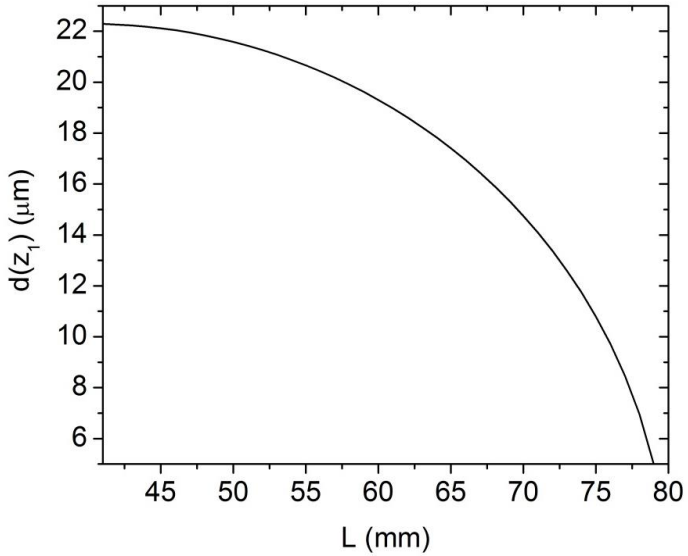

$$q(z_1) = \frac{Aq(z_1) + B}{Cq(z_1) + D}$$

$R = 40\ mm$
$\lambda = 3.5\ \mu m$

5.5 SPECTROSCOPY WITH RESONANT CAVITIES

5.5.4 Cavity-Ring Down Spectroscopy

Cavity ring-down spectroscopy (CRDS) is based on the measurement of the decay time of an optical resonator when filled with an absorbing gas species.

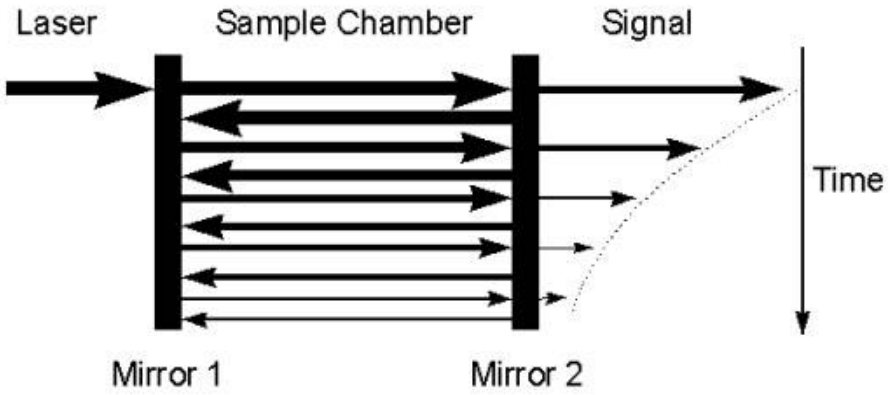

Let us consider a short laser pulse with P_0 as input power that is sent inside a linear cavity composed of two highly reflective mirrors (reflectivity $R_1 = R_2 = R$) and transmittivity equal to $T = 1 - R - A \ll 1$, where A includes all loss mechanisms occurring in the cavity (absorption loss, scattering loss, diffraction loss) except for the losses introduced by the absorption of the sample.

The pulse will be reflected back and forth by the mirrors and for each round-trip a small fraction of the light will be transmitted from the output mirror to reach the optical detector.

5.5 SPECTROSCOPY WITH RESONANT CAVITIES

5.5.4 Cavity-Ring Down Spectroscopy

The transmitted power of the first output pulse will be:

$$P_1 = T^2 e^{-\alpha L} P_0$$

where α is the absorption coefficient of the gas species within the L-length resonator. For each round-trip, the pulse power decreases by a factor of $R^2 e^{-2\alpha L}$.

After n round-trips, the power of the transmitted pulse is decreased by:

$$P_n = (R e^{-\alpha L})^{2n} P_1$$

which can be rewritten as (using the expression $R = e^{lnR}$):

$$P_n = P_1 e^{-2n(\alpha L - lnR)}$$

On the other hand, the mirror reflectivity R can be expressed as

$$\mathrm{R} = 1 - T - A$$

Since $R \gg T + A$, applying the logarithm operator to both members:

$$\ln \mathrm{R} = \ln[1 + (-T - A)] \approx -T - A$$

$\ln(1 + x) \approx \mathrm{x}$ per $x \to 0$

5.5 SPECTROSCOPY WITH RESONANT CAVITIES

5.5.4 Cavity-Ring Down Spectroscopy

Thus $P_n = P_1 e^{-2n(\alpha L - lnR)} = P_1 e^{-2n(T+A+\alpha L)}$

The delay time between two pulses transmitted by the cavity will be equal to the round-trip time of the cavity, namely $\tau_R = \frac{2L}{c}$. Then, the n-th pulse will be revealed at time $t = \frac{2nL}{c}$.

The discretization of the variable n can be "converted" to the continuous temporal variable t, by replacing $2n = \frac{ct}{L}$ in $P_n = P_1 e^{-2n(T+A+\alpha L)}$.

As a result, the detected signals will be a function of the time according to the following exponential function:

$$P(t) = P_1 e^{-\frac{ct}{L}(T+A+\alpha L)}$$

Introducing a decay time:

$$\tau_1 = \frac{\frac{L}{c}}{T + A + \alpha L}$$

you have: $P(t) = P_1 e^{-\frac{t}{\tau_1}}$

Without any absorbing gas species in the cavity ($\alpha = 0$), the resonator decay time will be:

$$\tau_2 = \frac{\frac{L}{c}}{T + A}$$

5.5 SPECTROSCOPY WITH RESONANT CAVITIES

5.5.4 Cavity-Ring Down Spectroscopy

The difference $\Delta\tau = \tau_2 - \tau_1$ will be:

$$\tau_1 = \frac{\frac{L}{c}}{T + A + \alpha L} \qquad \tau_2 = \frac{\frac{L}{c}}{T + A}$$

$$\Delta\tau = \tau_2 - \tau_1 = \frac{\alpha\frac{L}{c}}{(T + A)(T + A + \alpha L)} = \frac{\alpha\frac{L^2}{c}}{(1 - R)(T + A + \alpha L)}$$

Thus, we can express the product αL as:

$$\alpha L = (1 - R)\frac{\Delta\tau}{\tau_1}$$

The minimum detectable absorption $\alpha_{min}L$ is limited by the reflectivity R of the cavity mirrors and the accuracy in measuring the decay times.

As in cavity absorption spectroscopy, in CRDS the effective optical path is equal to $L_{eff} = L/(1 - R)$ because the laser pulse passes through the gas cell $1/(1 - R)$ times.

5.5 SPECTROSCOPY WITH RESONANT CAVITIES

5.5.4 Cavity-Ring Down Spectroscopy

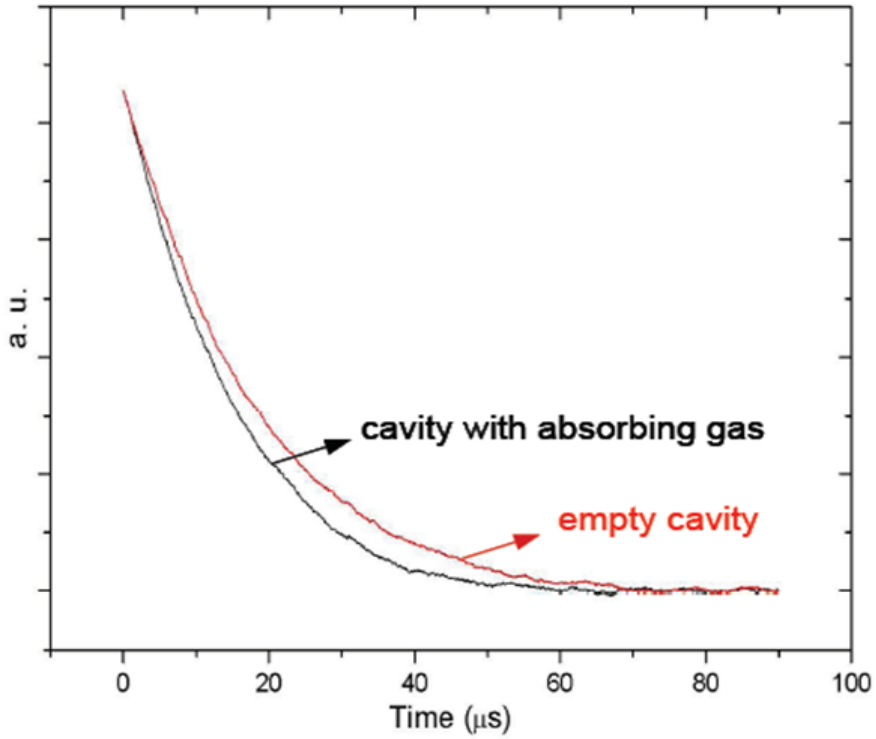

Advantages:

- It is independent of the laser power because the absorption of the gas is estimated starting from the exponent of the exponential trend. Thus, the system is not affected by fluctuations in the power of the source.
- It exploits multiple reflections in cavities, increasing the effective length of light-gas interaction.

Disadvatages:

- Decay time must be measured when there is no gas absorption (background reference signal)
- The measurement of the concentration cannot take place in real time, but a post-processing analysis is mandatory.

5.6 PHOTOACOUSTIC SPECTROSCOPY

The absorption techniques analyzed so far are called **direct absorption techniques** because they measure the absorption starting from the light transmitted by the sample.

Indirect absorption techniques measure the effect that an optical absorption produces within a sample.

An indirect absorption technique is the photoacoustic technique, which is based on the photoacoustic effect.

The photoacoustic effect was observed by Bell more than a century ago (1880) in a completely accidental way while working on perfectioning the photophone.

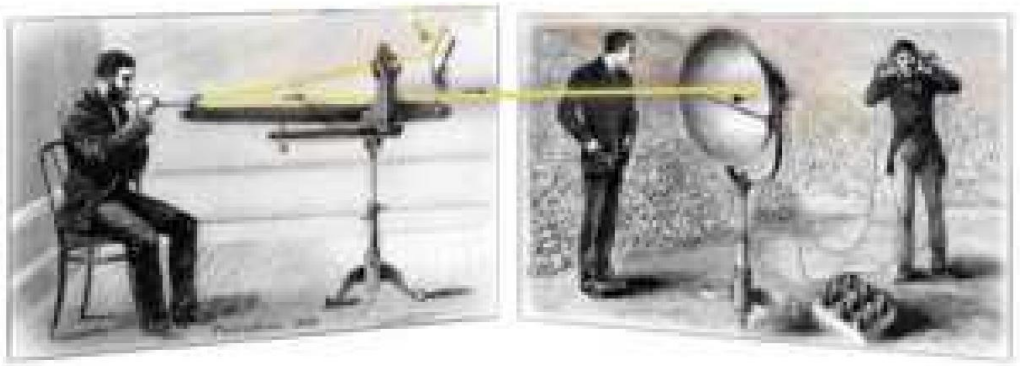

Fig. 1.2: Schema del fotofono di Bell.

5.6 PHOTOACOUSTIC SPECTROSCOPY

On June 3, 1880, Alexander Graham Bell realized a **photophone**, a device that allowed for the transmission of sound on a beam of light.

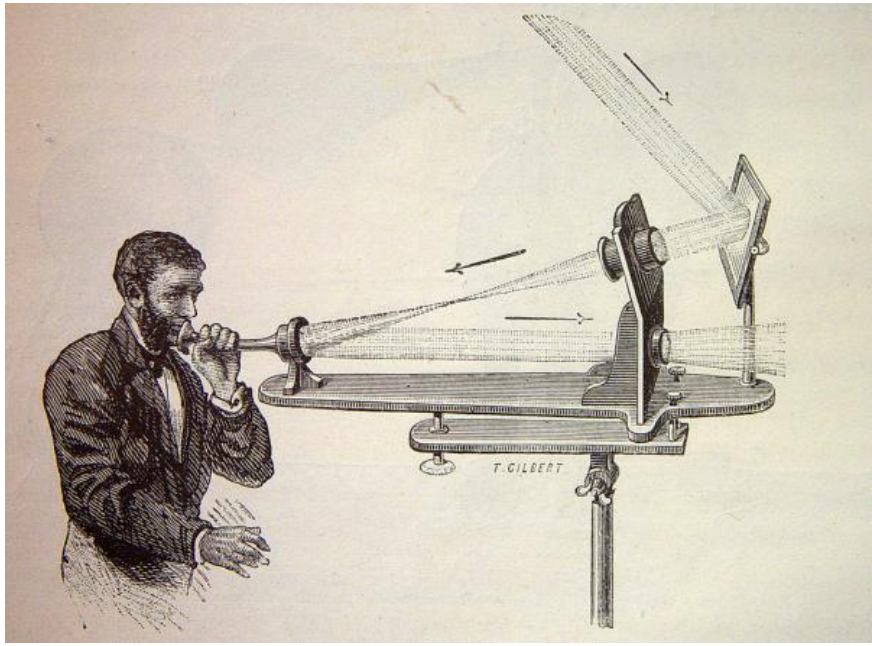

Bell directs sunlight into the mirror.

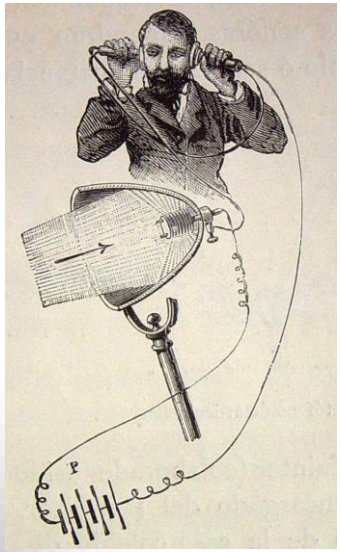

Vibrations in the voice causes oscillations in the shape of a flexible mirror.

The reflected beam results modulated by flexible mirror vibrations.

The photophone used crystalline selenium cells at the focal point of its parabolic receiver. This material's electrical resistance varies inversely with the illumination falling upon it, i.e., its resistance is higher when it is in the dark, and lower when it is exposed to light.

On June 3, 1880, Alexander Graham Bell invented **the first wireless telephone**

5.6 PHOTOACOUSTIC SPECTROSCOPY

The **photoacoustic effect** was observed by Graham Bell while he was working on the improvement of a photophone, in an accidental way.

Bell realized that when a light beam is periodically interrupted by a chopper and subsequently focused on a layer of thin material a sound wave is produced.

In addition, the generated acoustic signal increased in intensity when the layer exposed to the beam was dark in colour.

Thus, Bell realized that this effect was related to the absorption of light by the thin layer.

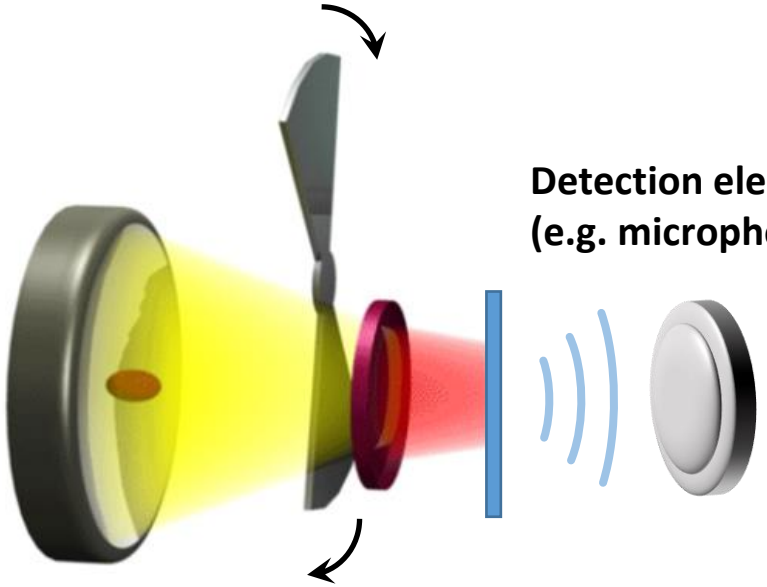

The photoacoustic effect occurs in all kind of materials (solids, liquids and gases)

However, due to the lack of appropriate equipment (such as light sources, microphones), the photoacoustic effect was completely forgotten for more than half a century.

5.6 PHOTOACOUSTIC SPECTROSCOPY

The photoacoustic effect for gas species can be divided into three main processes that can be analyzed separately:

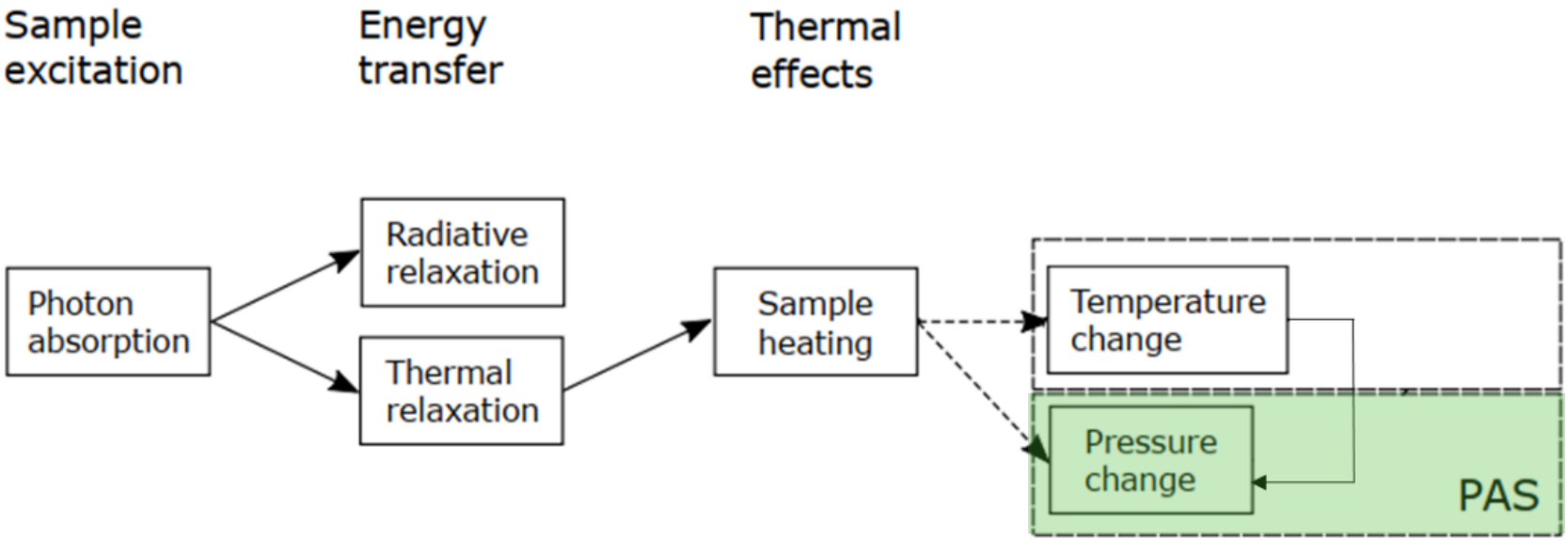

5.6 PHOTOACOUSTIC SPECTROSCOPY

4.6.1 Light absorption and heat generation

Molecules of the gas sample absorb optical radiation causing a local heating. This excess of energy is transferred to the surrounding molecules by collision processes.

When a molecule in the gas phase absorbs a photon, it passes from its ground energy state E_0 to an excited energy state E_1 , following the Planck relation $E_1 - E_0 = h\upsilon$, where $h\upsilon$ is the energy of the absorbed photon and υ its frequency.

The molecule can relax this extra-energy and return to its ground state by means of different decay processes:

- can emit a photon – radiative de-excitation;
- can cause a photochemical process;
- it can collide with another molecule of the same species, which is in the ground state E_0 and excite it to the E_1 state;
- it can collide with any other molecule in the gas and transfer the absorbed optical energy into translational or kinetic energy through collisions – non-radiative de-excitation. This process generates a local increase of the temperature of the gas.

5.6 PHOTOACOUSTIC SPECTROSCOPY

5.6.1 Light absorption and heat generation

If optical excitation occurs in the infrared range, the energy states involved are roto-vibrational ones.

The non-radiative decay time, at the pressures typically used in infrared spectroscopy applications (< 1bar), is of the order of $10^{-6} - 10^{-9}\ s$, while the radiative decay time varies between $10^{-1} - 10^{-3}\ s$. In addition, at these wavelengths, the energy of the photons is too small to induce chemical reactions, and this causes the absorbed optical energy to be released almost completely as heat, causing an increase of the kinetic energy of the molecules.

Let us suppose that a single molecule can be schematized with a two-level system:

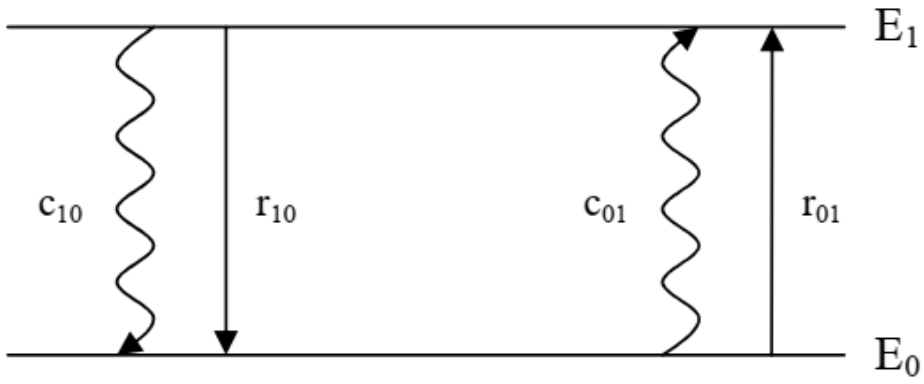

5.6 PHOTOACOUSTIC SPECTROSCOPY

5.6.1 Light absorption and heat generation

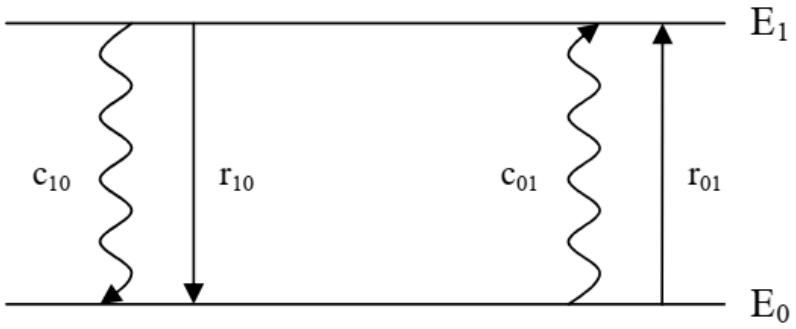

E_0 and E_1 represent the energies of the ground state and the excited state having population densities (number of molecules per unit volume) $N_0(\vec{r},t)$ and $N_1(\vec{r},t)$, respectively.

Being ρ_ν the energy density of the radiation at $\upsilon = \frac{E_1 - E_0}{h}$; B_{ij} the Einstein coefficient for absorption, $B_{ji} = B_{ij}$ the Einstein coefficient for stimulated emission; A_{ij} the Einstein coefficient for spontaneous emission, the radiative transition rate r_{ij} from the generic level i to the j level can be written as:

$$r_{ij} = \rho_\nu B_{ij} + A_{ij}$$

5.6 PHOTOACOUSTIC SPECTROSCOPY

5.6.1 Light absorption and heat generation

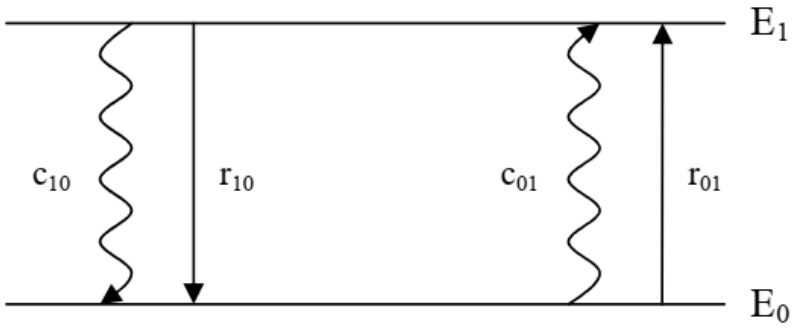

Being c_{ij} the non-radiative transition rate for collisions from the generic level i to the j level, the rate equation describing the temporal dependence of the population density of the excited energy level will be:

$$\frac{dN_1(\vec{r},t)}{dt} = (r_{01} + c_{01})N_0(\vec{r},t) - (r_{10} + c_{10})N_1(\vec{r},t)$$
$$= (\rho_\nu B_{01} + A_{01} + c_{01})N_0(\vec{r},t) - (\rho_\nu B_{10} + A_{10} + c_{10})N_1(\vec{r},t)$$

The probability for non-radiative transitions from the ground state to the excited one is close to zero, as it is thermally disadvantaged ($c_{01} = 0$) and that $A_{01} = 0$ because $E_1 > E_0$.

5.6 PHOTOACOUSTIC SPECTROSCOPY

5.6.1 Light absorption and heat generation

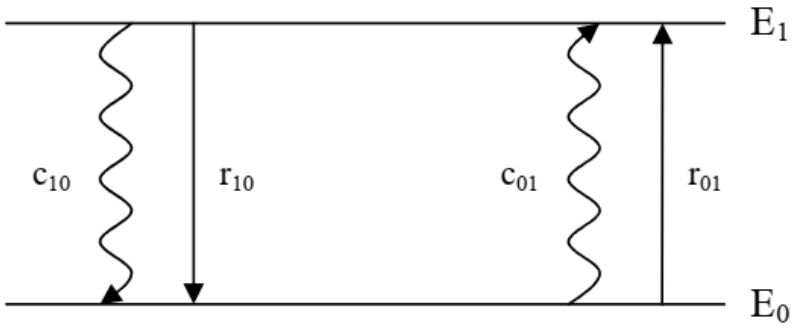

Including also that $B_{01} = B_{10}$, the above equation becomes:

$$\frac{dN_1(\vec{r},t)}{dt} = (\rho_\nu B_{01} + A_{01} + c_{01})N_0(\vec{r},t) - (\rho_\nu B_{10} + A_{10} + c_{10})N_1(\vec{r},t)$$

$$\frac{dN_1}{dt} = \rho_\nu B_{10}(N_0 - N_1) - (A_{10} + c_{10})N_1$$

Let us define τ as the total lifetime of the excited level, τ^{-1} can be expressed as the sum of the reciprocals of the radiative ($\tau_r = 1/A_{10}$) and non-radiative ($\tau_{nr} = 1/c_{10}$) relaxation times:

$$\frac{1}{\tau} = \frac{1}{\tau_r} + \frac{1}{\tau_{nr}}$$

5.6 PHOTOACOUSTIC SPECTROSCOPY

5.6.1 Light absorption and heat generation

The above equation becomes:

$$\frac{dN_1}{dt} = \rho_\nu B_{10}(N_0 - N_1) - (A_{10} + c_{10})N_1$$

$$\frac{dN_1}{dt} = \rho_\nu B_{10}(N_0 - N_1) - \frac{N_1}{\tau}$$

In the hypothesis of weakly absorbent gas $N_1 \ll N_0$, we have:

$$\frac{dN_1}{dt} = \rho_\nu B_{10} N_0 - \frac{N_1}{\tau}$$

with N_0 almost constant and approximately independent of time. $\rho_\nu B_{10}$ represents the optical absorption rate, that we can express as the flux F of incident photons for the cross section σ of the absorption process:

$$\rho_\nu B_{10} = F\sigma$$

5.6 PHOTOACOUSTIC SPECTROSCOPY

5.6.1 Light absorption and heat generation

If the photons flux is modulated at a frequency ω, its dependence on the position $\vec{r}$ and time t is given by:

$$F(\vec{r},t) = F_0(\vec{r})\left(1 + \delta e^{i\omega t}\right)$$

If $\delta \ll 1$, we are in the conditions where the laser light is polarized continuously, with a sinusoidal dither of small amplitude applied to the continuum.

Substituting these two relations in the expression for $\frac{dN_1}{dt}$, we get:

$$\frac{dN_1}{dt} = \left[\sigma F_0(\vec{r}) + \sigma F_0(\vec{r})\delta e^{i\omega t}\right]N_0 - \frac{N_1}{\tau}$$

$$\frac{dN_1}{dt} = \rho_\nu B_{10} N_0 - \frac{N_1}{\tau}$$

$$\rho_\nu B_{10} = F\sigma$$

Neglecting the time-independent term, this represents a complete first-order differential equation in the variable t. Its solution, which describes how the population density of the excited state changes over time due to the absorption of modulated light radiation, is given by:

5.6 PHOTOACOUSTIC SPECTROSCOPY

5.6.1 Light absorption and heat generation

$$N_1(\vec{r},t) = \frac{N_0 \sigma F_0(\vec{r}) \delta}{\sqrt{1+\omega^2\tau^2}} \tau e^{i(\omega\tau - \vartheta)}$$

with $\vartheta = arct(\omega\tau)$ indicates the phase shift between N_1 and the photons flux F.

The generated heat rate $H(\vec{r},t)$ can be assumed proportional to $N_1(\vec{r},t)$ by the relation:

$$H(\vec{r},t) = \frac{N_1(\vec{r},t) \cdot E'}{\tau_{nr}}$$

where E' is the average thermal energy released by a molecule following the non-radiative de-excitation process of the excited state.

During this process, the molecule moves from the excited state to the fundamental one, so E' corresponds to the energy $h\upsilon$ of the absorbed photon.

5.6 PHOTOACOUSTIC SPECTROSCOPY

5.6.1 Light absorption and heat generation

Neglecting the no-radiative relaxation and thus imposing $\tau = \tau_{nr}$ in the $N_1(\vec{r}, t)$ expression, the heat rate becomes:

$$H(\vec{r}, t) = \frac{N_0 \sigma F_0(\vec{r}) \delta h\upsilon}{\sqrt{1 + \omega^2 \tau^2}} e^{i(\omega\tau - \vartheta)} = H_0(\vec{r}) \delta e^{i(\omega\tau - \vartheta)}$$

where $H_0(\vec{r}) = \frac{N_0 \sigma F_0(\vec{r}) h\upsilon}{\sqrt{1+\omega^2\tau^2}}$

The photons flux multiplied by the energy of the single photon represents the intensity of the radiation field, namely:

$$I_0(\vec{r}) = F_0(\vec{r}) h\upsilon$$

then $H_0(\vec{r})$ can be expressed as:

$$H_0(\vec{r}) = \frac{N_0 \sigma I_0(\vec{r})}{\sqrt{1 + \omega^2 \tau^2}}$$

5.6 PHOTOACOUSTIC SPECTROSCOPY

5.6.1 Light absorption and heat generation

If $\omega\tau \ll 1$, namely $\omega \ll 10^6$ rad/s

$$H_0(\vec{r}) = N_0\sigma I_0(\vec{r})$$

$$H_0(\vec{r}) = \frac{N_0\sigma I_0(\vec{r})}{\sqrt{1+\omega^2\tau^2}}$$

$$H(\vec{r},t) = H_0(\vec{r})\delta e^{i(\omega t-\vartheta)}$$

and the heat rate becomes:

$$H(\vec{r},t) = H_0(\vec{r})\delta e^{i(\omega t-\vartheta)} = N_0\sigma I_0(\vec{r})\delta e^{i(\omega t-\vartheta)} = \alpha I_0(\vec{r})\delta e^{i(\omega t-\vartheta)}$$

where α is the optical absorption coefficient of the gas.

If the absorbing molecules are in traces within the carrier gas (carrier gas or matrix), being N_{TOT} the total number of molecules per unit volume, we have:

$$\alpha = N_0\sigma = \frac{N_0}{N_{TOT}}N_{TOT}\sigma = cN_{TOT}\sigma$$

where N_0 identifies the density of the absorbing molecules and c its relative concentration.

5.6 PHOTOACOUSTIC SPECTROSCOPY

5.6.1 Light absorption and heat generation

When the phase shift $\theta = 0$, the modulation of $H(\vec{r}, t)$ follows the modulation of the incident radiation directly without any phase delay.

$$H(\vec{r}, t) = H_0(\vec{r})\delta e^{i(\omega t - \vartheta)}$$

This model constitutes the basis of detection of trace gas absorption detected by photoacoustic spectroscopy. These equations are valid in the assumptions that:

- $F\sigma$ is small anough to avoid the saturation, so that the population density of the excited state is small ($N_1 \ll N_0$), and the stimulated emission can be neglected;
- Low modulation frequencies: $\omega << \tau^{-1}$.

The above hypotheses are both generally satisfied in applications of photoacoustic spectroscopy for the detection of gas traces. The first is verified because absorbing gases are, in most cases, present only at low concentrations (in traces). The second hypothesis, on the other hand, is verified for modulation frequencies smaller than MHz.

5.6 PHOTOACOUSTIC SPECTROSCOPY

5.6.2 Acoustic wave generation

The second process to consider is the generation of the acoustic wave because of the periodic variation of the pressure, as a consequence of the periodic heating of the sample due to the non-radiative relaxation processes.

A model for describing the generation of the acoustic wave is based on the combination of the **fluid mechanics** and **thermodynamics**.

We consider the case of an ideal fluid, uniform and continuous, elastic, at rest, at thermodynamic equilibrium except for the motion produced by the pressure wave, small enough to neglect non-linear effects.

The effect of gravitational force will also be neglected so that the pressure at the equilibrium P_0 $[N/m^3]$ and the density at equilibrium ρ_0 $[kg/m^3]$ can be considered constant within the fluid.

Dissipative terms due to viscosity and heat diffusion will also not be considered in the initial discussion. They will be introduced later as a disruptive effect of the solution.

The propagation of an acoustic wave produces in the fluid variations in pressure, density and temperature; each variation is proportional to the amplitude of the acoustic wave.

5.6 PHOTOACOUSTIC SPECTROSCOPY

5.6.2 Acoustic wave generation

For this reason, the acoustic wave that is generated is usually described by a sound pressure $p(\vec{r}, t)$ defined as the difference between the instantaneous pressure P and the pressure at the equilibrium P_0 :

$$p = P - P_0$$

The physical equations governing the generation in acoustic wave gases are:

- Ideal gas law:

$$pV = nRT$$

that we can rewrite in a different way. The number of moles n can be expressed as the ratio of the total mass M_{TOT} to the molar mass M, $n = M_{TOT}/M$

$$\frac{p}{\frac{M_{TOT}}{V}} = R\frac{T}{M}$$

5.6 PHOTOACOUSTIC SPECTROSCOPY

5.6.2 Acoustic wave generation

Since $\rho = \frac{M_{TOT}}{V}$, by using Mayer relation $C_P - C_V = R$, one obtain:

$$\frac{p}{\rho} = (\gamma - 1)\frac{C_V}{M}T$$

$$\frac{p}{\frac{M_{TOT}}{V}} = R\frac{T}{M}$$

where $\gamma = \frac{C_P}{C_V}$ is the ratio of the specific heat at constant pressure and the specific heat at constant volume.

- the mass conservation law

$$-\frac{1}{\rho}\frac{\partial \rho}{\partial t} = \vec{\nabla} \cdot \vec{v}$$

where $\vec{v}(\vec{r}, t)$ is the velocity vector field

- the law of conservation of the momentum

$$\rho\frac{\partial \vec{v}}{\partial t} = -\vec{\nabla}p$$

5.6 PHOTOACOUSTIC SPECTROSCOPY

5.6.2 Acoustic wave generation

- the energy conservation law

$$\rho \frac{C_V}{M} \frac{\partial T}{\partial t} + p\vec{\nabla} \cdot \vec{v} = \frac{\partial Q}{\partial t}$$

where Q is the heat produced as a result of non-radiative relaxation processes of the absorbing molecules after the absorption of modulated light.

The four equations that regulate the dynamics of the pressure field and the thermal gradient are:

$$\frac{p}{\rho} = (\gamma - 1)\frac{C_V}{M}T$$

$$-\frac{1}{\rho}\frac{\partial \rho}{\partial t} = \vec{\nabla} \cdot \vec{v}$$

$$\rho \frac{\partial \vec{v}}{\partial t} = -\vec{\nabla} p$$

$$\rho \frac{C_V}{M} \frac{\partial T}{\partial t} + p\vec{\nabla} \cdot \vec{v} = \frac{\partial Q}{\partial t}$$

5.6 PHOTOACOUSTIC SPECTROSCOPY

5.6.2 Acoustic wave generation

It is possible to couple the above equations to obtain a differential equation in the pressure field variable $p(\vec{r}, t\,)$:

$$\nabla^2 p(\vec{r}, t\,) - \frac{1}{c^2}\frac{\partial^2 p(\vec{r}, t\,)}{\partial t^2} = -\frac{\gamma - 1}{c^2}\frac{\partial H}{\partial t}$$

where $c = \sqrt{\frac{\gamma RT}{M}}$ is the sound velocity in the gas and $H = \frac{\partial Q}{\partial t}$ is the heat rate generated by the optical absorption.

We have obtained that the pressure field $p(\vec{r}, t\,)$ propagates according to the D'Alembert equation, thus solutions are waves.

For a sinusoidal modulation of the incident radiation, it is convenient to rewrite the differential equation in the frequency domain, applying the Fourier transform to both members:

$$\left(\nabla^2 + \frac{\omega^2}{c^2}\right) p(\vec{r}, \omega) = \frac{\gamma - 1}{c^2} i\omega H(\vec{r}, \omega)$$

5.6 PHOTOACOUSTIC SPECTROSCOPY

5.6.2 Acoustic wave generation

The Fourier's theorem gives also the relations for the expressions in the time and in the frequency domains:

$$p(\vec{r},t) = \int_{-\infty}^{+\infty} p(\vec{r},\omega)e^{-i\omega}d\omega$$

$$H(\vec{r},t) = \int_{-\infty}^{+\infty} H(\vec{r},\omega)e^{-i\omega}d\omega$$

$$\nabla^2 p(\vec{r},t) - \frac{1}{c^2}\frac{\partial^2 p(\vec{r},t)}{\partial t^2} = -\frac{\gamma-1}{c^2}\frac{\partial H}{\partial t}$$

$$\left(\nabla^2 + \frac{\omega^2}{c^2}\right) p(\vec{r},\omega) = \frac{\gamma-1}{c^2} i\omega H(\vec{r},\omega)$$

The solution $p(\vec{r},\omega)$ can be expressed as an infinite series of acoustic modes $p_k(\vec{r})$:

$$p(\vec{r},\omega) = \sum_k A_k(\omega)p_k(\vec{r})$$

with $A_k(\omega)$ amplitude of the k-th mode.

$p_k(\vec{r})$ is the solution of the associated homogeneous equation:

$$\left(\nabla^2 + \frac{{\omega_k}^2}{c^2}\right) p_k(\vec{r}) = 0$$

with ω_k is the angular frequency of the normal mode $p_k(\vec{r})$.

5.6 PHOTOACOUSTIC SPECTROSCOPY

5.6.3 Thermal diffusion mode

The equations can be coupled to study the propagation of the thermal gradient by eliminating the pressure dependence.

$$\frac{p}{\rho} = (\gamma - 1)\frac{C_V}{M}T$$

$$-\frac{1}{\rho}\frac{\partial \rho}{\partial t} = \vec{\nabla} \cdot \vec{v}$$

$$\rho \frac{\partial \vec{v}}{\partial t} = -\vec{\nabla} p$$

$$\rho \frac{C_V}{M}\frac{\partial T}{\partial t} + p\vec{\nabla} \cdot \vec{v} = \frac{\partial Q}{\partial t}$$

The thermal diffusion equation is obtained:

$$\frac{\partial T}{\partial t} - D_T \nabla^2 T = \frac{H}{\rho C_P}$$

where D_T is the thermal diffusivity, defined as:

$$D_T = \frac{\lambda}{\rho C_P}$$

with λ thermal conductivity defined as the ratio of the thermal current density to the thermal gradient.

A solution of the diffusion equation can be obtained using the Laplace transform. The thermal perturbation per unit of energy induced by a point source $H(\vec{r}, t\,)$ will be:

$$T(x, y, z, t) = \frac{1}{\rho C_P}\frac{1}{(4\pi D_T t)^{3/2}} e^{-\frac{x^2+y^2+z^2}{4D_T t}} \qquad t \geq 0$$

5.6 PHOTOACOUSTIC SPECTROSCOPY

5.6.3 Thermal diffusion mode

The exponent $\tau_{diff} = \frac{l^2}{4D_T}$ is the diffusion time and represents the time necessary for the heat to propagate at a distance l from the heat source.

$$T(x,y,z,t) = \frac{1}{\rho C_P}\frac{1}{(4\pi D_T t)^{3/2}} e^{-\frac{x^2+y^2+z^2}{4D_T t}}$$

Thermal variations can be converted into density variations using the definition of the volumetric thermal expansion coefficient:

$$\beta = -\frac{1}{\rho}\left(\frac{\partial \rho}{\partial T}\right)_P$$

Thus, the density variations result:

$$\rho(x,y,z,t) = -\frac{\beta}{C_P}\frac{1}{(4\pi D_T t)^{3/2}} e^{-\frac{x^2+y^2+z^2}{4D_T t}} \qquad t \geq 0$$

This solution can be generalized for each thermal source, using the convolution operation between the real thermal source and the response to a point source.

5.6 PHOTOACOUSTIC SPECTROSCOPY

5.6.3 Thermal diffusion mode

The study of the hydrodynamic response of a system with a photothermal excitation causes both a local thermal diffusion and a propagation of an acoustic wave within the gas.

The two phenomena do not interfere with each other. This can be easily demonstrated by comparing the characteristic time it takes for the acoustic and thermal wave to propagate.

In air, considering $D_T = 1.06 \cdot 10^{-5}\, m^2/s$, the time required by the thermal perturbation to spread up to $l = 1\ cm$ far from the source is:

$$\tau_{diff} = \frac{l^2}{4D_T} \approx \frac{10^{-4} m^2}{4 \cdot 10^{-5}\, m^2/s} = 2.5\ s$$

$$\tau_{diff} = \frac{l^2}{4D_T}$$

The same distance will be covered by the acoustic wave in a time equal to (sound velocity $c = 343\ m/s$)

$$\tau_a = \frac{l}{c} \approx \frac{10^{-2} m}{343\, m/s} = 3 \cdot 10^{-5} s$$

The two phenomena are non-interfering at distances greater than few millimeters because they occur on different time scales.

5.6 PHOTOACOUSTIC SPECTROSCOPY

5.6.3 Thermal diffusion mode

It follows that the spatial and temporal evolution of the acoustic wave and the thermal diffusion are different.

In the following graph, the change in density $\delta\rho$ as a function of distance x from the heat source and as a function of time is shown for one-dimensional propagation along the x-axis with an excitation pulse generated in the y−z plane

The thermal and acoustic contributions are well recognizable: the thermal diffusion is presented as a negative variation of the density, whose maximum is located in x = 0, with a narrow broadening in space and time; acoustic propagation occurs in two directions opposite, at the speed of sound.

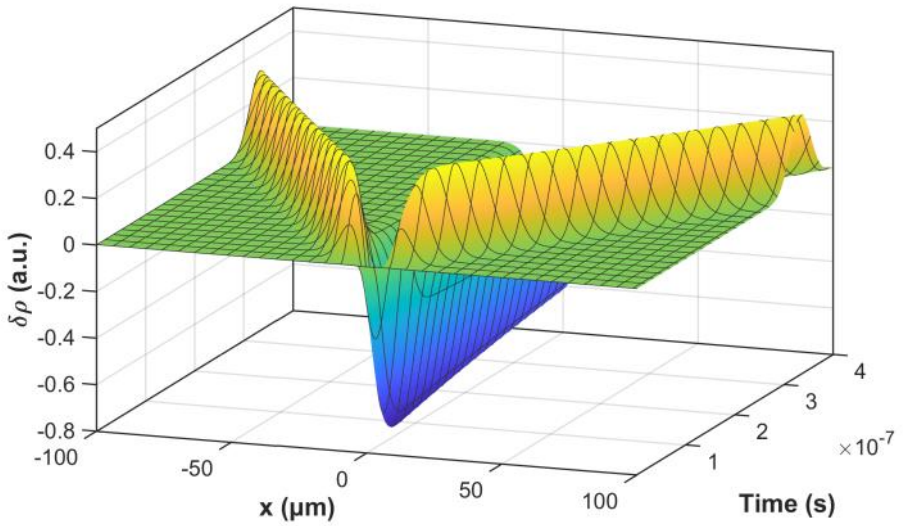

5.6 PHOTOACOUSTIC SPECTROSCOPY

5.6.3 Thermal diffusion mode

How can we measure local temperature changes?

The easiest approach is to measure the changes in refractive index induced by thermal effects. This technique is known as **photothermal spectroscopy**.

The refractive index of a gas depends on the temperature. Therefore, infinitesimal variations of the temperature δT cause variations in the refractive index:

$$\delta n(T,\rho) = \left(\frac{dn}{dT}\right)\delta T$$

In the Clausius-Mossotti approximation: $\frac{dn}{dT} = -\frac{n_0^2 - 1}{2T_0}$

where T_0 is the absolute temperature and n_0 is the refractive index of the unperturbed gas.

Since $n_0 \approx 1$, the previous equation becomes:

$$\delta n = -\frac{(n_0 - 1)(n_0 + 1)}{2T_0}\delta T \approx -\frac{(n_0 - 1)}{T_0}\delta T$$

5.6 PHOTOACOUSTIC SPECTROSCOPY

5.6.3 Thermal diffusion mode

The most efficient way to monitor refractive index changes is to use an optical interferometer, monitoring the relative phase change of light passing through the gas sample.

The relationship between the phase shift $\delta\varphi$ of the beam at the wavelength λ induced on an optical path L by a change in the refractive index (caused in turn by a local change of the temperature) will be:

$$\delta\phi = \frac{2\pi L}{\lambda}\delta n = -\frac{2\pi L}{\lambda}\frac{(n_0 - 1)}{T_0}\delta T$$

The most used interferometer is the Mach-Zender interferometer.

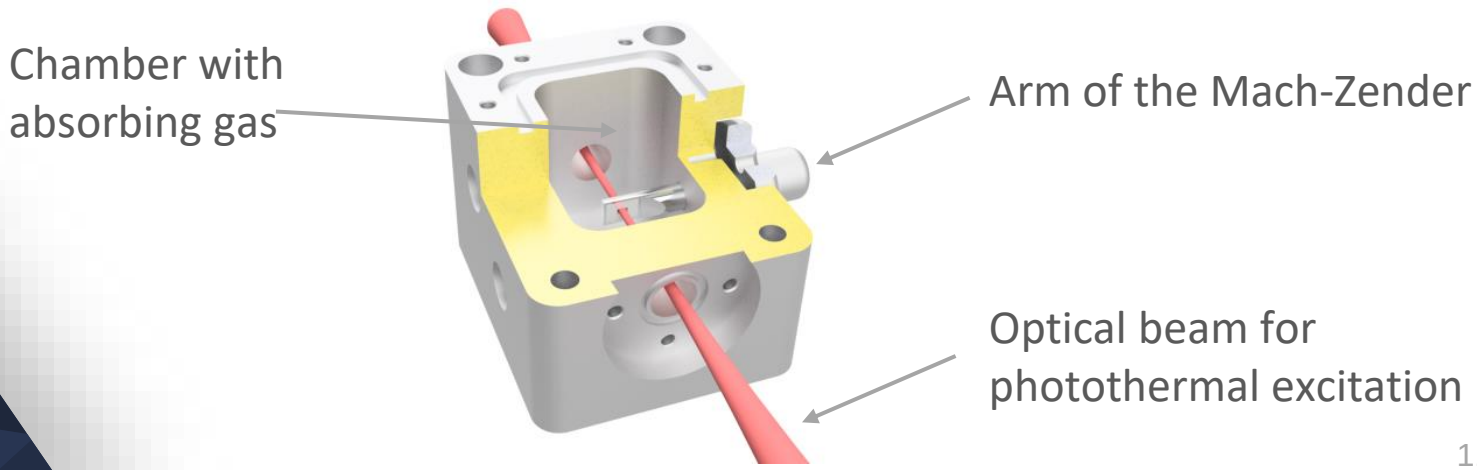

5.6 PHOTOACOUSTIC SPECTROSCOPY

5.6.4 Acoustic wave detection

The detection of the acoustic wave takes place mainly using a microphone.

In photoacoustic spectroscopy, the gas is enclosed within an acoustic cell in which optical absorption also takes place. The acoustic cell acts as an acoustic resonator that amplifies only the acoustic frequencies corresponding to the acoustic modes of the cell.

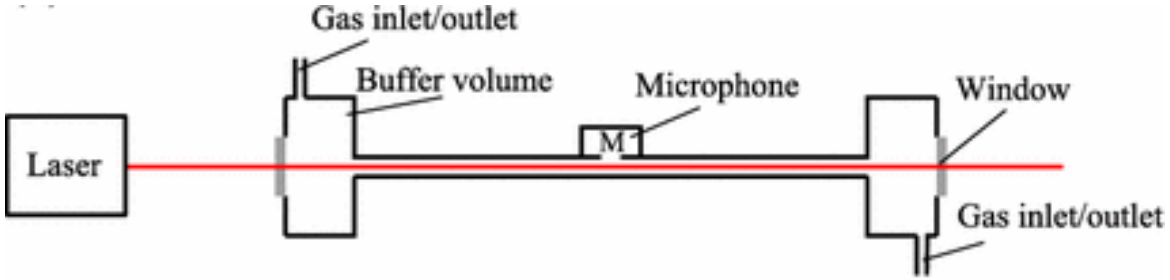

- The laser source is modulated to the frequency of the fundamental acoustic mode of the acoustic cell.
- A microphone is located inside the acoustic cell at the antinode point of the acoustic mode, in order to detect the maximum strength of the acoustic pattern.
- The acoustic cell has an input and an exit window for the laser beam.
- The geometry and size of the cell determine its resonance properties.

5.6 PHOTOACOUSTIC SPECTROSCOPY

5.6.4 Acoustic wave detection

The calculation of normal acoustic modes is determined by imposing the right boundary conditions, so it is highly dependent on the geometry of the acoustic cell.

Although several theoretical models allow to calculate with excellent precision the frequencies of the cavity modes, it is still preferred to measure them. The most used method is to send a white sound into the acoustic cell in the audible spectrum (20 Hz ÷20 KHz) and to detect the response of the cavity with the microphone.

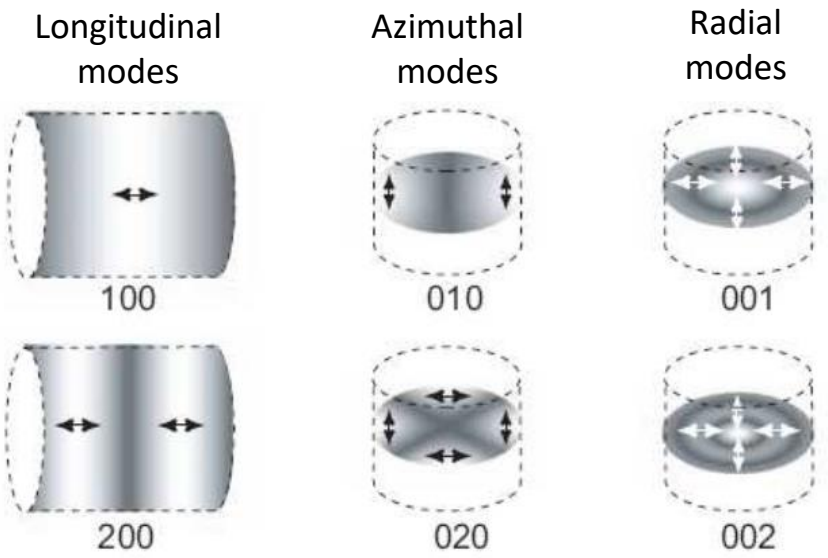

When the modulation frequency matches one of the frequencies of the cavity modes $\omega = \omega_k$, the acoustic energy accumulates in a standing wave and the system works as an acoustic amplifier.

5.6 PHOTOACOUSTIC SPECTROSCOPY

5.6.4 Acoustic wave detection

The resulting amplification of the acoustic wave is determined by the total losses of the resonator.

It is defined in terms of the quality factor Q_k of the resonance mode :

$$Q_k = 2\pi \frac{stored\ energy}{energy\ loss\ per\ cycle}$$

Experimentally, Q_k is calculated as the ratio of the resonance frequency ω_k of the mode to the full-width half maximum $\Delta\omega_k$ value of the resonance curve of the mode:

$$Q_k = \frac{\omega_k}{\Delta\omega_k}$$

The amplitude of the k-th mode p_k at the resonance frequency ω_k is proportional to:

$$A_k(\omega_k) = \frac{(\gamma - 1)\alpha P L Q_k}{\omega_k V_0}$$

Thus, the photoacoustic signal is proportional to the absorption coefficient α, to the incident optical power P and to the interaction length L; it is inversely proportional to the modulation frequency ω_k and the volume of the cell V_0.

5.7 QUARTZ-ENHANCED PHOTOACOUSTIC SPECTROSCOPY

In traditional photoacoustic spectroscopy, the common approach to detect the acoustic signal generated by modulated laser radiation in an absorbing gas uses an acoustic resonator filled with the gas sample and a microphone as a detector.

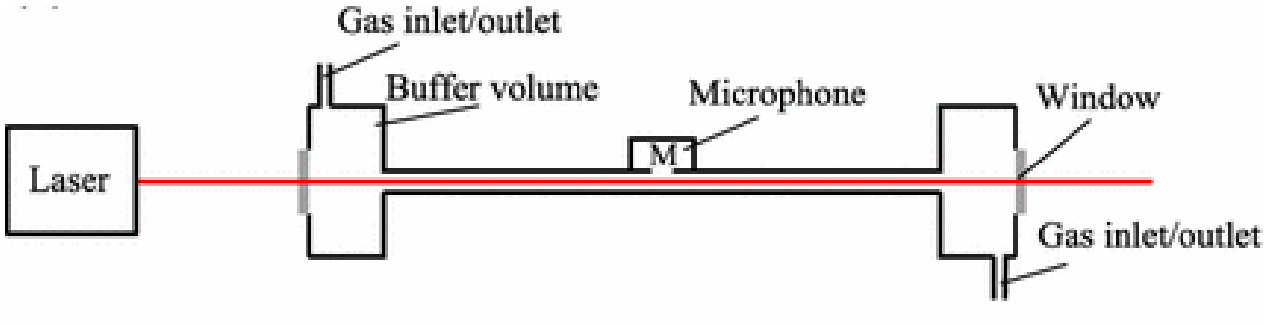

The ultimate detection sensitivity is strongly influenced by:

- the capability to build acoustic cells that are excellent resonators. The resonance frequencies are typically in the range of 1 to 4 kHz and the quality factor at atmospheric pressure does not exceed a few hundred;
    - the performance of the microphone, i.e., the minimum sound wave intensity that the microphone can detect, together with its state of isolation from the surrounding environment, which can generate a significant noise contribution within its detection band.

5.7 QUARTZ-ENHANCED PHOTOACOUSTIC SPECTROSCOPY

An alternative approach for photoacoustic detection of gas traces is to use a quartz tuning fork as an acoustic transducer.

Let us suppose to focus a collimated beam inside a cell containing the gas sample.

The energy density is high at the beam waist of the beam and therefore it makes sense to assume that the acoustic wave has as its source at the beam waist of the beam.

If we place the tuning fork so that the beam waist is between the prongs of the tuning fork, the acoustic wave will deflect the two prongs by putting them in oscillation.

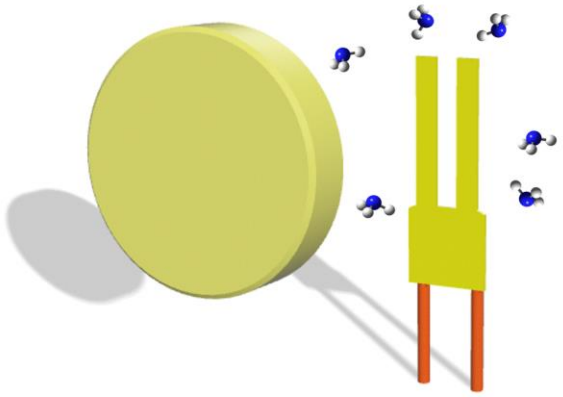

This variant of the photoacoustic spectroscopy is known as **quartz-enhanced photoacustic spectroscopy**, **QEPAS**.

5.7 QUARTZ-ENHANCED PHOTOACOUSTIC SPECTROSCOPY

The laser beam is focused between prongs of the QTF

A sound wave is generated between prongs (photoacoustic effect)

The sound wave generates a stress field T_{ij} that puts prongs in vibration (antisymmetric flexural mode)

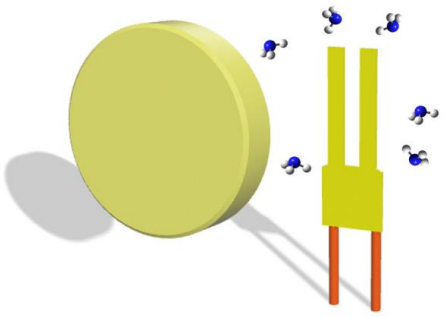

The stress field T_{ij} generates a strain field S_{ij}

$$T_i = Y_{ij}^E S_j$$

Piezoelectric effect generates charges proportional to the strain field

$$D_i = d_{ij} S_j$$

5.7 QUARTZ-ENHANCED PHOTOACOUSTIC SPECTROSCOPY

If the tuning fork is placed inside a cell containing the gas and the modulated laser beam focused between the prongs of the tuning fork, the acoustic wave will deflect the two prongs in two opposite directions, exciting an in-plane mode of vibration, called antisymmetric flexural vibration mode.

The antisymmetric flexural vibration is piezo-electrically active, and electric charges are generated on the surface.

Conversely, the symmetric flexural vibration (mode of vibration in the plane of the tuning fork with the two prongs moving in the same direction) is piezo-electrically inactive.

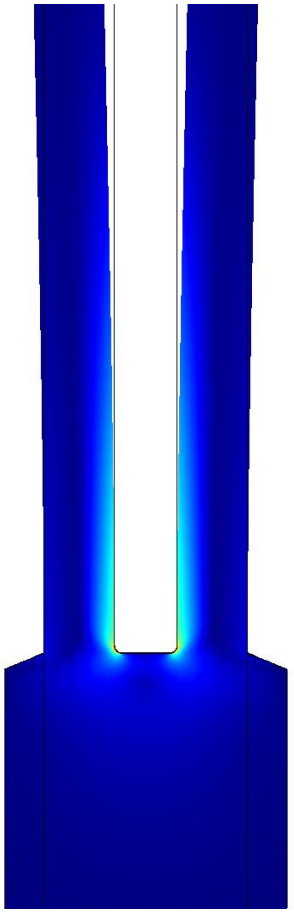

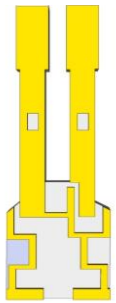

The charges are therefore collected by thin layers of gold or silver deposited on the quartz surface. They can be collected and measured as a voltage or current signal, depending on the electronic circuit used.

5.7 QUARTZ-ENHANCED PHOTOACOUSTIC SPECTROSCOPY

Until 2013, tuning forks used for QEPAS were those typically employed in watches and smartphones.

The frequency of the fundamental antisymmetric flexural mode is $f_0 = 32768\ \text{Hz}$ (2^{15} Hz)

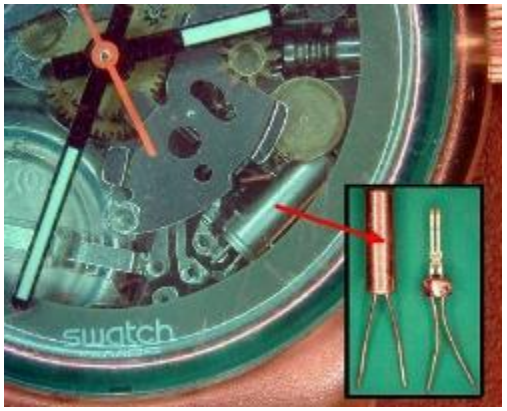

with a quality factor of about $Q_0 = 13{,}000$-$15{,}000$ at atmospheric pressure but can reach 100,000 in a vacuum.

These features make QEPAS devices highly immune to acoustic noise because:

- the ambient noise density follows the $1/f$-dependency and it is very low above 10 KHz;

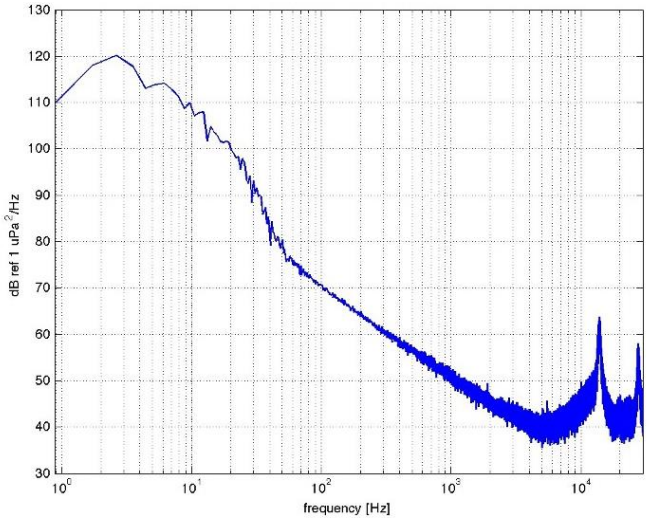

5.7 QUARTZ-ENHANCED PHOTOACOUSTIC SPECTROSCOPY

- Sound waves from an external source tend to apply a force in the same direction on the two prongs of the tuning fork. This does not excite the antisymmetric (piezoelectrically active) flexural mode in which the two prongs move in opposite directions.

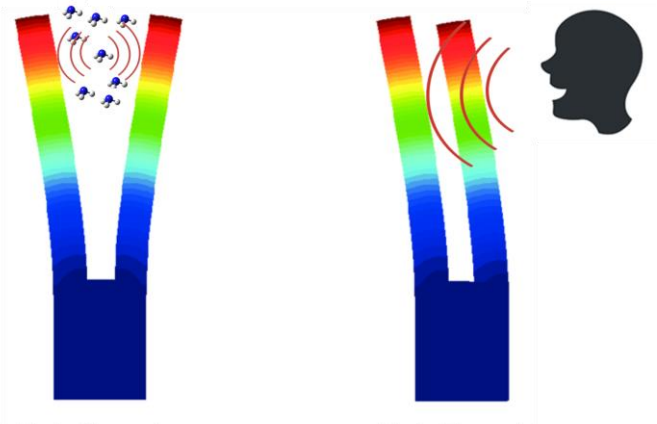

  - the full-width half maximum $\Delta\omega_k$ value of the resonance curve of the tuning fork at normal pressure is less than 3 Hz ($\Delta f = f_0/Q_0$), and only the frequencies contained in this very narrow spectral band can produce an efficient excitation of the flexural vibrational mode.

5.7 QUARTZ-ENHANCED PHOTOACOUSTIC SPECTROSCOPY

The photoacoustic signal for QEPAS will follow the same dependencies found for photoacoustic spectroscopy: the substantial difference is that the tuning fork itself acts as both an acoustic resonator and a transducer.

Then we can adapt the expression previously found for photoacoustic spectroscopy with microphones:

$$S_{QEPAS} \propto \frac{\alpha P Q_0}{f_0}$$

$$A_k(\omega_k) = \frac{(\gamma - 1)\alpha P L Q_k}{\omega_k V_0}$$

We note that compared to traditional photoacoustics, in QEPAS:

- the size of the acoustic cell is no longer important because the tuning fork itself acts as a resonator
- The tuning fork has a quality factor one order of magnitude larger
- It operates at higher frequencies.

The straightforward approach to increase the performance of the QEPAS technique, the resonance frequency of the tuning fork should be decreased while keeping high the quality factor.

5.7 QUARTZ-ENHANCED PHOTOACOUSTIC SPECTROSCOPY

5.7.1 Quartz tuning fork: flexural modes

In order to study the dependence of the geometry and material of the tuning fork on the frequency of the antisymmetric flexural mode, a mechanical model for flexural oscillations must be introduced.

The main assumptions for the mechanical model for flexural oscillations are:

- each prong operates as a cantilever, with one end clamped at the base and the other one free to move
  - the center of mass of each prong does not change while prongs are oscillating.
  - Despite vibrate simultaneously, the vibrations of the two prongs are independent of each other, in other words, the oscillation of a prong does not affect the oscillation of the other.

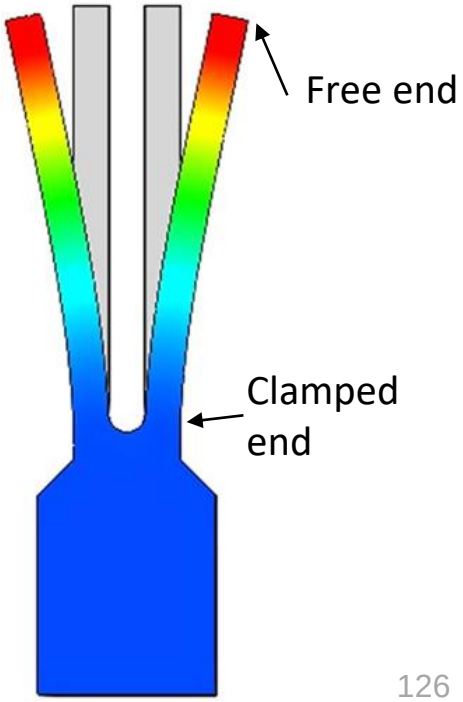

5.7 QUARTZ-ENHANCED PHOTOACOUSTIC SPECTROSCOPY

5.7.1 Quartz tuning fork: flexural modes

With those assumptions, being E the Young's modulus (one-dimensional) of quartz crystal, ρ its volumetric density, I the moment of inertia and A the area of the cross section of the prong, the description of the motion of each prong is given by the classical Euler-Bernoulli theory described by a fourth-order differential equation :

$$EI\frac{\partial^4 y(x,t)}{\partial x^4} + \rho A\frac{\partial^2 y(x,t)}{\partial t^2} = 0$$

The Euler-Bernoulli equation can be solved by assuming that the prong displacement can be separated into two contributions, one dependent on position and the other on time (method of separation of variables):

$$y(x,t) = X(x)f(t)$$

Replacing:

$$\frac{EI}{\rho AX(x)}\frac{\partial^4 X(x)}{\partial x^4} = -\frac{1}{f(t)}\frac{\partial^2 f(t)}{\partial t^2}$$

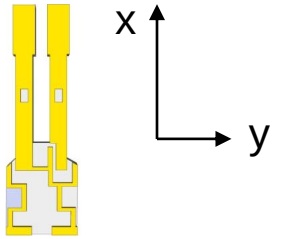

Since the left member does not change as t changes, the right member must be constant. The same is for the right-hand side.

5.7 QUARTZ-ENHANCED PHOTOACOUSTIC SPECTROSCOPY

5.7.1 Quartz tuning fork: flexural modes

If we denote this constant as ω_n^2, we will have that:

$$\frac{EI}{\rho A X(x)}\frac{\partial^4 X(x)}{\partial x^4} = \omega_n^2$$

$$\frac{EI}{\rho A X(x)}\frac{\partial^4 X(x)}{\partial x^4} = -\frac{1}{f(t)}\frac{\partial^2 f(t)}{\partial t^2}$$

So, we can rewrite it as:

$$\frac{\partial^4 X(x)}{\partial x^4} - k_n^4 X(x) = 0$$

with $k_n^4 = \frac{\omega_n^2 \rho A}{EI}$

It can be shown that the general solution is a linear combination of trigonometric functions:

$$\begin{aligned} &X(x) \\ &= C_1[\cos(k_n x) + \cosh(k_n x)] + C_2[\cos(k_n x) - \cosh(k_n x)] \\ &+ C_3[\text{sen}(k_n x) + \text{senh}(k_n x)] + C_4[\text{sen}(k_n x) - \text{senh}(k_n x)] \end{aligned}$$

5.7 QUARTZ-ENHANCED PHOTOACOUSTIC SPECTROSCOPY

5.7.1 Quartz tuning fork: flexural modes

To determine the 4 constants C_1, we need to impose the boundary conditions.

We impose that the clamped end of the prong (the one connected to the support) must have zero displacement and velocity, while the free end cannot be subject to a bending moment or a shear force, namely it is free to oscillate.

These boundary conditions are known in the literature as clamped-free boundary conditions.

Fixing to $x = 0$ the end of the prong clamped to the support, $x = L$ will identify the free end of the prong. Then, the boundary conditions become:

$$X(0) = 0$$

$$\frac{\partial X(0)}{\partial x} = 0$$

$$\frac{\partial^2 X(L)}{\partial x^2} = 0$$

$$\frac{\partial^3 X(L)}{\partial x^3} = 0$$

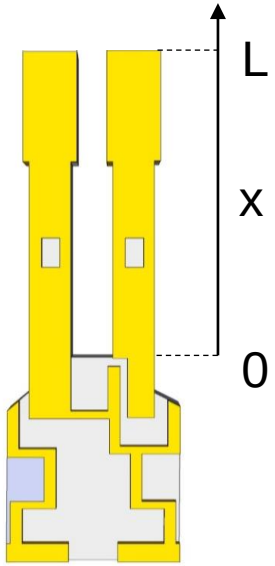

5.7 QUARTZ-ENHANCED PHOTOACOUSTIC SPECTROSCOPY

5.7.1 Quartz tuning fork: flexural modes

- Using the first condition, we get (with $senh0 = 0$ and $cosh0 = 1$):

$$X(0) = 0 = 2C_1$$

$$X(x) = C_1[\cos(k_n x) + \cosh(k_n x)] + C_2[\cos(k_n x) - \cosh(k_n x)] + C_3[\mathrm{sen}(k_n x) + \mathrm{senh}(k_n x)] + C_4[\mathrm{sen}(k_n x) - \mathrm{senh}(k_n x)]$$

leading to $C_1 = 0$

- With the second condition imposed, deriving respect to x ($\frac{\partial senhx}{\partial x} = coshx$ and $\frac{\partial coshx}{\partial x} = senhx$):

$$\frac{\partial X(x)}{\partial x} = C_2[-\mathrm{sen}(k_n x) - \mathrm{senh}(k_n x)] + C_3[\cos(k_n x) + \cosh(k_n x)] + C_4[\cos(k_n x) - \cosh(k_n x)]$$

Imposing:

$$\frac{\partial X(0)}{\partial x} = 0 = 2C_3$$

then $C_3 = 0$

5.7 QUARTZ-ENHANCED PHOTOACOUSTIC SPECTROSCOPY

5.7.1 Quartz tuning fork: flexural modes

With $C_1 = C_3 = 0$, the general solution becomes:

$$X(x) = C_2[\cos(k_n x) - \cosh(k_n x)] + C_4[\text{sen}(k_n x) - \text{senh}(k_n x)]$$

- Let's impose the third condition: $\frac{\partial X(x)}{\partial x} = C_2[-\text{sen}(k_n x) - \text{senh}(k_n x)] + C_4[\cos(k_n x) - \cosh(k_n x)]$

$$\frac{\partial^2 X(L)}{\partial x^2} = C_2[-\cos(k_n L) - \cosh(k_n L)] + C_4[-\text{sen}(k_n L) - \text{senh}(k_n L)] = 0$$

giving:

$$C_4 = C_2 \frac{-\cos(k_n L) - \cosh(k_n L)}{\text{sen}(k_n L) + \text{senh}(k_n L)}$$

Finally, the solution $X_n(x)$ with the imposed conditions becomes:

$$X_n(x) = C_2 \left\{ [\cos(k_n x) - \cosh(k_n x)] + \left[\frac{-\cos(k_n L) - \cosh(k_n L)}{\text{sen}(k_n L) + \text{senh}(k_n L)} \right] [\text{sen}(k_n x) - \text{senh}(k_n x)] \right\}$$

5.7 QUARTZ-ENHANCED PHOTOACOUSTIC SPECTROSCOPY

5.7.1 Quartz tuning fork: flexural modes

- The fourth boundary condition will be used to determine the eigenfrequencies:

$$\frac{\partial^2 X(x)}{\partial x^2} = C_2[-\cos(k_n x) - \cosh(k_n x)] + C_4[-\text{sen}(k_n x) - \text{senh}(k_n x)]$$

$$C_4 = C_2 \frac{-\cos(k_n L) - \cosh(k_n L)}{\text{sen}(k_n L) + \text{senh}(k_n L)}$$

$$\frac{\partial^3 X(L)}{\partial x^3} = C_2[\text{sen}(k_n L) - \text{senh}(k_n L)] + C_2 \left[\frac{-\cos(k_n L) - \cosh(k_n L)}{\text{sen}(k_n L) + \text{senh}(k_n L)}\right][-\cos(k_n L) - \cosh(k_n L)] = 0$$

then:

$$\text{sen}(k_n L) - \text{senh}(k_n L) = -\left[\frac{\cos(k_n L) + \cosh(k_n L)}{\text{sen}(k_n L) + \text{senh}(k_n L)}\right][\cos(k_n L) + \cosh(k_n L)]$$

from which:

$$\text{sen}^2(k_n L) - \text{senh}^2(k_n L) = -[\cos(k_n L) + \cosh(k_n L)]^2$$

Expanding the square:

$$\text{sen}^2(k_n L) - \text{senh}^2(k_n L) = -\cos^2(k_n L) - \cosh^2(k_n L) - 2\cos(k_n L)\cosh(k_n L)$$

5.7 QUARTZ-ENHANCED PHOTOACOUSTIC SPECTROSCOPY

5.7.1 Quartz tuning fork: flexural modes

$$\text{sen}^2(k_nL) - \text{senh}^2(k_nL) = -\cos^2(k_nL) - \cosh^2(k_nL) - 2\cos(k_nL)\cosh(k_nL)$$

Being $\text{sen}^2 x + \cos^2 x = 1$ and $\cosh^2 x - \text{senh}^2 x = 1$, then :

$$\cos(k_nL)\cosh(k_nL) = -1$$

This equation can be solved graphically in the variable k_nL.

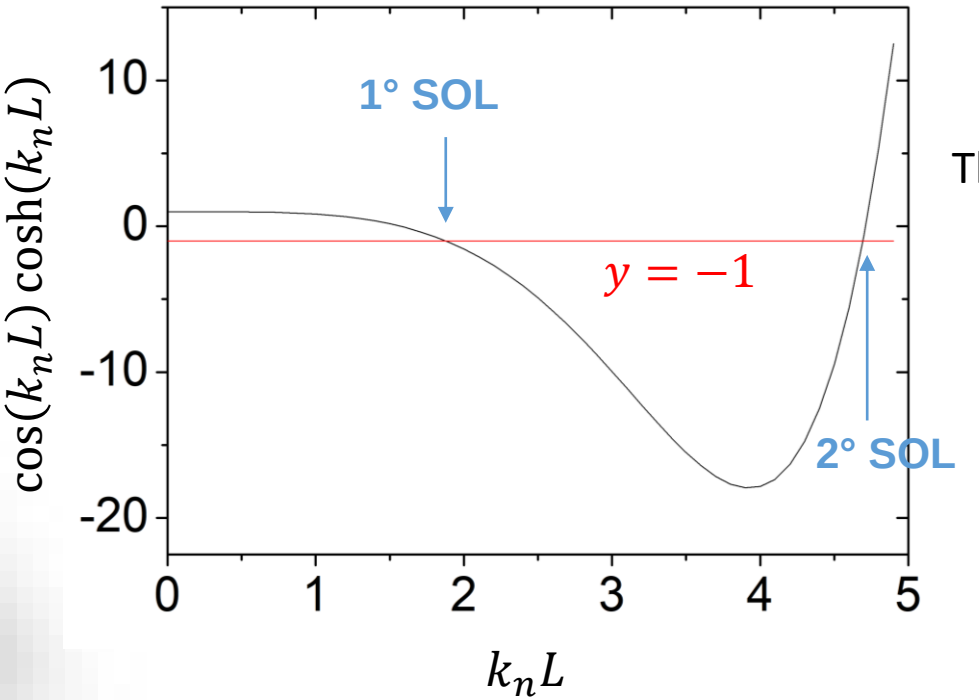

The first three solutions are:

n	k_nL
1	1.875
2	4.694
3	7.855

5.7 QUARTZ-ENHANCED PHOTOACOUSTIC SPECTROSCOPY

5.7.1 Quartz tuning fork: flexural modes

With the assumption made:

$$k_n^4 = \frac{\omega_n^2 \rho A}{EI}$$

We can directly determine the eigenfrequencies of the first three antisymmetric flexural modes :

$$f_n = \frac{\omega_n}{2\pi} = \frac{1}{2\pi}\sqrt{\frac{EI}{\rho A}}k_n^2$$

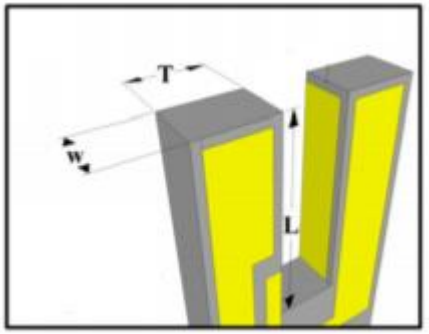

For a cantilever with a rectangular section, it can be shown that $\sqrt{\frac{I}{A}} = \sqrt{\frac{1}{12}}T$, where T is the thickness of the prong.

Using the values reported in the Table, defining $(k_n L)^2 = v^2$, the eigenfrequencies are determined:

$$f_n = \frac{1}{2\sqrt{12}\pi}\sqrt{\frac{E}{\rho}}\frac{T}{L^2}v^2$$

n	$k_n L$
1	1.875
2	4.694
3	7.855

5.7 QUARTZ-ENHANCED PHOTOACOUSTIC SPECTROSCOPY

5.7.1 Quartz tuning fork: flexural modes

$$f_n = \frac{1}{2\sqrt{12}\pi}\sqrt{\frac{E}{\rho}\frac{T}{L^2}}\upsilon^2$$

where $\upsilon = 1.875$ identifies the fundamental flexural mode

$\upsilon = 4.694$ the first flexural overtone mode;

$\upsilon = 7.855$ the second flexural overtone mode,

and so on for the higher harmonics.

It is easy to verify that the first overtone mode ($n = 1$) has a frequency 6.26 times higher than the fundamental one ($n = 0$):

$$\frac{f_1}{f_0} = \frac{4.694^2}{1.875^2} \approx 6.26$$

In addition, the frequency f_n of flexural modes depends:

- by the type of material (Young's modulus and density)

5.7 QUARTZ-ENHANCED PHOTOACOUSTIC SPECTROSCOPY

5.7.1 Quartz tuning fork: flexural modes

$$f_n = \frac{1}{2\sqrt{12}\pi}\sqrt{\frac{E}{\rho}}\frac{T}{L^2}v^2$$

- depends on the geometry of the prong as: $\frac{T}{L^2}$
- it does not depend on the thickness w of the crystal. This because the model considers only motions in the plane of the tuning fork, and therefore the thickness is neglected. Therefore, the model can be applied for all cases in which both w and L are larger than w.

Ultimately, we can change the comb of the flexural modes of a quartz tuning fork by varying the size and the geometry of its prongs.

Using the expression found for

$$X_n(x) = C_2\left\{[\cos(k_n x) - \cosh(k_n x)] + \left[\frac{-\cos(k_n L) - \cosh(k_n L)}{\text{sen}(k_n L) + \text{senh}(k_n L)}\right][\text{sen}(k_n x) - \text{senh}(k_n x)]\right\}$$

we can graphically represent the lateral displacement of the prong while it is vibrating at the fundamental and at the first overtone mode.

5.7 QUARTZ-ENHANCED PHOTOACOUSTIC SPECTROSCOPY

5.7.1 Quartz tuning fork: flexural modes

$$X_n(x) = C_2\left\{[\cos(k_n x) - \cosh(k_n x)] + \left[\frac{-\cos(k_n L) - \cosh(k_n L)}{\text{sen}(k_n L) + \text{senh}(k_n L)}\right][\text{sen}(k_n x) - \text{senh}(k_n x)]\right\}$$

n	$k_n L$
1	1.875
2	4.694

Fundamental Mode

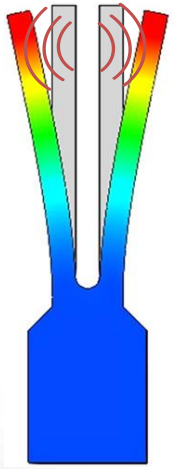

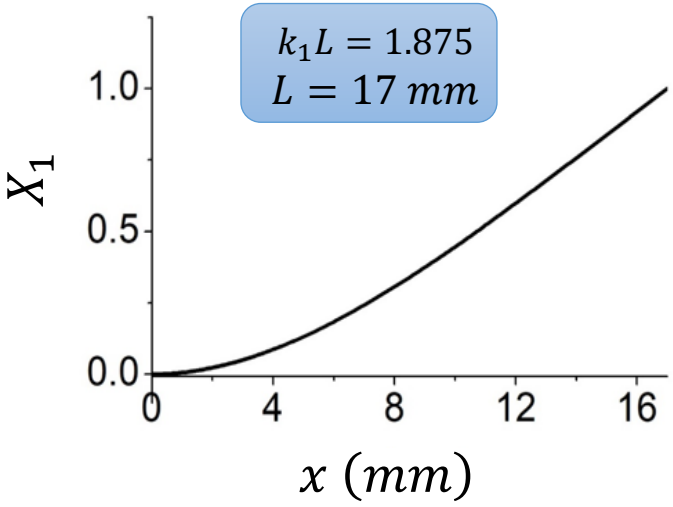

1° Overtone Mode

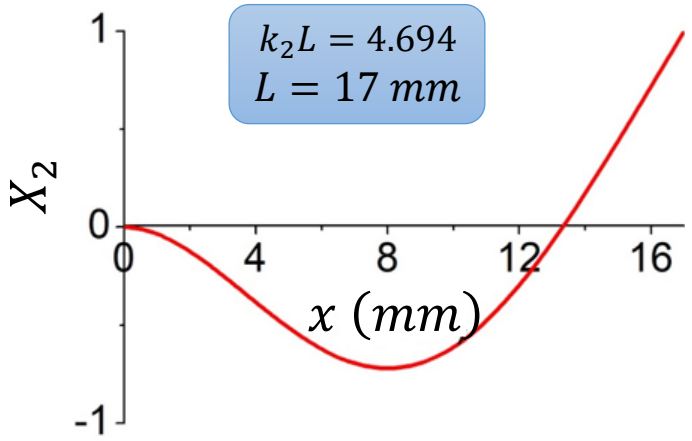

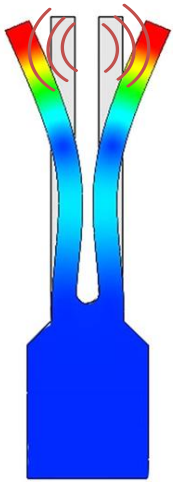

The fundamental mode has a node point (at the base of the prong) and an antinode point (at the free end)

The first overtone mode has two node points and two antinode points (one at the free end and the other almost at the half of the prong length)

5.7 QUARTZ-ENHANCED PHOTOACOUSTIC SPECTROSCOPY

5.7.2 Damping effects due to pressure

Considerations on the quality factor are more difficult to be treated with an analytical model.

The quality factor is related to the losses of the system while it is oscillating.

The factors contributing to the losses are:

- *air damping*
- *support losses*
- Thermoelastic damping

It is difficult to determine an analytical model that considers all three loss mechanisms. As a first assumption, we can consider that the most relevant loss mechanism is the interaction with air and neglect the other two.

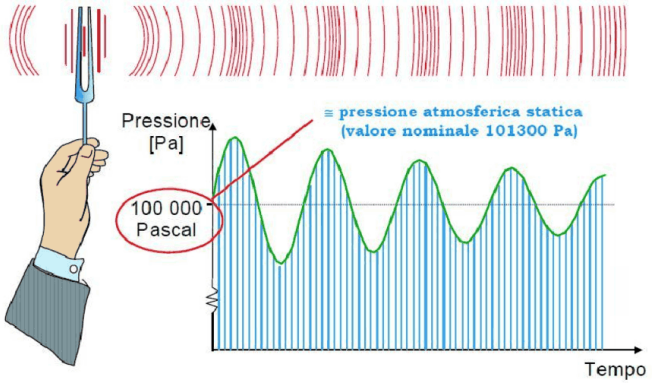

5.7 QUARTZ-ENHANCED PHOTOACOUSTIC SPECTROSCOPY

5.7.2 Damping effects due to pressure

In QEPAS the tuning fork is immersed in the gas to be detected.

What happens to the resonance properties of the tuning fork (the frequency and the quality factor) when the thermodynamic parameters of gas change?

If we assume that the tuning fork is at thermal equilibrium, the study can be reduced to analyze the dependence of the tuning fork resonance properties on gas pressure.

When the tuning fork undergoes harmonic oscillations of small amplitude in a fluid, it tends to induce particles motion in the fluid which gives rise to energy loss and additional inertia. Since the molecular mean free path is much smaller than the characteristic length of the structure, the gas behaves entirely as a continuous fluid. This generates:

- a virtual increase of the oscillating mass that in the Euler-Bernoulli equation is included as an additive mass term
- a viscous friction proportional to speed of molecules

The Euler-Bernoulli equation will change as:

$$EI\frac{\partial^4 y(x,t)}{\partial x^4} + \rho A\frac{\partial^2 y(x,t)}{\partial t^2} = 0$$

$$EI\frac{\partial^4 y(x,t)}{\partial x^4} + C_d\frac{\partial y(x,t)}{\partial t} + (\rho A + u)\frac{\partial^2 y(x,t)}{\partial t^2} = 0$$

where C_d is the damping parameter and u the added mass per unit length.

5.7 QUARTZ-ENHANCED PHOTOACOUSTIC SPECTROSCOPY

5.7.2 Damping effects due to pressure

Let's suppose that the eigenfrequencies are not affected by viscous damping, but are mainly influenced by the additional mass (a legitimate hypothesis if we consider that the resonance frequencies strongly depend on the geometry of the tuning fork).

In this approximation, the resonance frequencies will change as:

$$f'_n = \frac{1}{2\sqrt{12}\pi}\sqrt{\frac{EI}{(\rho A + u)}}k_n^2$$

$$f_n = \frac{1}{2\pi}\sqrt{\frac{EI}{\rho A}}k_n^2$$

We can estimate the change in frequency Δf due to the presence of a gas compared to the case in which the tuning fork oscillates in a vacuum:

$$\Delta f = \frac{f_n - f'_n}{f_n} = \frac{\frac{1}{\sqrt{\rho A}} - \frac{1}{\sqrt{(\rho A + u)}}}{\frac{1}{\sqrt{\rho A}}} = 1 - \sqrt{\frac{\rho A}{\rho A + u}} = 1 - \sqrt{\frac{1}{1 + \frac{u}{\rho A}}}$$

5.7 QUARTZ-ENHANCED PHOTOACOUSTIC SPECTROSCOPY

5.7.2 Damping effects due to pressure

Assuming that $u \ll \rho A$, $\frac{u}{\rho A} \ll 1$ and using: $\sqrt{\frac{1}{1+x}} \approx 1 - \frac{x}{2}$ for $x \ll 1$, one obtain:

$$\Delta f = -\frac{1}{2}\frac{u}{\rho A}$$

$$\Delta f = 1 - \sqrt{\frac{1}{1+\frac{u}{\rho A}}}$$

The frequency of the tuning fork decreases linearly while the added mass increases.

The rigorous derivation of the additional mass u is a problem of not ease solution even for simple structures or geometries; in a first approximation, the additional mass can be supposed proportional to the density ρ_0 of the surrounding gas.

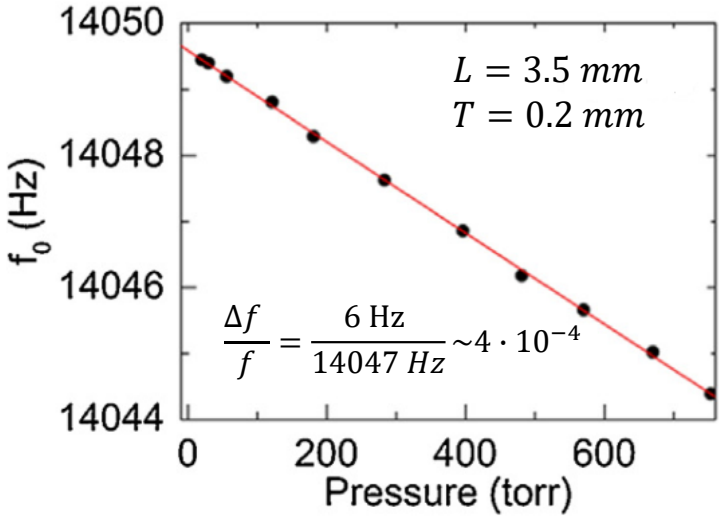

Since the relationship between pressure and density for a gas is of simple proportionality: $P \propto \rho_0$, we can conclude that Δf varies linearly with the gas pressure.

5.7 QUARTZ-ENHANCED PHOTOACOUSTIC SPECTROSCOPY

5.7.2 Damping effects due to pressure

However, the damping of the motion by the gas negatively affects also the quality factor: in fact, the reaction force to the vibration motion causes energy dissipation.

Assuming that the viscous drag force of the gas is the only source of damping, as prescribed by the Euler-Bernoulli theory, the gas damping parameter is proportional to $C_d \propto \sqrt{\rho_0}$

Using the ideal gas law, $C_d = a\sqrt{P}$, where a is the constant of proportionality.

The influence of damping on the quality factor Q can be expressed in terms of energy dissipation $1/Q(P)$ at gas pressure P, thus:

$$C_d = \frac{1}{Q(P)} - \frac{1}{Q_0}$$

where Q_0 is the Q factor contribution in vacuum which depends exclusively on internal losses (support losses and thermoelastic damping).

5.7 QUARTZ-ENHANCED PHOTOACOUSTIC SPECTROSCOPY

5.7.2 Damping effects due to pressure

Including $C_d = a\sqrt{P}$, we can derive the dependence of the quality factor on pressure:

$$Q(P) = \frac{Q_0}{1 + Q_0 a\sqrt{P}}$$

$$C_d = \frac{1}{Q(P)} - \frac{1}{Q_0}$$

Thus, it is expected that the QEPAS sensitivity is a function of the gas sample pressure because the QEPAS signal is proportional to the quality factor of the tuning fork.

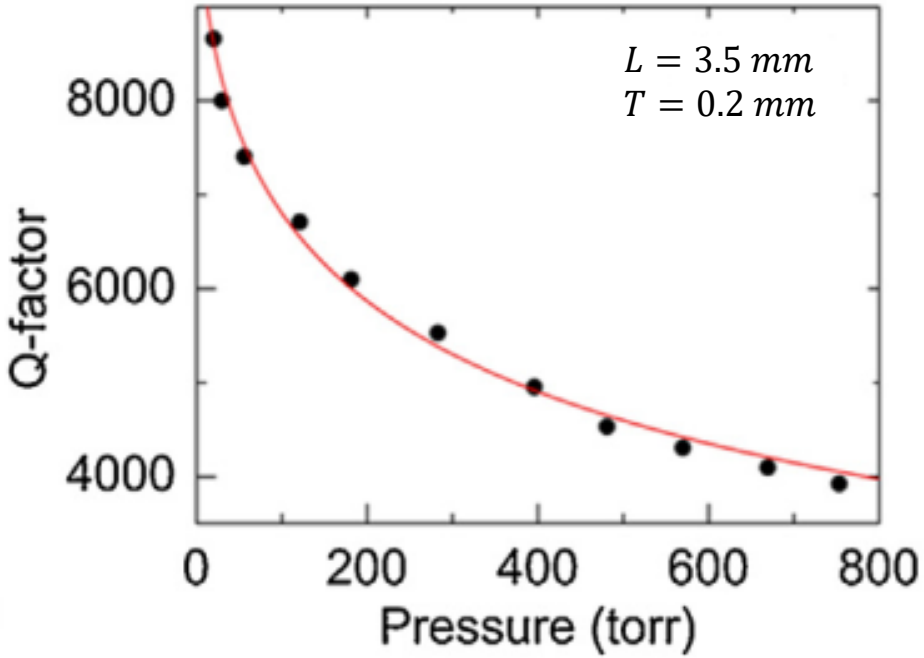

5.7 QUARTZ-ENHANCED PHOTOACOUSTIC SPECTROSCOPY

5.7.2 Damping effects due to pressure

What happens to the QEPAS signal if the gas pressure changes?

$$S_{QEPAS} \propto \frac{\alpha P_L Q(P)}{f(P)}$$

Variations in frequency due to pressure are negligible, so only Q(P) will give its contribution.

As the pressure changes, there are two trends to be considered:

- the Q factor decreases with increasing pressure
- the transfer of energy in the no radiative relaxation processes are faster at higher pressure (because each molecule can count on more nearest neighbors), resulting in a more efficient generation of the sound wave.

Since these two trends are in opposition, this suggests that the QEPAS signal can be optimized as a function of pressure, in a sort of trade-off between these two trends.

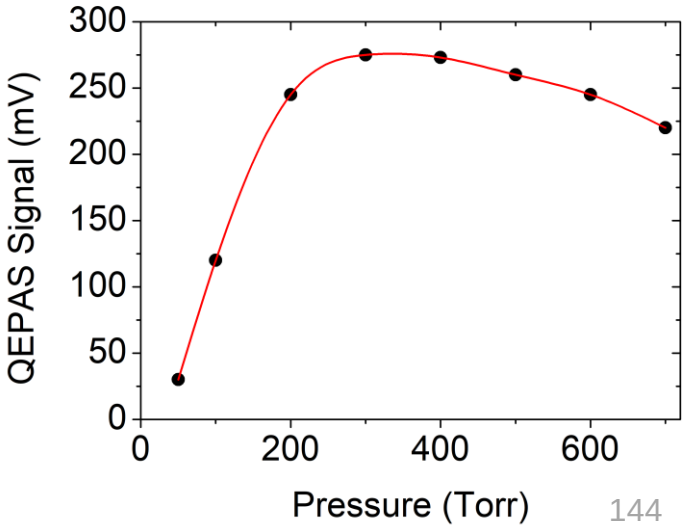

5.8 COMPARING DIFFERENT SPECTROSCOPIC TECHNIQUES

Comparing different spectroscopic techniques is a complicated problem.

The objective is to find a figure of merit that can be used for all spectroscopic techniques. This figure of merit must then be normalized with respect to operating parameters that affect the ultimate performance, but not the technique itself.

The starting point is to determine the detection limit of a sensor. This is usually expressed in terms of Noise Equivalent Concentration (NEC) and is strictly defined as the concentration of the gas to be detected whose signal equals the noise level. In other words, the NEC is estimated at a signal-to-noise ratio (SNR) of 1.

The noise level is calculated as the standard deviation (1σ) of the sensor response in the condition of no optical absorption.

The noise level can be calculated in the following way. Let us consider a generic gas sensor:

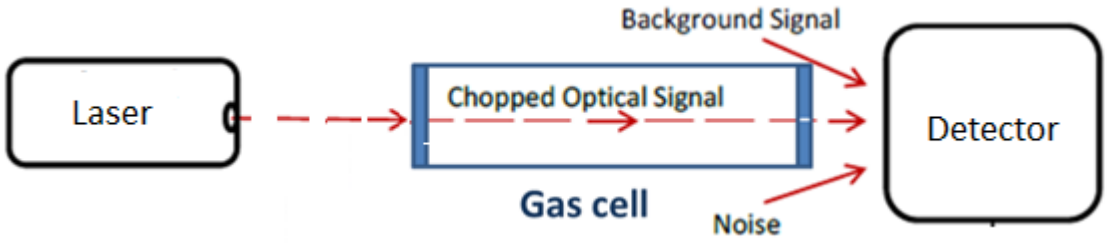

5.8 COMPARING DIFFERENT SPECTROSCOPIC TECHNIQUES

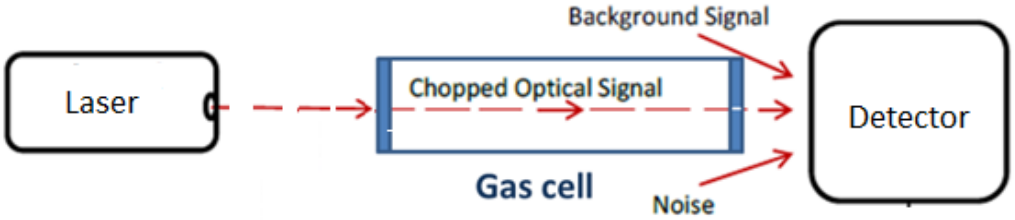

The condition of no optical absorption can be achieved under two conditions:

- **Removing the target gas concentration from the absorption cell**

This condition could be achieved by completely emptying the absorption cell.

This way is not the best one because the experimental condition that would be realized for the measurement of noise is substantially different from the condition in which there is the gas in the cell.

To preserve the experimental conditions as much as possible, it is convenient to fill the cell with the same gas matrix, but without the target gas.

If, for example, the sensor detects carbon dioxide (concentration 400 parts per million) in air, the noise measurement can be done by filling the cell with pure nitrogen (N_2) at atmospheric pressure, being the air composed of about 78% nitrogen.

5.8 COMPARING DIFFERENT SPECTROSCOPIC TECHNIQUES

- **Tuning the laser to a wavelength far from the absorption curve of the gaseous species**

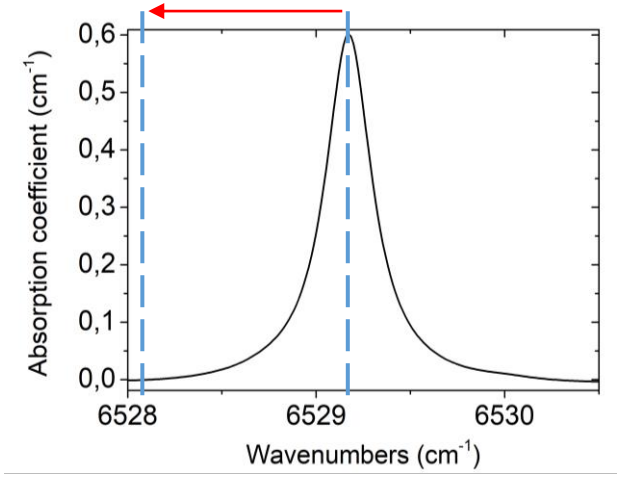

Of course, the two conditions can also be realized simultaneously.

We then proceed to acquire the detector signal with a sampling Δt for a total time T.

When $N = T/\Delta t$ samples are acquired, a statistical analysis can be performed to determine the 1σ standard deviation

$$1\sigma = \sqrt{\sum_{i=1}^{N} \frac{(x_i - \bar{x})^2}{N}} \qquad \text{with} \qquad \bar{x} = \frac{1}{N}\sum_{i=1}^{N} x_i$$

where N is the number of samples x_i acquired in a time interval T.

5.8 COMPARING DIFFERENT SPECTROSCOPIC TECHNIQUES

$N = 15000$ samples acquired every $\Delta t = 0.1\ s$ for a total time of $T = 25\ minutes$

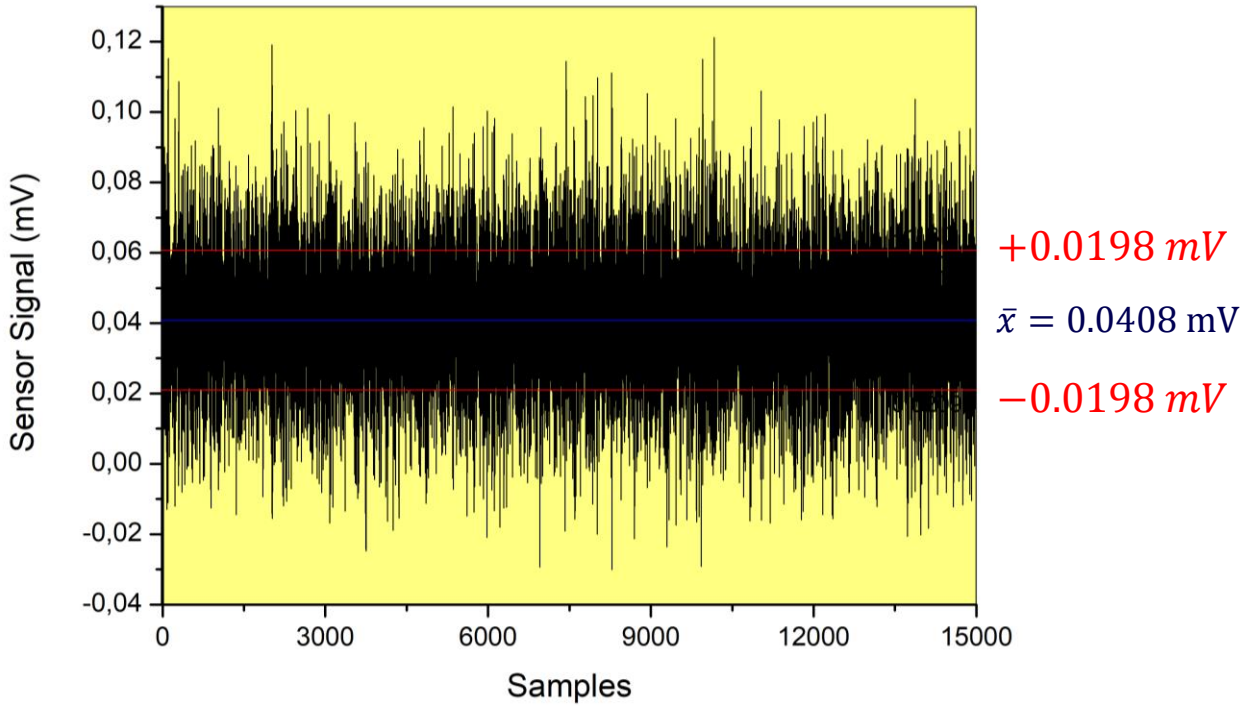

The mean value of $\bar{x}$=0.0408 mV represents the signal in the absence of absorption. It is typically referred to as an **offset** and can be subtracted from the signal measured in the presence of absorption.

The noise level measured at 1σ (1σ-noise level) is ±0.0198 mV

5.8 COMPARING DIFFERENT SPECTROSCOPIC TECHNIQUES

5.8.1 Minimum absorption coefficient

The minimum absorption coefficient α_{min} represents the estimated absorption coefficient at the minimum detectable concentration, namely NEC.

Let's start from the expression of the absorption coefficient for a generic optical transition $|i\rangle \rightarrow |k\rangle$:

$$\alpha_{ik}(\omega) = N_i \sigma_{ik}(\omega)$$

with N_i density of absorbent molecules, $\sigma_{ik}(\omega)$ optical absorption cross section.

The cross section of the process can be expressed as the product between the linestrength S of the transition and its normalized Lorentzian line profile $I(\omega - \omega_0)$:

$$\sigma_{ik}(\omega) = SI(\omega - \omega_0) = \frac{S}{\pi} \frac{\gamma}{(\omega - \omega_0)^2 + \gamma^2}$$

where ω_0 is the frequency at the maximum absorption and γ the FWHM

The cross section at the absorption peak ($\omega = \omega_0$) will be:

$$\sigma_{ik}(\omega_0) = \frac{S}{\gamma \pi}$$

5.8 COMPARING DIFFERENT SPECTROSCOPIC TECHNIQUES

5.8.1 Minimum absorption coefficient

The minimum absorption coefficient α_{min} at the absorption peak (i.e. with the laser tuned to $\omega = \omega_0$) will be:

$$\alpha_{min} = N_i \sigma = N_i \frac{S}{\gamma \pi}$$

$$\alpha_{ik}(\omega) = N_i \sigma_{ik}(\omega)$$
$$\sigma_{ik}(\omega_0) = \frac{S}{\gamma \pi}$$

The N_i density of the absorbing molecules can be expressed as the product with the molecular density N_{TOT} and the minimum detectable concentration c_{min} of the target molecules, i.e.

$$N_i = c_{min} N_{TOT}$$

Considering the equation of the ideal gas law:

$$PV = nRT$$

where P is the gas pressure, V the volume, T the temperature, n the number of moles, and R the ideal gas constant.

The number of moles is equal to the total number of molecules n_{TOT} divided by the Avogadro number N_A:

$$n = \frac{n_{TOT}}{N_A}$$

5.8 COMPARING DIFFERENT SPECTROSCOPIC TECHNIQUES

5.8.1 Minimum absorption coefficient

The equation of the ideal gas law becomes:

$$PV = \frac{n_{TOT}}{N_A} RT$$

$PV = nRT$

$n = \frac{n_{TOT}}{N_A}$

Whereas the molecular density is equal to:

$$N_{TOT} = \frac{n_{TOT}}{V}$$

from the equation of the ideal gas law we get

$$N_{TOT} = \frac{PN_A}{RT}$$

Finally, the minimum absorption coefficient α_{min} can be expressed as a function of c_{min} and of thermodynamic parameters of the gas sample:

$$\alpha_{min} = N_i \sigma = c_{min} \frac{PN_A}{RT} \frac{S}{\gamma\pi}$$

$\alpha_{min} = N_i \sigma = N_i \frac{S}{\gamma\pi}$

$N_i = c_{min} N_{TOT}$

5.8 COMPARING DIFFERENT SPECTROSCOPIC TECHNIQUES

5.8.1 Minimum absorption coefficient

The concentration of a gaseous species is therefore defined as the percentage (fraction) of absorbing molecules compared to the total number of molecules of the gas sample.

It is therefore a dimensionless quantity, and the following nomenclature in English is largely employed in literature.

Fraction	Name	Symbol
$1:100$	Percent	%
$1:10^3$	Part-per-thousand	‰
$1:10^6$	Part-per-million	ppm
$1:10^9$	Part-per-billion	ppb
$1:10^{12}$	Part-per-trillion	ppt
$1:10^{15}$	Part-per-quadrillion	ppq

5.8 COMPARING DIFFERENT SPECTROSCOPIC TECHNIQUES

5.8.2 Normalized Noise Equivalent Absorption (NNEA)

The minimum absorption coefficient α_{min} estimates the minimum detectable absorption.

However, it is a parameter that depends exclusively on the chosen absorption line, the thermodynamic conditions of the gas sample and the noise level of the acquired signal.

It does not consider two fundamental operating parameters:

- The power of the laser. Comparing two sensors with the same estimated α_{min}, the sensor that uses less laser power is to be considered as more efficient.
- The integration time of the detector signal. Comparing two sensors with the same estimated α_{min}, the sensor that uses lower integration times (and therefore fast response time) is to be considered more efficient.

Therefore, the Normalized Noise Equivalent Absorption (NNEA) is introduced as a figure of merit and defined as α_{min} normalized with respect to the power of the laser P_L and the bandwidth of the detector Δf :

$$NNEA = \frac{P_L \cdot \alpha_{min}}{\sqrt{\Delta f}}$$

5.8 COMPARING DIFFERENT SPECTROSCOPIC TECHNIQUES

5.8.2 Normalized Noise Equivalent Absorption (NNEA)

$$NNEA = \frac{P_L \cdot \alpha_{min}}{\sqrt{\Delta f}}$$

where the bandwidth of a detector is related to the integration time τ of the signal by the relation:

$$\tau \propto \frac{1}{2\pi\Delta f}$$

The unit of NNEA is:

$$NNEA \left[\frac{W cm^{-1}}{Hz^{1/2}}\right]$$

As it has been defined, comparing different sensors with each other, the sensor that shows lower NNEAs is to be considered more performing.

5.8 COMPARING DIFFERENT SPECTROSCOPIC TECHNIQUES

5.8.2 Normalized Noise Equivalent Absorption (NNEA)

The NNEA is largely used in literature to compare different optical techniques. The graph shows the NNEAs achieved by the various techniques as a function of the effective optical pathlength.

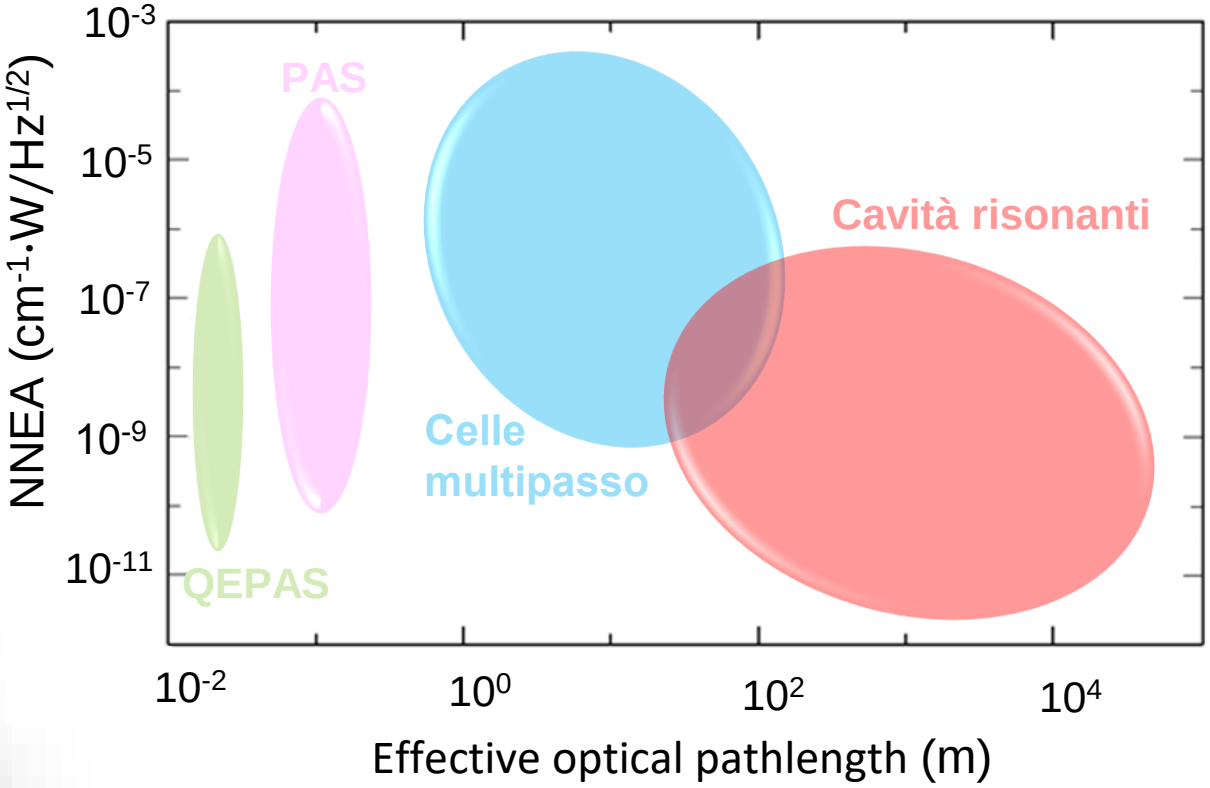

EXERCISE

ESERCIZIO 1

An optical sensor for sulfur dioxide (SO_2) detection uses a multipass cell and a quantum cascade laser tuned at the SO_2 absorption line centered at 1350.82 cm^{-1}, having a linestrength of S = $4.85 \cdot 10^{-20}$ cm/molecules and a spectral broadening of 0.0051 cm^{-1} at a working pressure P = 50 torr. When the SO_2 concentration SO2 in N_2 is equal to 20 ppm, the acquired signal is 158 µV with fluctuations having a standard deviation (1σ) equal to 2.2 µV, with a signal acquisition time of τ = 100 ms. Being the laser power equal to P_L = 5 mW, determine the NNEA of the sulfur dioxide sensor.

To determine the NNEA of the sensor, the minimum absorption coefficient α_{min} must first be estimated:

$$\alpha_{min} = N_{min}\sigma$$

with N_{min} is the minimum detectable density of SO_2 molecules and σ the optical cross-section.

EXERCISE

The cross section will be equal to:

$$\sigma = \frac{S}{\gamma\pi} = \frac{4.85 \cdot 10^{-20}\ \frac{cm}{molecole}}{0.0051\ cm^{-1} \cdot 3.14} = 3.03 \cdot 10^{-18}\ \frac{cm^2}{molecole}$$

Using the ideal gas law, we have seen that the molecular density N_{min} an be related to the minimum detectable concentration of SO_2 molecules:

$$N_{min} = c_{min}\frac{PN_A}{RT}$$

where $P = 50\ torr = 0.0658\ atm$ is the gas pressure,$R = 82.1\ \frac{cm^3 \cdot atm}{molecole \cdot K}$ is the ideal gas constant, $T = 295\ K$ is the temperature, and $N_A = 6 \cdot 10^{23}\ \frac{molecole}{moli}$ is the Avogadro number.

c_{min} is the minimum detectable concentration, corresponding to a signal-to-noise ratio of 1:

$$c_{min} = \frac{Rumore\ (1\sigma)}{Segnale} \cdot 20\ ppm = \frac{2.2\ \mu V}{158\ \mu V} \cdot 20\ ppm = 278\ ppb$$

EXERCISE 1

$$N_{min} = c_{min}\frac{PN_A}{RT} = 278 \cdot 10^{-9}\frac{0.0658\ atm \cdot 6 \cdot 10^{23}\frac{molecole}{moli}}{82.1\frac{cm^3 \cdot atm}{moli \cdot K} \cdot 295K} = 4.53 \cdot 10^{11}\frac{molecole}{cm^3}$$

Thus, the minimum absorption coefficient will be:

$$\alpha_{min} = N_{min}\sigma = 4.53 \cdot 10^{11}\frac{molecole}{cm^3} \cdot 3.03 \cdot 10^{-18}\frac{cm^2}{molecole} = 1.37 \cdot 10^{-6}cm^{-1}$$

and the $NNEA$ will be:

$$NNEA = \frac{P_L \cdot \alpha_{min}}{\sqrt{\Delta f}}$$

For τ=100 ms the bandwidth of the photodetector will be:

$$\Delta f \propto \frac{1}{2\pi\tau} = 1.59\ Hz$$

leading to:

$$NNEA = \frac{P_L \cdot \alpha_{min}}{\sqrt{\Delta f}} = \frac{0.005\ W \cdot 1.37 \cdot 10^{-6}cm^{-1}}{\sqrt{1.59\ Hz}} = 5.43 \cdot 10^{-9}\frac{W cm^{-1}}{\sqrt{Hz}}$$